Mediators of Inflammation

Novel Approaches in Diagnosing the Role of Inflammation in the Onset Cardiovascular Disorders

Lead Guest Editor: Adrian Doroszko
Guest Editors: Aneta Radziwon-Balicka, Robert P. Skomro, and Piotr Dobrowolski

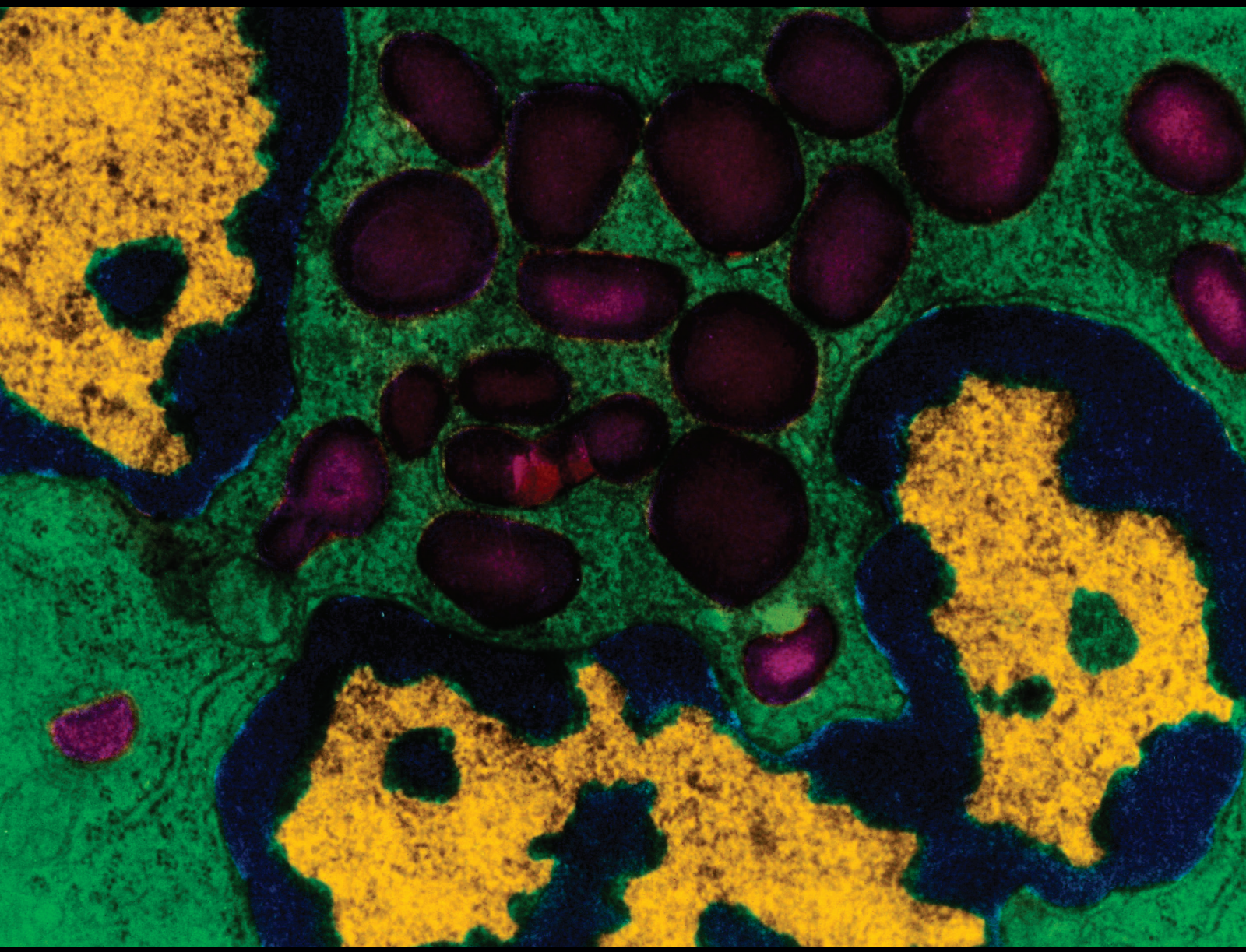

Novel Approaches in Diagnosing the Role of Inflammation in the Onset Cardiovascular Disorders

Mediators of Inflammation

Novel Approaches in Diagnosing the Role of Inflammation in the Onset Cardiovascular Disorders

Lead Guest Editor: Adrian Doroszko
Guest Editors: Aneta Radziwon-Balicka, Robert P. Skomro, and Piotr Dobrowolski

Editorial Board

Contents

Hindawi
Mediators of Inflammation
Volume 2018, Article ID 8234063, 2 pages
https://doi.org/10.1155/2018/8234063

Editorial

Novel Approaches in Diagnosing the Role of Inflammation in the Onset Cardiovascular Disorders

Adrian Doroszko,[1] **Piotr Dobrowolski**,[2] **Aneta Radziwon-Balicka**,[3] **and Robert Skomro**[4]

[1]*Department of Internal Medicine, Occupational Diseases and Hypertension, Wroclaw Medical University, Wroclaw, Poland*
[2]*Department of Congenital Heart Diseases, Institute of Cardiology, Warsaw, Poland*
[3]*Department of Clinical Experimental Research, Glostrup Research Institute, Rigshospitalet, Glostrup, Denmark*
[4]*Division of Respirology, Critical Care and Sleep Medicine, Department of Medicine, University of Saskatchewan, Saskatoon, Canada*

Correspondence should be addressed to Adrian Doroszko; adrian.doroszko@umed.wroc.pl

Received 24 September 2018; Accepted 24 September 2018; Published 18 October 2018

Cardiovascular disease remains among the major healthcare problems of the world population, and understanding its determinants is pivotal for designing novel effective interventions. Advances in molecular medicine have enabled us to identify the critical pathways involved in cell survival or death in the myocardium, endothelial cells, vascular wall, and brain. What is more, some crucial regulators of these pathways have been newly identified, resulting in the development of novel strategies for treatment of coronary artery disease, hypertension, and congestive heart failure. There are a number of chemical mediators and pathways involved in the inflammatory onset of cardiovascular disorders. Thus, from a therapeutic point of view, it would be most important to focus on the active mediators of inflammation and apoptosis and to manipulate these in order to improve cell function and survival. The cellular mechanisms involved in the pathogenesis of cardiovascular inflammatory injury are complex and involve the interactions of various cells, including coronary endothelial cells, circulating blood cells, and cardiac myocytes. The intracellular signalling pathways that mediate stress responses and determine cell death or survival have not been fully investigated. Protein kinase activation potentially regulates the onset of injury. A substantial amount of basic research has defined many of the details regarding the role of inflammation in the kinase pathway organization and activation; nevertheless, the role of individual signalling pathways in pathogenesis of various forms of cardiovascular disease is still investigated.

This special issue is aiming at stimulating the continuing effort to understand the molecular mechanisms underlying cardiovascular damage mediated by inflammation.

Selenoprotein S (SelS) has been identified in endothelial cells and is associated with inflammation. S. Cui et al. demonstrated that the upregulation of SelS enhances the levels of nitric oxide and endothelial nitric oxide synthase in tumour necrosis factor-α-treated human umbilical vein endothelial cells. The authors postulate that SelS protects endothelial cells against TNF-α-induced dysfunction by inhibiting the activation of p38 MAPK and NF-κB pathways and implicate it as a possible modulator of vascular inflammatory diseases.

Oxysterols may affect cholesterol metabolism, membrane fluidity regulation, and intracellular signalling pathways. They are implicated in a pathophysiology of type 2 diabetes mellitus and neurodegenerative disorder as well as in malignancies. Some studies postulate that oxysterols may play a role in atherogenesis. T. Wielkoszyński et al., in their experimental study, have shown that the oxidized cholesterol

metabolites are postulated to exert atherogenic effect and thus adversely affect vascular endothelium. The authors demonstrate that oxidized cholesterol derivatives exert cytotoxic effect on vascular endothelial cells, causing endothelial dysfunction, the severity of which depends on the duration of exposure. What is more, combined administration of oxysterols and cholesterol was shown to increase their angiotoxic effect.

Despite advances in critical care treatment and increased understanding of the sepsis pathophysiology, the mortality rate of affected patients remains high, ca. 50% even in developed countries, and is mostly attributed to cardiovascular dysfunction. Endothelial dysfunction (ED) occurring with an overproduction of endothelium-derived contracting factor (EDCF) plays a key role in the pathogenesis of cardiovascular disease. Overproduction of nitric oxide and other molecules of vasodilatory action may result in uncontrolled vasodilation leading in turn to the development of hemodynamic shock. W. Han et al., in an interesting paper, found that inhibition of the mTOR pathway plays a cardioprotective role in a sepsis-induced myocardial dysfunction and that this effect may be mediated by acceleration of autophagy. The mTOR is a sensor of energetic status and induces autophagy upon energy depletion, which is a major cause of myocardial dysfunction during sepsis. Hence, the mTOR pathway seems to play an important role in myocardial dysfunction induced by sepsis. The authors found that the mTOR pathway was inhibited and rapamycin significantly alleviated cardiac dysfunction and improved myocardial anoxia in septic cardiomyopathy.

A. Stanek et al. in their study investigate the impact of whole-body cryotherapy on cardiovascular risk factors in patients with ankylosing spondylitis, which—according to the results presented—might be a useful additional method preventing development of atherosclerosis. The authors postulate that the whole-body cryotherapy with subsequent kinesiotherapy may facilitate the decrease in oxidative stress, lipid profile, atherosclerosis plaque, and its instability, as well as inflammatory parameters.

Peripheral artery disease (PAD) affects ca. 25% of population over 60 years old. Inflammation and mitochondrial dysfunction may predispose to PAD, which is associated with other highly prevalent disorders, including diabetes, dyslipidaemia, and hypertension. In a research study by A. Hernández-Aguilera, using metabolomic approach, the authors have demonstrated a relevant correlation between plasma concentrations of energy-balance-associated metabolites, oxidative stress, and inflammation in subjects with peripheral artery disease. The authors postulate that (iso)citrate and glutamate could constitute novel biomarkers for discriminating PAD patients without symptomatic disease.

In summary, the papers presented in this special issue demonstrate the recent developments in understanding the role of inflammation in the onset of cardiovascular disease. We believe that some of the presented studies will provide new evidence, which could lead to the discovery of potential biomarkers and drug targets for the development of novel therapeutic approaches for combating cardiovascular disease in the future.

Conflicts of Interest

The authors declare that there is no conflict of interest regarding the publication of this article.

Adrian Doroszko
Piotr Dobrowolski
Aneta Radziwon-Balicka
Robert Skomro

Hindawi
Mediators of Inflammation
Volume 2018, Article ID 2760272, 12 pages
https://doi.org/10.1155/2018/2760272

Research Article

Plasma Energy-Balance Metabolites Discriminate Asymptomatic Patients with Peripheral Artery Disease

Anna Hernández-Aguilera,[1] **Salvador Fernández-Arroyo**,[2] **Noemí Cabre**,[2] **Fedra Luciano-Mateo**,[2] **Gerard Baiges-Gaya**,[2] **Montserrat Fibla**,[1] **Vicente Martín-Paredero**,[3] **Javier A. Menendez**,[4,5] **Jordi Camps**,[1] **and Jorge Joven**[1,2,6]

[1]*Unitat de Recerca Biomèdica, Hospital Universitari Sant Joan, Institut d'Investigació Sanitària Pere Virgili, C. Sant Joan s/n, 43201 Reus, Spain*
[2]*Universitat Rovira i Virgili, C. Escorxador s/n, 43003 Tarragona, Spain*
[3]*Department of Vascular Surgery, Hospital Universitari Joan XXIII, C/ Dr. Mallafré Guasch 4, 43005 Tarragona, Spain*
[4]*Program Against Cancer Therapeutic Resistance (ProCURE), Metabolism and Cancer Group, Catalan Institute of Oncology, Girona, Spain*
[5]*Girona Biomedical Research Institute (IDIBGI), Girona, Spain*
[6]*The Campus of International Excellence Southern Catalonia, Tarragona, Spain*

Correspondence should be addressed to Jordi Camps; jcamps@grupsagessa.com

Received 16 March 2018; Accepted 15 July 2018; Published 20 September 2018

Academic Editor: Adrian Doroszko

Peripheral artery disease (PAD) is a common disease affecting 20–25% of population over 60 years old. Early diagnosis is difficult because symptoms only become evident in advanced stages of the disease. Inflammation, impaired metabolism, and mitochondrial dysfunction predispose to PAD, which is normally associated with other highly prevalent and related conditions, such as diabetes, dyslipidemia, and hypertension. We have measured energy-balance-associated metabolite concentrations in the plasma of PAD patients segregated by the severity of the disease and in plasma of healthy volunteers using a quantitative and targeted metabolomic approach. We found relevant associations between several metabolites (3-hydroxybutirate, aconitate, (iso)citrate, glutamate, and serine) with markers of oxidative stress and inflammation. Metabolomic profiling also revealed that (iso)citrate and glutamate are metabolites with high ability to discriminate between healthy participants and PAD patients without symptoms. Collectively, our data suggest that metabolomics provide significant information on the pathogenesis of PAD and useful biomarkers for the diagnosis and assessment of progression.

1. Introduction

The prevalence of peripheral artery disease (PAD) is now higher than 20% in population over 60 years, and affected patients have a several-fold increased risk of all-cause mortality compared to people without the disease [1]. Age, hypertension, hypercholesterolemia, diabetes, and smoking are recognized risk factors, but the disease progresses silently for decades, with the consequence that if appropriate, effective measures are applied too late, or not implemented at all, will result in atherosclerosis affecting wide portions of the arteries in the lower extremities [2]. Tissue ischemia is a common finding in PAD patients, and an increasing body of evidence supports the notion that inflammation plays an important role in the pathogenesis of this disease, linking oxidative stress, metabolic adaptation, and immunity [3–6]. Consequently, the combined action of abnormal mitochondrial function, increased production of reactive oxygen spe-

Table 1: Clinical characteristics, blood count, and biochemical characteristics of the control group and PAD patients.

	Control ($n = 48$)	PAD ($n = 201$)	p value
BMI (kg/m^2)	24 (22.5–25.3)	25 (22.5–28)	0.021
Diabetes (%)	—	64.1	<0.001
Hypertension (%)	—	69.2	<0.001
Dyslipidemia	—	37.9	<0.001
Red blood cells, $\times 10^{12}$/l	4.9 (4.4–5.2)	4.16 (3.57–4.66)	<0.001
Hemoglobin, mmol/l	8.94 (8.32–9.43)	13.30 (11.50–14.90)	0.001
Leukocytes, $\times 10^9$/l	6.8 (5.4–8.2)	8.17 (6.50–10.22)	0.003
Platelets, $\times 10^9$/l	233 (205–273)	253 (200–329)	ns
Total cholesterol, mmol/l	4.85 (4.40–5.85)	3.90 (3.31–4.94)	<0.001
HDL cholesterol, mmol/l	1.34 (1.14–1.61)	0.96 (0.78–1.19)	<0.001
LDL cholesterol, mmol/l	2.82 (2.40–3.86)	2.26 (1.77–2.79)	<0.001
Triglycerides, mmol/l	0.90 (0.70–1.38)	1.99 (1.40–3.08)	<0.001
Glucose, mmol/l	4.70 (4.37–4.92)	5.61 (4.60–6.88)	<0.001
ALT, U/l	20 (13.5–24.9)	21.5 (15–34.8)	ns
AST, U/l	20 (17.7–24)	21 (16–32)	ns

BMI: Body mass index; HDL: high-density lipoprotein; LDL: low-density lipoprotein; ALT: alanine aminotransferase; AST: aspartate aminotransferase; ns: not significant. Nonparametric variables are shown as medians, and IQR are in parentheses. Qualitative variables are expressed as percentage of total participants.

cies, impaired energy metabolism, and the subsequent inflammatory response complicates vascular remodeling, perfusion recovery, and atherosclerosis [7–10].

One of the main challenges clinicians face is early diagnosis of PAD (i.e., during the asymptomatic stages), and many biomarker candidates have been proposed with limited success [11–13]. The emerging metabolomic approaches are providing new clues in understanding atherosclerosis-related cardiovascular disease [14–20], but efforts on PAD have been scarce. Previous studies from our group suggested that serum paraoxonase-1 (PON1) and the chemokine (C-C) motif ligand 2 (CCL2) might be useful biomarkers of PAD [21, 22]: PON1 being a scavenger of excessive reactive oxygen species [23] and CCL2 an inducer of monocyte migration and differentiation into macrophages [24]. As mitochondrial dysfunction and inflammation result in disrupted metabolism [25, 26], we report here that metabolomic profiling of plasma may be useful for identifying patients at increased risk of PAD and that energy-balance metabolites are associated with inflammation and oxidation in these patients. Our results might suggest new biomarkers and therapeutic targets.

2. Materials and Methods

2.1. Participants and Study Design. We performed an observational, cross-sectional study in 201 men with clinically diagnosed PAD attending our vascular surgery department between 2010 and 2015. Patients were classified according to the Fontaine classification in nonsymptomatic stage (grade I), intermittent claudication (grade II), rest pain (grade III), and tissue damage, and necrosis (grade IV) [27]. Diagnostic criteria involved ankle-brachial index (ABI), noninvasive imaging techniques (computerized tomography scan or magnetic resonance imaging), and arteriography when indicated. The exclusion criteria were the presence of acute ischemia, signs of infection, renal failure, liver disease, cancer, or autoimmune disease. Clinical data and laboratory variables were obtained from patients' clinical records. For comparisons, we used biobanked samples ($n = 48$) from healthy, age-matched men and normal ABI values, whose details have been previously described [28]. Plasma and serum samples from all participants were collected and stored at −80°C until use. Procedures were approved by the Comité d'Ètica d'Investigació Clínica of Hospital Universitari de Sant Joan (EPINOLS/12-03-09/3proj6 and INFLAMET/15-04-30/4proj6), and written informed consent was obtained from all participants.

2.2. Metabolomic Analyses. To detect and quantify metabolites of energy metabolism, we used a previously described method [6]. Briefly, metabolites from plasma (100 μl) were extracted using 400 μl of methanol/water (8 : 2, v/v) and proteins were precipitated for two hours at −20°C. After centrifugation at 14,000 rpm for 10 minutes at 4°C, the supernatant was collected and dried under N_2 flow. Metabolites were then derivatized with methoxyamine in pyridine (40 mg/ml) and N-methyl-N-(trimethylsilyl)-trifluoroacetamide and injected into a gas chromatograph coupled with a quadrupole time-of-flight mass spectrometer by an electron impact source. Metabolites were detected and quantified with the use of proper calibration curves.

2.3. Biochemical Analyses. The true physiological substrates for PON1 have not been yet identified. Since PON1 has lactonase and esterase activities [23], we opted to analyze the catalytic activity of PON1 using two different substrates: paraoxon (an ester) and 5-thiobutyl butyrolactone (TBBL; a synthetic lactone). Serum PON1 paraoxonase activity was determined as the rate of hydrolysis of paraoxon at 410 nm and 37°C in a 0.05 mM glycine buffer, pH 10.5 with 1 mM $CaCl_2$. Activities were expressed as U/l (1 U = 1 μmol of paraoxon hydrolyzed per minute). Serum PON1 lactonase activity was measured in an assay containing 1 mM $CaCl_2$,

Metabolite	Control (μM)	PAD (μM)	PAD-to-control ratio	ρ-value
3-Hydroxybutirate	0.12 (0.11–0.13)	0.22 (0.14–0.40)	1.83	<0.001
Aconitate	0.47 (0.39–0.63)	4.42 (2.45–6.26)	9.40	<0.001
α-Ketoglutarate	2.91 (2.15–3.97)	4.67 (2.85–7.07)	1.60	<0.001
Alanine	199.95 (163.83–252.32)	208.71 (147.51–274.36)	1.04	ns
Aspartate	132.46 (114.27–147.78)	181.61 (142.32–229.68)	1.37	<0.001
(Iso)citrate	267.20 (200.34–329.55)	687.82 (561.31–921.93)	2.57	<0.001
Fumarate	0.31 (0.23–0.41)	0.25 (0.19–0.39)	−1.24	0.032
Glucose	4718.45 (4407.71–5073.74)	4878.41 (4312.48–5658.30)	1.03	ns
Glutamate	168.57 (106.17–258.28)	1417.56 (711.82–2669–54)	8.41	<0.001
Glutamine	1705.99 (990.44–2736.23)	5073.46 (2616.13–9189.28)	2.97	<0.001
Isoleucine	48.28 (40.66–55.59)	61.55 (52.22–73.56)	1.27	<0.001
Lactate	399.68 (348.17–429.08)	358.59 (305.02–440.07)	−1.11	ns
Leucine	71.25 (62.95–80.77)	88.41 (71.57–107.83)	1.24	<0.001
Malate	1.43 (1.15–1.77)	2.51 (1.90–3.88)	1.76	<0.001
Pyruvate	9.12 (6.47–13.49)	13.49 (3.79–23.04)	1.48	ns
Serine	103.49 (93.41–112.86)	135.86 (105.32–167.17)	1.31	<0.001
Succinate	10.52 (10.25–11.09)	9.40 (8.44–15.07)	−1.12	0.021
Succinyl-CoA	7.27 (5.27–9.76)	10.45 (7.58–15.54)	1.44	<0.001
Valine	92.81 (82.87–104.55)	105.44 (83.91–135.10)	1.14	0.004

(a)

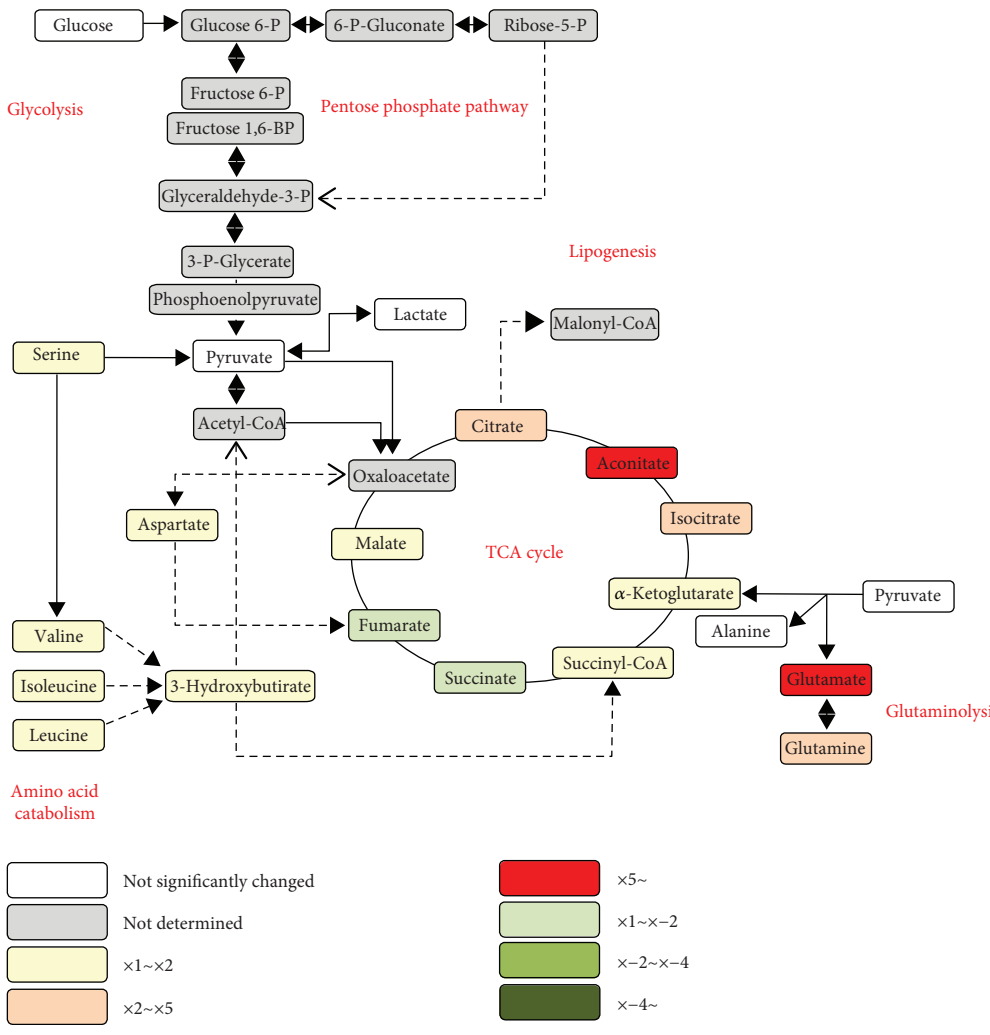

(b)

Figure 1

Table 2: Spearman's correlation coefficients for PON1 concentration, PON1 paraoxonase activity, PON1 lactonase activity, CCL2 concentration, and related metabolites.

	PON1 concentration		Paraoxonase activity		Lactonase activity		CCL2 concentration	
	Spearman's rho	p value	Spearman's rho	p value	Spearman's rho	p value	Spearman's rho	p value
3-hydroxybutirate	−0.640	<0.001	−0.309	<0.001	−0.496	<0.001	0.241	0.009
α-Ketoglutarate	−0.021	ns	−0.183	0.029	−0.029	ns	−0.045	ns
Aconitate	−0.641	<0.001	−0.394	<0.001	−0.552	<0.001	0.345	<0.001
Alanine	0.153	ns	0.253	0.002	0.275	0.001	−0.155	ns
Aspartate	−0.241	0.004	−0.187	0.026	−0.349	<0.001	0.184	0.046
(Iso)citrate	−0.592	<0.001	−0.166	0.048	−0.381	<0.001	0.303	0.001
Fumarate	0.295	<0.001	−0.053	ns	0.166	0.048	−0.014	ns
Glucose	0.011	ns	0.109	ns	0.053	ns	−0.098	ns
Glutamate	−0.590	<0.001	−0.425	<0.001	−0.589	<0.001	.0171	ns
Glutamine	−0.263	0.002	−0.059	ns	−0.198	0.018	0.187	0.043
Isoleucine	−0.342	<0.001	−0.101	ns	−0.299	<0.001	0.167	ns
Lactate	0.277	0.001	0.086	ns	0.175	0.036	−0.104	ns
Leucine	−0.229	0.006	0.008	ns	−0.136	ns	0.079	ns
Malate	−0.356	<0.001	−0.240	0.004	−0.279	0.001	0.225	0.014
Pyruvate	0.356	<0.001	−0.034	ns	0.158	ns	−0.163	ns
Serine	−0.595	<0.001	−0.294	<0.001	−0.534	<0.001	0.295	0.001
Succinate	−0.355	<0.001	−0.194	0.021	−0.342	<0.001	0.110	ns
Succinyl-CoA	−0.223	0.008	−0.101	ns	−0.154	ns	0.025	ns
Valine	−0.035	ns	0.155	ns	0.076	ns	−0.009	ns

PON1: Paraoxonase 1; CCL2: chemokine (C-C) motif ligand 2; ns: not significant.

0.25 mM 5-thiobutyl butyrolactone, and 0.5 mM 5,5′-dithiobis-2-nitrobenzoic acid (DTNB) in 0.05 mM Tris-HCl buffer, pH = 8.0. The change in absorbance was monitored at 412 nm. Activities were expressed as U/l (1 U = 1 mmol of TBBL hydrolyzed per minute) [29]. Serum PON1 concentrations were determined by an in-house enzyme-linked immunosorbent assay (ELISA) with a rabbit polyclonal antibody generated against the synthetic peptide CRNHQSSYQTRLNALREVQ which is sequence specific for mature PON1 [30]. CCL2 metabolites were measured by ELISA (PeproTech, London, UK). Serum lipid, liver profiles, and glucose concentrations were analyzed by standard tests in a Roche Modular Analytics P800 system. Blood count was analyzed in a Roche Sysmex XT-1800i counter (Roche Diagnostics, Basel, Switzerland).

2.4. Statistical Analysis. Differences between groups were assessed by Student's t-test (parametric) or Mann–Whitney U test (nonparametric). Correlations between variables were assessed by Spearman's rho test. The relative magnitude of observed changes was evaluated using random forest analysis [31]. Receiver operating characteristic (ROC) curves were used to assess the diagnostic accuracy of the measured variables. This analysis represents plots of all the sensitivity/specificity pairs resulting from varying decision thresholds. Sensitivity (or true-positive rate) is the proportion of the sample correctly identified as having a specific disease. Specificity (or true-negative rate) is the proportion of the subjects correctly identified as not having a specific disease. False-positive rate is calculated as 1 − specificity. The area under the curve (AUC) and 95% confidence interval (CI) were calculated. The AUC represents the ability of the test to correctly classify patients according to the investigated alteration. The values of AUC can range between 1 (perfect test) and 0.5 (worthless test) [32]. Statistical analyses were performed with SPSS 22.0 (IBM Corp., Chicago, IL, USA). MetaboAnalyst 3.0 (http://www.metaboanalyst.ca/) was used to generate scores/loading plots and random forest analyses.

3. Results

3.1. Participants' Characteristics. Clinical characteristics and biochemical variables of PAD patients and the control group are shown in Table 1. PAD patients had a mildly higher BMI than those in the control group, and they often had diabetes, hypertension, or dyslipidemia. Serum glucose and triglyceride concentrations were higher in patients, while cholesterol was lower, which is probably the result of medication.

3.2. Alterations in Energy-Balance-Associated Metabolites. The plasma concentrations of most energy metabolism intermediates were significantly higher in PAD patients than those in the control group, with the exceptions of fumarate, lactate, and succinate, that were decreased (Figure 1(a)). Glutaminolysis was disrupted in PAD, as shown by glutamate and glutamine increases. Moreover, reactions involving amino acid metabolism seemed to be inhibited in PAD, as serine, valine, isoleucine, and leucine concentrations were increased. TCA cycle was strongly disturbed since

Table 3: Metabolite concentration in patients segregated according to the presence of diabetes.

Metabolite	Diabetes	
	No	Yes
3-hydroxybutirate	0.27 (0.13–0.39)	0.27 (0.14–0.40)
Aconitate	3.75 (2.38–6.50)	4.60 (2.67–6.28)
α-Ketoglutarate	4.24 (2.56–7.22)	4.13 (2.76–6.50)
Alanine	210.6 (147.5–266.3)	189.6 (139.0–271.4)
Aspartate	172.5 (133.3–215.8)	179.7 (143.0–225.1)
(Iso)citrate	721.7 (584.42–867.3)	665.6 (538.0–880.5)
Fumarate	0.26 (0.19–0.41)	0.24 (0.18–0.37)
Glucose	4546.0 (4104.0–5115.5)	4959.3 (4040.8–5804.9)[a]
Glutamate	1457.2 (743.0–2912.4)	1416.9 (671.7–2684.2)
Glutamine	5073.4 (3054.2–7754.5)	4742.5 (1842.3–8881.2)
Isoleucine	57.14 (47.71–63.99)	63.68 (52.83–75.20)[a]
Lactate	367.2 (283.9–423.6)	341.0 (297.1–441.6)
Leucine	85.07 (70.62–94.86)	86.68 (69.33–109.65)
Malate	2.38 (1.85–4.31)	2.45 (1.88–3.56)
Pyruvate	12.47 (3.64–22.87)	12.83 (3.55–21.89)
Serine	147.5 (101.7–167.4)	137.6 (109.4–169.5)
Succinate	9.57 (8.35–15.11)	9.70 (8.47–15.23)
Succinyl-CoA	10.14 (7.74–15.12)	10.46 (7.37–17.62)
Valine	102.0 (83.0–129.4)	104.1 (80.7–138.9)

[a]$p < 0.01$.

Table 4: Metabolite concentrations in patients segregated according to the presence of hypertension.

Metabolite	Hypertension	
	No	Yes
3-hydroxybutirate	0.21 (0.14–0.38)	0.35 (0.14–0.42)
Aconitate	4.59 (2.54–6.65)	4.13 (2.60–6.60)
α-Ketoglutarate	4.71 (2.81–6.67)	3.70 (2.51–7.07)
Alanine	213.5 (152.7–273.7)	184.3 (137.3–255.1)
Aspartate	181.6 (141.4–239.5)	173.1 (137.3–200.4)
(Iso)citrate	721.8 (566.6–934.0)	654.2 (476.5–815.9)
Fumarate	0.27 (0.19–0.40)	0.22 (0.17–0.30)[a]
Glucose	4955.9 (4459.1–5679.9)	4418.1 (4134.8–5191.7)[b]
Glutamate	1335.8 (725.0–2628.5)	1786.6 (691.1–2891.7)
Glutamine	5083.3 (2842.0–9072.2)	4742.5 (1700.9–7003.8)
Isoleucine	63.52 (52.24–75.19)	57.88 (51.23–63.22)[a]
Lactate	373.5 (308.3–452.5)	332.3 (279.5–405.9)[a]
Leucine	90.17 (71.33–109.35)	84.54 (69.77–93.84)
Malate	2.79 (1.96–4.09)	2.23 (1.75–3.08)[a]
Pyruvate	13.86 (3.85–24.11)	8.78 (2.72–18.15)[a]
Serine	135.3 (106.1–162.1)	161.0 (103.6–172.0)[a]
Succinate	9.15 (8.42–15.04)	11.71 (8.49–15.47)
Succinyl-CoA	11.21 (7.72–16.31)	9.94 (7.52–14.25)
Valine	107.3 (86.6–136.8)	96.6 (78.8–134.8)

[a]$p < 0.05$; [b]$p < 0.01$.

Table 5: Metabolite concentrations in patients segregated according to the presence of dyslipidemia.

Metabolite	Dyslipidemia	
	No	Yes
3-hydroxybutirate	0.31 (0.16–0.40)	0.19 (0.13–0.419)
Aconitate	4.64 (2.91–6.61)	4.22 (2.36–6.16)
α-Ketoglutarate	3.99 (2.44–6.55)	5.05 (3.05-6.90)
Alanine	180.5 (125.1–247.5)	233.6 (171.4–302.8)[b]
Aspartate	168.6 (134.1–205.4)	191.7 (148.8–253.2)[a]
(Iso)citrate	678.6 (545.4–864.5)	712.3 (566.1–959.1)
Fumarate	0.23 (0.18–0.36)	0.27 (0.19–0.40)
Glucose	4663.9 (4172.3–5417.5)	4925.3 (4503.6–5684.9)[a]
Glutamate	1556.2 (679.8–2785.7)	1342.5 (763.7–2372.1)
Glutamine	4742.5 (2007.9–7169.0)	5073.4 (2219.3–10427.7)
Isoleucine	57.90 (49.81–68.46)	65.02 (55.35–77.95)[b]
Lactate	334.7 (274.2–435.6)	393.3 (323.2–457.6)[b]
Leucine	83.96 (66.70–98.71)	92.19 (76.10–109.92)[a]
Malate	2.37 (1.83–3.66)	2.87 (2.12–3.80)
Pyruvate	9.50 (3.08–21.00)	13.58 (6.00–25.78)
Serine	150.0 (104.9–170.3)	131.9 (106.0–18.8)
Succinate	10.82 (8.44–15.23)	9.11 (8.46–15.15)
Succinyl-CoA	9.79 (6.71–14.00)	13.36 (8.90–18.47)[b]
Valine	99.3 (78.6–125.5)	113.3 (89.6–139.4)[b]

[a]$p < 0.05$; [b]$p < 0.01$.

(iso)citrate, aconitate, α-ketoglutarate, succinyl-CoA, and malate concentrations were increased, and fumarate and succinate concentrations were decreased in PAD (Figure 1(b)).

3.3. Relationships between Energy-Balance-Associated Metabolites, PON1 and CCL2. We observed significant inverse correlations between metabolites and PON1-related variables and direct correlations between metabolites and CCL2. The strongest correlations were observed between serum PON1 concentration and PON1 lactonase activity with 3-hydroxybutirate, aconitate, (iso)citrate, glutamate, and serine (Table 2).

3.4. Metabolites Are Linked to PAD Comorbidities, Age, and BMI. Univariate analyses confirmed that many metabolites were associated with diabetes, hypertension, or dyslipidemia (Tables 3–5), while multivariate analyses (principal component analyses) revealed that the combination of these metabolites was not able to separate groups regarding hypertension (Figure 2(a)) and dyslipidemia (Figure 2(b)). Random forest analysis showed that glucose and isoleucine were associated with diabetes in PAD patients and glucose (as expected) had the highest discriminant capacity (Figure 2(c)). Hyperlipidemic and normolipemic patients showed significant differences in alanine, aspartate, glucose, isoleucine, lactate, leucine, succinyl-CoA, and valine concentrations and, among them, isoleucine had the highest discriminant capacity (Figure 2(d)). Fumarate, glucose, isoleucine, lactate, malate, serine, and pyruvate were associated with hypertension in

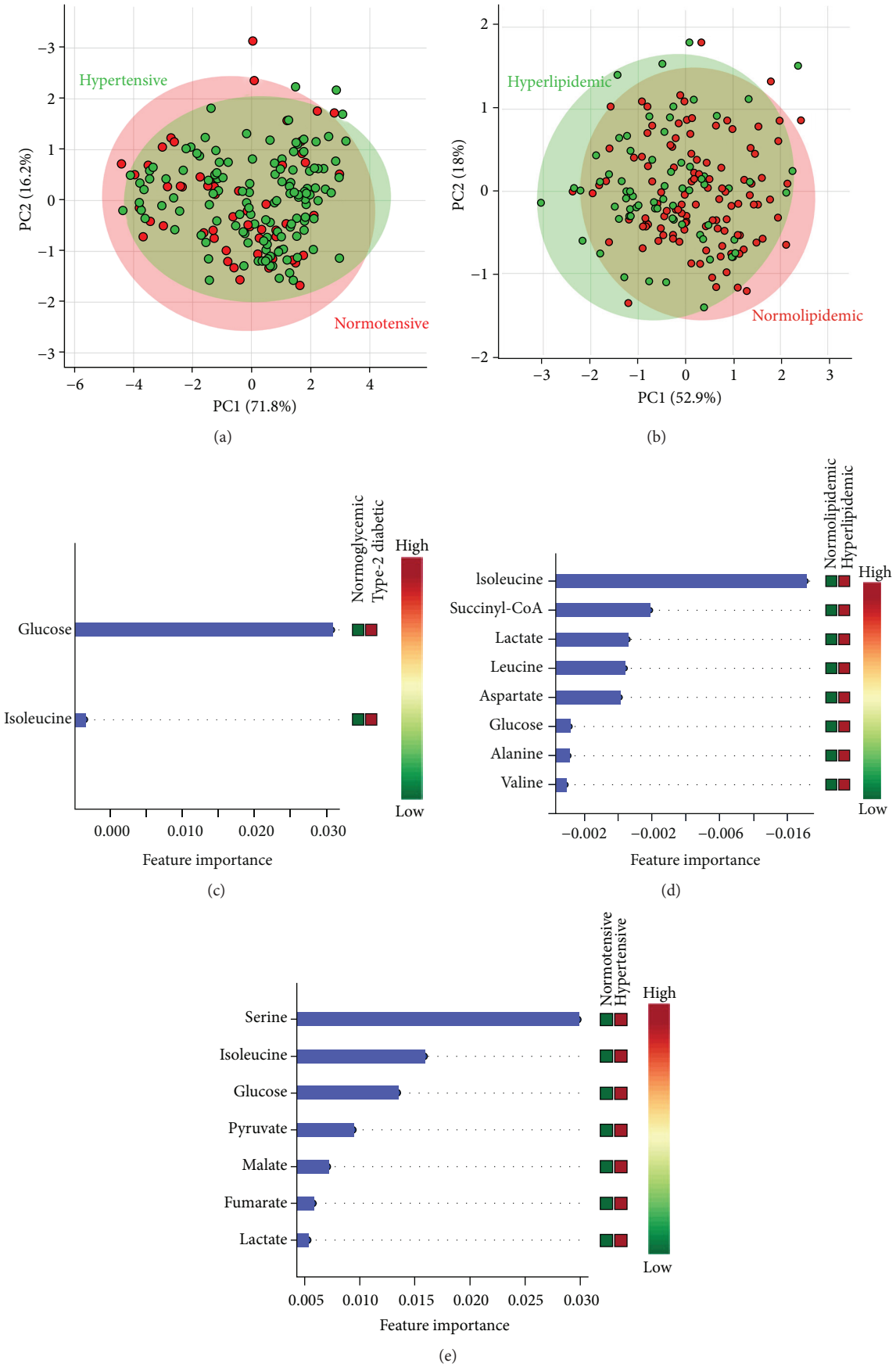
Hypertensive
Normotensive
PC2 (16.2%)
PC1 (71.8%)
(a)
Hyperlipidemic
Normolipidemic
PC2 (18%)
PC1 (52.9%)
(b)
Normoglycemic
Type-2 diabetic
High
Low
Glucose
Isoleucine
0.000
0.010
0.020
0.030
Feature importance
(c)
Normolipidemic
Hyperlipidemic
High
Low
Isoleucine
Succinyl-CoA
Lactate
Leucine
Aspartate
Glucose
Alanine
Valine
−0.002
−0.002
−0.006
−0.016
Feature importance
(d)
Normotensive
Hypertensive
High
Low
Serine
Isoleucine
Glucose
Pyruvate
Malate
Fumarate
Lactate
0.005
0.010
0.015
0.020
0.025
0.030
Feature importance
(e)

Figure 2

Table 6: Spearman's correlation coefficients for age, body mass index, and related metabolites.

	Age		BMI	
	Spearman's rho	p value	Spearman's rho	p value
3-Hydroxybutirate	0.057	ns	0.022	ns
Aconitate	0.205	0.003	−0.236	0.010
α-Ketoglutarate	0.054	ns	−0.031	ns
Alanine	−0.081	ns	0.230	0.013
Aspartate	0.083	ns	0.256	0.005
(Iso)citrate	0.113	ns	0.147	ns
Fumarate	0.220	0.002	−0.085	ns
Glucose	−0.031	ns	0.202	0.029
Glutamate	0.063	ns	−0.032	ns
Glutamine	0.007	ns	0.157	ns
Isoleucine	0.124	ns	0.194	0.036
Lactate	−0.023	ns	0.034	ns
Leucine	−0.005	ns	0.220	0.017
Malate	0.248	<0.001	−0.079	ns
Pyruvate	−0.009	ns	0.103	ns
Serine	0.062	ns	−0.112	ns
Succinate	0.011	ns	−0.145	ns
Succinyl-CoA	0.038	ns	0.134	ns
Valine	−0.122	ns	0.241	0.009

BMI: Body mass index; ns: not significant.

PAD patients, and serine was the metabolite with the best discriminant capacity (Figure 2(e)). Aconitate, fumarate, and malate were associated with age, and aconitate, alanine, aspartate, glucose, isoleucine, leucine, and valine were correlated with BMI (Table 6 and Figure 3). All these metabolites were excluded for further analysis as candidates for PAD biomarker in order to avoid the influence of confounding factors.

3.5. Metabolic Biomarkers of PAD. Metabolites included in further analysis were (iso)citrate, glutamate, succinate, 3-hydroxybutirate, α-ketoglutarate, and glutamine. From them, (iso)citrate and glutamate were those showing the greatest differences between patients and controls and between the different patient groups according to the Fontaine scale (Figure 4). To evaluate the capacity of these metabolites to discriminate between groups, we performed random forest analyses and ROC curves confirming that (iso)citrate and glutamate were the most powerful metabolites to separate the healthy individuals from PAD patients (Figures 5(a) and 5(b)), and the healthy individuals from asymptomatic or nearly asymptomatic patients (grades I and II), with AUC > 0.95 (Figures 5(c) and 5(d)). They were also useful to discriminate between the different subgroups of patients (Figure 5(e)).

4. Discussion

Energy-balance-associated metabolites are related to oxidative stress and inflammation. We found in PAD patients significant alterations in energy metabolism, particularly evident through the citrate-aconitate-(iso)citrate conversions. The mitochondrial enzymes involved in these reactions are (iso)citrate dehydrogenase (IDH2) and aconitase 2 (ACO2). Both enzymes are crucial for normal mitochondrial function [33]. In mice, decreased IDH2 expression contributes to atherosclerosis progression by increasing oxidative stress [34]. An oxidative environment inactivates aconitase, which in turn undergoes age-dependent oxidative modification. Whether IDH2 and ACO2 may be the cause or consequence of mitochondrial dysfunction in PAD requires further studies [8].

Mitochondrial dysfunction, oxidative stress, and inflammation are closely related [24, 25]. The present study shows the existence of significant inverse correlations between various metabolites and PON1-related variables and direct correlations with CCL2. These correlations are stronger for PON1 concentration and lactonase activity. This may be due to the observation that PON1 is located (among other cellular organelles) in the membranes of the mitochondria, protecting them from oxidative stress [25]. Therefore, alterations in the TCA cycle may directly affect PON1. The correlations between metabolites and paraoxonase activity are weaker than those found for lactonase activity, but this is probably due to the differential impact of genetic polymorphisms [23]. Metabolites showing the strongest and more consistent correlations with PON1 and CCl2 were 3-hydroxybutirate, aconitate, (iso)citrate, glutamate, and serine. 3-Hydroxybutirate is a ketone body, and studies on the effects of ketones on oxidative stress and inflammation are contradictory. For example, it has been reported that these

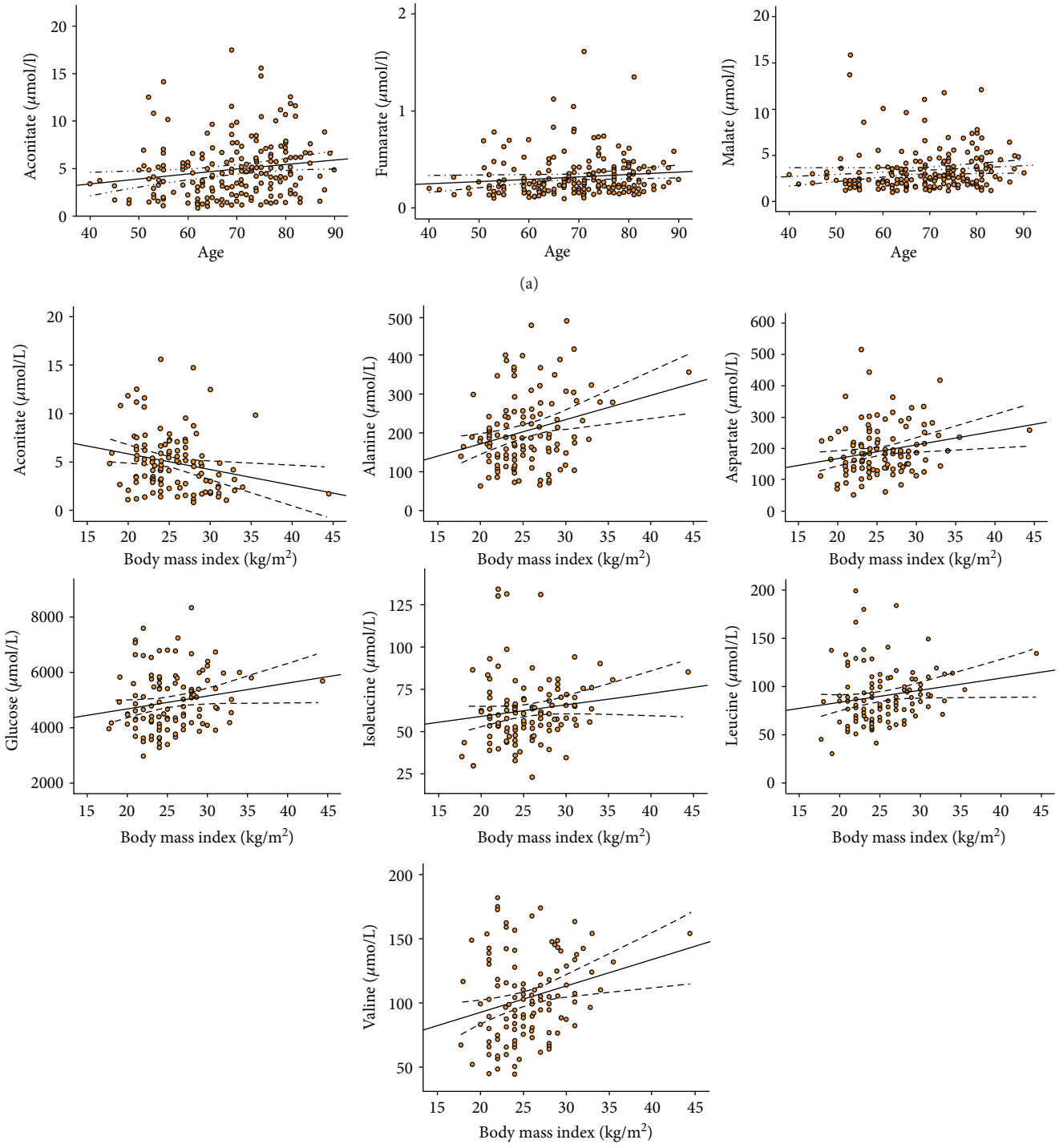

Figure 3

compounds inhibit mitochondrial production of reactive oxygen species in rat and mice neurons [35–37] while they activate NF-κB, upregulate NADPH oxidase, elevate oxidative stress, and induce the expression of proinflammatory cytokines in endothelial cells and hepatocytes [38, 39]. Our results are in agreement with this latter possibility. It has been suggested that these contradictory findings reflect tissue-specific differences because the source of reactive oxygen species in neurons differ from that in nonneuronal cells [35]. Aconitate is the precursor of itaconate, and this metabolite regulates metabolic remodeling and mitochondrial respiration in inflammatory macrophages [40]. There

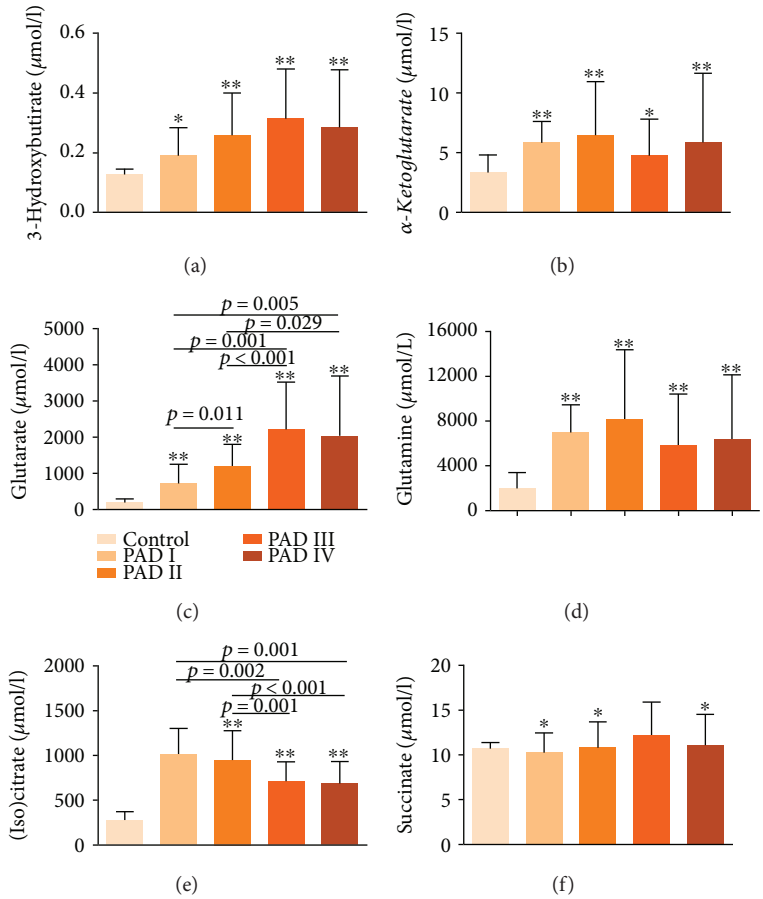

Figure 4: $^{*}p < 0.05$ and $^{**}p < 0.001$ for the control samples.

is little information on the associations of (iso)citrate, glutamate, and serine with oxidative stress and inflammation, but studies suggest that glutamate is pro-oxidant and pro-inflammatory [41] while (iso)citrate and serine may elicit the opposite effect [42, 43].

Energy-balance-associated metabolites might be considered as PAD biomarkers. Early diagnosis is important in these patients because preventive treatment has potential benefits in the progression of PAD. Current biomarkers are indeed risk factors [11, 13], and dyslipidemia, hypertension, or diabetes plays independent roles in atherogenesis. In our population, approximately 80% of patients had one or more of these complications. Their effect on metabolite concentrations is unknown but probably multifactorial. For instance, branched-chain amino acids (BCAA) were influenced by hypertension, diabetes, and dyslipidemia confirming previous associations [44–47]. We therefore discarded metabolites influenced by confounding variables, and we found six candidates with statistically significant differences in concentration between the control group and PAD patients: 3-hydroxybutyrate, α-ketoglutarate, glutamate, glutamine, (iso)citrate, and succinate. These candidates were useful to distinguish between PAD patients and the control group and also to discriminate between different clinical stages. The conversion of (iso)citrate to α-ketoglutarate is mediated by IDH2, and increased concentrations of this metabolite have been associated with a worse cardiovascular prognosis [48]. Interestingly, glutamate, another metabolite with a good discriminant capacity, is the substrate for many enzymes located in the mitochondria [49] and plays an important role in the mechanical function of the ischemic myocardium [50]. Understanding glutamate overproduction in the blood of patients with atherosclerosis requires further research. Our more interesting finding indicates that (iso)citrate and glutamate may discriminate healthy participants from PAD patients in the asymptomatic or early symptomatic stages (Fontaine grades I and II). Simple measurements may then provide clinical tools to assess patients at risk but without symptoms. Larger studies using sensitive metabolomic techniques are warranted to confirm these findings and to identify specific metabolic pathways associated with increased risk of PAD.

5. Conclusion

Our metabolomic approach supports a relevant association of plasma concentrations of energy-balance-associated metabolites with oxidative stress and inflammation and reveals (iso)citrate and glutamate as candidate biomarkers for discriminating PAD patients without symptomatic disease.

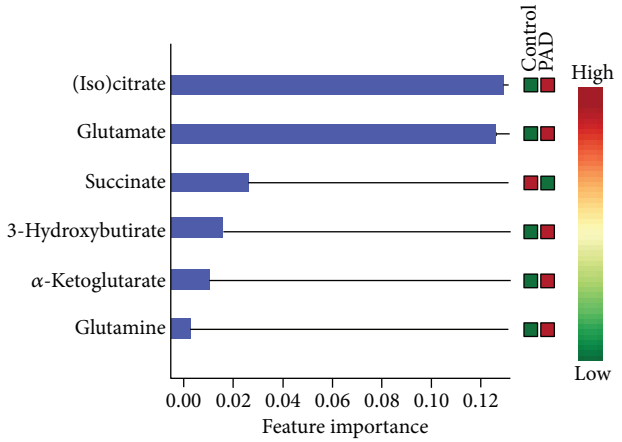

(a)

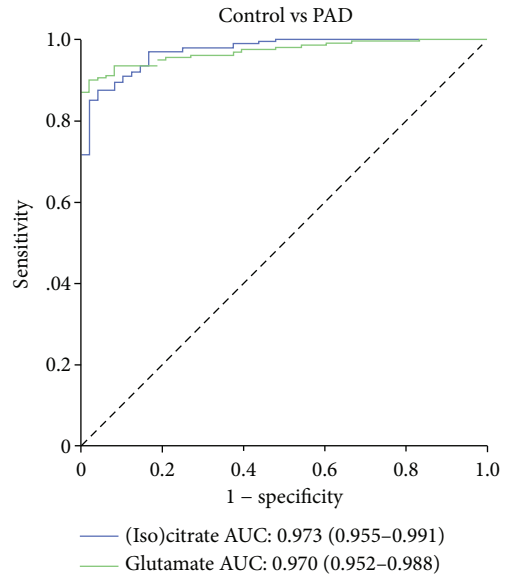

(b)

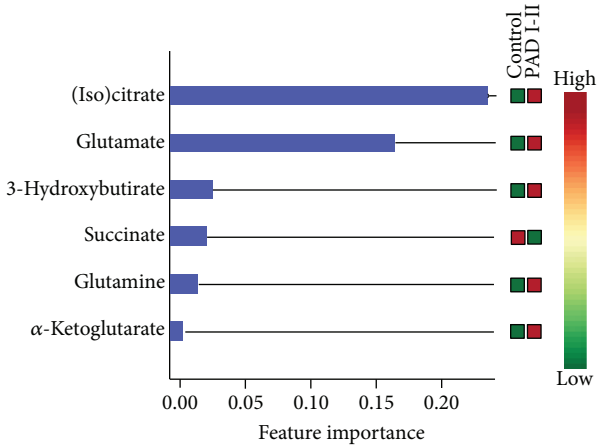

(c)

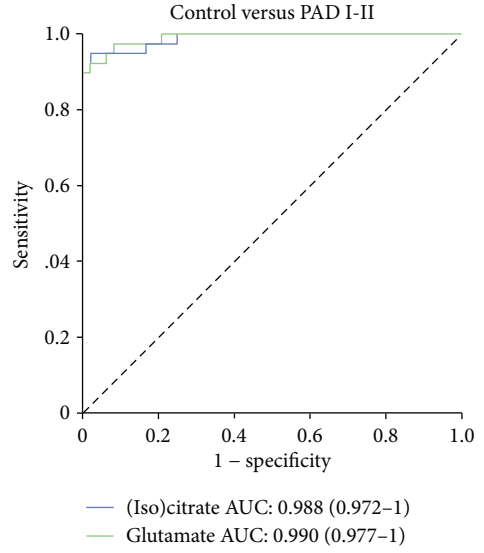

(d)

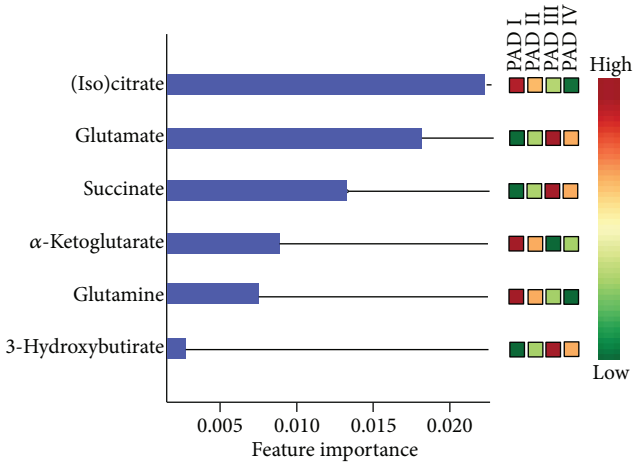

(e)

Figure 5

Data Availability

The data used to support the findings of this study are available from the corresponding author upon request.

Conflicts of Interest

The authors declare that they have no conflicts of interest.

Authors' Contributions

Anna Hernández-Aguilera and Salvador Fernández-Arroyo contributed equally to this work.

Acknowledgments

This work was supported by grants from the Plan Nacional de I+D+I, Spain, Instituto de Salud Carlos III (Grant no. PI15/00285, co-founded by the European Regional Development Fund (EU FEDER)) to Jorge Joven and the Ministerio de Ciencia e Innovación (Grant no. SAF2012–38914) to Javier A. Menendez. The authors also acknowledge the support by the Agència de Gestió d'Ajuts Universitaris i de Recerca (AGAUR) (Grant nos. 2014 SGR1227 and 2014 SGR229) and the Fundació La Marató de TV3.

References

[1] F. G. R. Fowkes, D. Rudan, I. Rudan et al., "Comparison of global estimates of prevalence and risk factors for peripheral artery disease in 2000 and 2010: a systematic review and analysis," *Lancet*, vol. 382, no. 9901, pp. 1329–1340, 2013.

[2] M. H. Criqui, "Peripheral arterial disease - epidemiological aspects," *Vascular Medicine*, vol. 6, Supplement 1, pp. 3–7, 2017.

[3] K. E. Wellen and G. S. Hotamisligil, "Inflammation, stress, and diabetes," *The Journal of Clinical Investigation*, vol. 115, no. 5, pp. 1111–1119, 2005.

[4] G. S. Hotamisligil, "Inflammation and metabolic disorders," *Nature*, vol. 444, no. 7121, pp. 860–867, 2006.

[5] C. Bernal-Mizrachi, A. C. Gates, S. Weng et al., "Vascular respiratory uncoupling increases blood pressure and atherosclerosis," *Nature*, vol. 435, no. 7041, pp. 502–506, 2005.

[6] M. Riera-Borrull, E. Rodríguez-Gallego, A. Hernández-Aguilera et al., "Exploring the process of energy generation in pathophysiology by targeted metabolomics: performance of a simple and quantitative method," *Journal of the American Society for Mass Spectrometry*, vol. 27, no. 1, pp. 168–177, 2016.

[7] P. Bénit, E. Letouzé, M. Rak et al., "Unsuspected task for an old team: succinate, fumarate and other Krebs cycle acids in metabolic remodeling," *Biochimica et Biophysica Acta (BBA) - Bioenergetics*, vol. 1837, no. 8, pp. 1330–1337, 2014.

[8] M. Calderón-Santiago, F. Priego-Capote, J. G. Galache-Osuna, and M. D. Luque de Castro, "Method based on GC-MS to study the influence of tricarboxylic acid cycle metabolites on cardiovascular risk factors," *Journal of Pharmaceutical and Biomedical Analysis*, vol. 74, pp. 178–185, 2013.

[9] K. I. Makris, A. A. Nella, Z. Zhu et al., "Mitochondriopathy of peripheral arterial disease," *Vascular*, vol. 15, no. 6, pp. 336–343, 2007.

[10] G. J. Kemp, "Mitochondrial dysfunction in chronic ischemia and peripheral vascular disease," *Mitochondrion*, vol. 4, no. 5-6, pp. 629–640, 2004.

[11] S. Hazarika and B. H. Annex, "Biomarkers and genetics in peripheral artery disease," *Clinical Chemistry*, vol. 63, no. 1, pp. 236–244, 2016.

[12] E. S. H. Kim, K. Wattanakit, and H. L. Gornik, "Using the ankle-brachial index to diagnose peripheral artery disease and assess cardiovascular risk," *Cleveland Clinic Journal of Medicine*, vol. 79, no. 9, pp. 651–661, 2012.

[13] R. K. Upadhyay, "Emerging risk biomarkers in cardiovascular diseases and disorders," *Journal of Lipids*, vol. 2015, Article ID 971453, 50 pages, 2015.

[14] J. R. Ussher, S. Elmariah, R. E. Gerszten, and J. R. B. Dyck, "The emerging role of metabolomics in the diagnosis and prognosis of cardiovascular disease," *Journal of the American College of Cardiology*, vol. 68, no. 25, pp. 2850–2870, 2016.

[15] R. Laaksonen, "Identifying new risk markers and potential targets for coronary artery disease: the value of the lipidome and metabolome," *Cardiovascular Drugs and Therapy*, vol. 30, no. 1, pp. 19–32, 2016.

[16] G. D. Lewis, A. Asnani, and R. E. Gerszten, "Application of metabolomics to cardiovascular biomarker and pathway discovery," *Journal of the American College of Cardiology*, vol. 52, no. 2, pp. 117–123, 2008.

[17] J. B. German, B. D. Hammock, and S. M. Watkins, "Metabolomics: building on a century of biochemistry to guide human health," *Metabolomics*, vol. 1, no. 1, pp. 3–9, 2005.

[18] H. Matthews, J. Hanison, and N. Nirmalan, ""Omics"-informed drug and biomarker discovery: opportunities, challenges and future perspectives," *Proteomes*, vol. 4, no. 3, 2016.

[19] C. K. Ward-Caviness, T. Xu, T. Aspelund et al., "Improvement of myocardial infarction risk prediction via inflammation-associated metabolite biomarkers," *Heart*, vol. 103, no. 16, pp. 1278–1285, 2017.

[20] S. E. Ali, M. A. Farag, P. Holvoet, R. S. Hanafi, and M. Z. Gad, "A comparative metabolomics approach reveals early biomarkers for metabolic response to acute myocardial infarction," *Scientific Reports*, vol. 6, no. 1, article 36359, 2016.

[21] A. Rull, R. Garcia, L. Fernandez-Sender et al., "The role of combined assessment of defense against oxidative stress and inflammation in the evaluation of peripheral arterial disease," *Current Molecular Medicine*, vol. 11, no. 6, pp. 453–464, 2011.

[22] A. Hernández-Aguilera, J. Sepúlveda, E. Rodríguez-Gallego et al., "Immunohistochemical analysis of paraoxonases and chemokines in arteries of patients with peripheral artery disease," *International Journal of Molecular Sciences*, vol. 16, no. 12, pp. 11323–11338, 2015.

[23] J. Camps, J. Marsillach, and J. Joven, "The paraoxonases: role in human diseases and methodological difficulties in measurement," *Critical Reviews in Clinical Laboratory Sciences*, vol. 46, no. 2, pp. 83–106, 2009.

[24] J. Camps, E. Rodríguez-Gallego, A. García-Heredia et al., "Paraoxonases and chemokine (C-C motif) ligand-2 in non-communicable diseases," *Advances in Clinical Chemistry*, vol. 63, pp. 247–308, 2014.

[25] J. Camps, A. García-Heredia, A. Hernández-Aguilera, and J. Joven, "Paraoxonases, mitochondrial dysfunction and non-communicable diseases," *Chemico-Biological Interactions*, vol. 259, Part B, pp. 382–387, 2016.

[26] A. Hernández-Aguilera, A. Rull, E. Rodríguez-Gallego et al., "Mitochondrial dysfunction: a basic mechanism in inflammation-related non-communicable diseases and therapeutic opportunities," *Mediators of Inflammation*, vol. 2013, Article ID 135698, 13 pages, 2013.

[27] S. Novo, "Classification, epidemiology, risk factors, and natural history of peripheral arterial disease," *Diabetes, Obesity & Metabolism*, vol. 4, Supplement 2, pp. S1–S6, 2002.

[28] J. Joven, E. Espinel, A. Rull et al., "Serum fatty acid synthase concentration is increased in patients with hepatitis viral infection and may assist in the prediction of liver steatosis," *Journal of Clinical Virology*, vol. 51, no. 3, pp. 199–201, 2011.

[29] J. Marsillach, G. Aragonès, R. Beltrán et al., "The measurement of the lactonase activity of paraoxonase-1 in the clinical evaluation of patients with chronic liver impairment," *Clinical Biochemistry*, vol. 42, no. 1-2, pp. 91–98, 2009.

[30] N. Martinelli, A. García-Heredia, H. Roca et al., "Paraoxonase-1 status in patients with hereditary hemochromatosis," *Journal of Lipid Research*, vol. 54, no. 5, pp. 1484–1492, 2013.

[31] M. Grootveld, "Introduction to the applications of chemometric techniques in 'omics' research: common pitfalls, misconceptions and 'rights and wrongs'," in *Metabolic Profiling: Disease and Xenobiotics*, M. Grootveld, Ed., Royal Society of Chemistry, Cambridge, 2014.

[32] M. H. Zweig and G. Campbell, "Receiver-operating characteristic (ROC) plots: a fundamental evaluation tool in clinical medicine," *Clinical Chemistry*, vol. 39, no. 4, pp. 561–577, 1993.

[33] H. J. Ku, Y. Ahn, J. H. Lee, K. M. Park, and J.-W. Park, "IDH2 deficiency promotes mitochondrial dysfunction and cardiac hypertrophy in mice," *Free Radical Biology & Medicine*, vol. 80, pp. 84–92, 2015.

[34] X. Fu, X. Huang, P. Li, W. Chen, and M. Xia, "7-Ketocholesterol inhibits isocitrate dehydrogenase 2 expression and impairs endothelial function via microRNA-144," *Free Radical Biology & Medicine*, vol. 71, pp. 1–15, 2014.

[35] M. Maalouf, P. G. Sullivan, L. Davis, D. Y. Kim, and J. M. Rho, "Ketones inhibit mitochondrial production of reactive oxygen species production following glutamate excitotoxicity by increasing NADH oxidation," *Neuroscience*, vol. 145, no. 1, pp. 256–264, 2007.

[36] J. Yin, P. Han, Z. Tang, Q. Liu, and J. Shi, "Sirtuin 3 mediates neuroprotection of ketones against ischemic stroke," *Journal of Cerebral Blood Flow and Metabolism*, vol. 35, no. 11, pp. 1783–1789, 2015.

[37] K. Marosi, S. W. Kim, K. Moehl et al., "3-Hydroxybutyrate regulates energy metabolism and induces BDNF expression in cerebral cortical neurons," *Journal of Neurochemistry*, vol. 139, no. 5, pp. 769–781, 2016.

[38] P. Kanikarla-Marie and S. K. Jain, "Hyperketonemia (acetoacetate) upregulates NADPH oxidase 4 and elevates oxidative stress, ICAM-1, and monocyte adhesivity in endothelial cells," *Cellular Physiology and Biochemistry*, vol. 35, no. 1, pp. 364–373, 2015.

[39] X. Shi, X. Li, D. Li et al., "β-Hydroxybutyrate activates the NF-κB signaling pathway to promote the expression of pro-inflammatory factors in calf hepatocytes," *Cellular Physiology and Biochemistry*, vol. 33, no. 4, pp. 920–932, 2014.

[40] V. Lampropoulou, A. Sergushichev, M. Bambouskova et al., "Itaconate links inhibition of succinate dehydrogenase with macrophage metabolic remodeling and regulation of inflammation," *Cell Metabolism*, vol. 24, no. 1, pp. 158–166, 2016.

[41] H. Parfenova, S. Basuroy, S. Bhattacharya et al., "Glutamate induces oxidative stress and apoptosis in cerebral vascular endothelial cells: contributions of HO-1 and HO-2 to cytoprotection," *American Journal of Physiology. Cell Physiology*, vol. 290, no. 5, pp. C1399–C1410, 2006.

[42] B. A. Paim, J. A. Velho, R. F. Castilho, H. C. F. Oliveira, and A. E. Vercesi, "Oxidative stress in hypercholesterolemic LDL (low-density lipoprotein) receptor knockout mice is associated with low content of mitochondrial NADP-linked substrates and is partially reversed by citrate replacement," *Free Radical Biology & Medicine*, vol. 44, no. 3, pp. 444–451, 2008.

[43] M. N. Maralani, A. Movahedian, and Javanmard ShH, "Antioxidant and cytoprotective effects of L-serine on human endothelial cells," *Research in Pharmaceutical Sciences*, vol. 7, no. 4, pp. 209–215, 2012.

[44] T. J. Wang, M. G. Larson, R. S. Vasan et al., "Metabolite profiles and the risk of developing diabetes," *Nature Medicine*, vol. 17, no. 4, pp. 448–453, 2011.

[45] J. E. Ho, M. G. Larson, A. Ghorbani et al., "Metabolomic profiles of body mass index in the Framingham heart study reveal distinct cardiometabolic phenotypes," *PLoS One*, vol. 11, no. 2, article e0148361, 2016.

[46] P. Yang, W. Hu, Z. Fu et al., "The positive association of branched-chain amino acids and metabolic dyslipidemia in Chinese Han population," *Lipids in Health and Disease*, vol. 15, no. 1, p. 120, 2016.

[47] T. Fujii, S. Yura, K. Tatsumi et al., "Branched-chain amino acid supplemented diet during maternal food restriction prevents developmental hypertension in adult rat offspring," *Journal of Developmental Origins of Health and Disease*, vol. 2, no. 3, pp. 176–183, 2011.

[48] S. Cheng, M. G. Larson, E. L. McCabe et al., "Distinct metabolomic signatures are associated with longevity in humans," *Nature Communications*, vol. 6, no. 1, p. 6791, 2015.

[49] N. C. Danbolt, "Glutamate uptake," *Progress in Neurobiology*, vol. 65, no. 1, pp. 1–105, 2001.

[50] L. M. Dinkelborg, R. K. Kinne, and M. K. Grieshaber, "Transport and metabolism of L-glutamate during oxygenation, anoxia, and reoxygenation of rat cardiac myocytes," *The American Journal of Physiology*, vol. 270, 5, Part 2, pp. H1825–H1832, 1996.

Hindawi
Mediators of Inflammation
Volume 2018, Article ID 4798209, 9 pages
https://doi.org/10.1155/2018/4798209

Research Article

Inhibition of the mTOR Pathway Exerts Cardioprotective Effects Partly through Autophagy in CLP Rats

Wen Han, Hao Wang, Longxiang Su, Yun Long, Na Cui, and Dawei Liu

Department of Critical Care Medicine, Peking Union Medical College Hospital, Peking Union Medical College and Chinese Academy of Medical Science, Beijing 100730, China

Correspondence should be addressed to Na Cui; pumchcn@163.com and Dawei Liu; pumchkycn@163.com

Received 16 January 2018; Accepted 4 June 2018; Published 28 June 2018

Academic Editor: Adrian Doroszko

Background. Sepsis-induced myocardial dysfunction is a severe clinical problem. Recent studies have indicated that autophagy and myocardial energy depletion play a major role in myocardial dysfunction during sepsis, a mechanistic target of rapamycin (mTOR) as a master sensor of energy status and autophagy mediator; however, there are little data describing its role during sepsis in the heart. *Methods.* Cecal ligation and puncture (CLP) or sham operation (SHAM) was performed in rats. After treatment, pathological changes were determined by H&E staining, cardiac functions by echocardiography, the distribution of microtubule-associated protein light chain 3 (LC-3) type II and hypoxia-inducible factor 1α (HIF-1a) by immunohistochemical staining, and autophagic vacuoles by transmission electron microscopy. Moreover, the mTOR signaling pathway and LC3II, p62, and HIF-1a expression were measured by western blotting. *Results.* Rapamycin alleviated the pathological damage of myocardial tissue, attenuated cardiac dysfunction (left ventricular ejection fraction (LVEF), $p < 0.05$; fractional shortening (FS), $p < 0.05$), and reduced HIF-1a expression ($p < 0.05$). Expectedly, rapamycin decreased the activity of the mTOR pathway in both sham-operated rats ($p < 0.0001$) and CLP rats ($p < 0.01$). Interestingly, we also found inhibition of the mTOR pathway in CLP rats compared with sham-operated rats; phosphorylation of both mTOR ($p < 0.001$) and pS6K1 ($p < 0.01$) was significantly suppressed following CLP challenge. Furthermore, autophagic processes were elevated by CLP; the ratio of LC3II/LC3I ($p < 0.05$) was increased while p62 expression ($p < 0.001$) was decreased significantly; there were also more autophagic vacuoles in CLP rats; and rapamycin could further elevate the autophagic processes compared with CLP rats (LC3II/LC3I, $p < 0.05$; P62, $p < 0.05$). *Conclusion.* Inhibition of the mTOR pathway has cardioprotective effects on myocardial dysfunction during sepsis induced by CLP, which is partly mediated through autophagy.

1. Introduction

Sepsis as a systemic response to infection is a leading cause of morbidity and mortality worldwide. Despite advances in critical care treatment and increased understanding of the sepsis pathophysiology, the mortality rate of affected patients remains high (40%–60%), even in developed countries [1]. High mortality in septic patients is associated with cardiac dysfunction. When people suffer from severe heart failure, their mortality rate increases by 50% [2]. To develop more effective therapies for septic myocardial dysfunction, it is necessary to explore the mechanisms of cardiac dysfunction induced by sepsis.

Autophagy refers to any cellular degradative pathway that involves delivery of cytoplasmic cargo to the lysosome [3]. LC3-II and p62 are two major proteins in autophagy. LC3II functions at an early stage of phagophore expansion, while p62/SQSMT1 has an adaptor function to recognize ubiquitinated proteins that need to be removed from the cytoplasm during autophagy; its amount is generally considered to inversely correlate with autophagic activity [4–6]. In the basal state, autophagy is an important process in the heart, and a defect in this process can be detrimental [7]. It also plays an important role in the modulation of ischemia-reperfusion (I/R) injury. Evidence suggests that autophagy protects against I/R injury, and impaired autophagy

contributes to higher morbidity and mortality [8]. Recent studies have found that autophagy also plays an important role in septic myocardial depression. Accumulating evidence has shown that autophagic activity in cardiomyocytes changes during sepsis, but the results are unclear [9, 10].

Mammalian target of rapamycin (mTOR) is a master sensor of energy status and promotes autophagy when there is energy depletion [11]. Myocardial energy depletion plays a major role in myocardial dysfunction during sepsis [12, 13]. However, to the best of our knowledge, there is little data describing the role of the mTOR pathway during sepsis in the heart [10, 14]. Furthermore, the relationship between autophagy and the mTOR pathway in cardiac dysfunction caused by sepsis is still unknown, which was investigated in this study.

2. Methods

2.1. Animal Model. Healthy male Wistar rats, weighing 250 ± 10 g, were obtained from the Animal Facility Center, PUMCH. All animals were housed in a pathogen-free facility and treated according to protocols approved by the Institutional Animal Care and Use Committee of PUMCH. Rats were randomly divided into SHAM, SHAM + rapamycin (RAPA), cecal ligation and puncture (CLP), and CLP + RAPA groups (six mice per group). CLP was performed as previously described to establish a mid-grade sepsis model [15]. In brief, under chloral hydrate anesthesia, the cecum was exposed by a 3 cm midline laparotomy. The mesentery of the cecum was carefully dissected, and the cecum was ligated at half the distance between the distal pole and base of the cecum. Two cecal punctures were made with a 22 G needle, and a droplet of feces was forced out from both the mesenteric and antimesenteric penetration holes to ensure patency of the punctures. Sham-operated rats were subjected to the same laparotomy without CLP. After surgery, all animals immediately received a subcutaneous injection of sterile saline (0.9% NaCl, 5 ml per 100 g body weight) for resuscitation. Eighteen hours after surgery, the animals were killed, and the hearts were removed for further evaluation. In treatment groups, rapamycin (10 mg/kg BW) was administered intraperitoneally for the 7 consecutive days before CLP operation. In the vehicle-treated group, mice received the same volume of vehicle (10% DMSO, 4 ml/kg BW) intraperitoneally. The dose of rapamycin was chosen based on a previous study [9].

2.2. Hematoxylin and Eosin (H&E) Staining. The left ventricle hearts of rats were transversely cut at a 2 mm thickness, immediately fixed in 4% paraformaldehyde, and embedded in paraffin. Sections of 3 μm in thickness were affixed to slides, deparaffinized, and stained with H&E to evaluate morphological changes of the heart.

2.3. Transmission Electron Microscopy Analysis. Transmission electron microscopy was performed as described previously [16]. The heart was perfused with 0.5% glutaric dialdehyde in 0.1 M cacodylate buffer (perfusion fluid) at 3 ml/min for 5 min to fix the muscle in situ. Then, the freshly isolated cardiac tissue from mice was cut into small pieces and immediately fixed by immersion in perfusion fluid for 3 h. After washing with 0.1 M cacodylate buffer and 15% sucrose buffer, the samples were cut into thin sections (90 nm) that were viewed at 120 kV with a H7650 transmission electron microscope (HITACHI, Tokyo, Japan). Micrographs were obtained using a Philips CM12 (10–15 per sample) by random sampling.

2.4. Western Blot Analysis. The left ventricle tissues were homogenized in lysis buffer. Tissue lysates were centrifuged at 17,000g for 10 min. An aliquot of the supernatant was used to determine the protein concentration. Protein samples were mixed with 4× lithium dodecyl sulfate sample buffer, electrophoresed on SDS-polyacrylamide gels, and then transferred electrophoretically onto nitrocellulose. The membranes were immunoblotted with antibodies against LC3B (ab48394, Abcam, 1 : 1000 dilution), p62 (#9234, Cell Signaling Technology, 1 : 1000 dilution), phospho-mTOR (Ser2448) (#5536, Cell Signaling Technology, 1 : 8500 dilution), phospho-p70S6 kinase (Thr389) (#9234, Cell Signaling Technology, 1 : 500 dilution), HIF-1a (ab2185, Abcam, 1 : 1000 dilution), and actin. A horseradish peroxidase-conjugated goat anti-rabbit secondary antibody was used. After the final wash, the membranes were developed using enhanced chemiluminescence (Amersham, Piscataway, NJ) and autoradiographed. Actin was used as a loading control.

2.5. Immunohistochemistry. Formalin-fixed, paraffin-embedded sections of rat hearts were subjected to immunohistochemical analysis as described previously [17]. Briefly, 3 μm thick tissue sections were deparaffinized and rehydrated, followed by antigen retrieval in a microwave, according to the standard procedures. The sections were sequentially blocked with avidin and biotin and then incubated at 4°C overnight with a 1/1000-diluted anti-LC3 antibody (ab48394, Abcam) and 1/1000-diluted anti-HIF-1a antibody (ab2185, Abcam). Following repeated washes, the sections were incubated at 25°C for 30 min with biotinylated IgG. Diaminobenzidine was used as a development substrate. The sections were dehydrated and mounted with DePex.

2.6. Echocardiography Examination. Rats were anaesthetized intraperitoneally with pentobarbital (70–80 mg/kg) at 18 h after CLP and situated in the supine position on a warming pad. An ultrasonic machine (M-Turbo Sonosite, USA) equipped with a 15 MHz transducer was used for noninvasive transthoracic echocardiography. The left ventricular end-diastolic and end-systolic dimensions were measured. The left ventricular ejection fraction (LVEF) and fractional shortening (FS) were also calculated from M-mode echocardiograms. Data from three consecutive selected cardiac cycles were analyzed and averaged.

2.7. Statistical Analysis. Data were analyzed by SPSS 18.0 software (SPSS Inc., IBM Corp., Armonk, NY, USA). All data for continuous variables in this study had normal distributions and are shown as the mean ± standard deviation. Differences were assessed using analysis of variance followed

by the least significant difference (LSD). A p value of less than 0.05 was considered as statistically significant.

3. Results

3.1. Pathological Changes in the Myocardial Tissue of Model Rats. H&E staining revealed that the myocardium of SHAM rats had a normal architecture and clear myocyte boundaries, whereas CLP rats after 18 h of sepsis showed marked myocardial injury with myocardial necrosis and interstitial edema adjacent to localized extravasation of red blood cells. These results indicated cardiomyopathy of the sepsis model established by CLP. Pathological damage of myocardial tissue was significantly alleviated by rapamycin treatment (Figure 1).

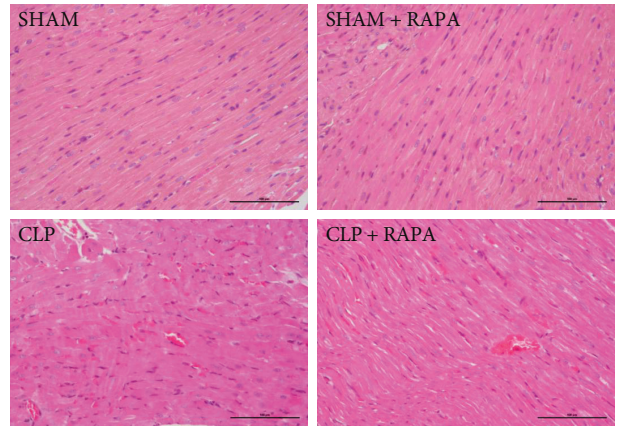

Figure 1: Representative H&E staining of the left ventricle sections. Original magnification, ×200. SHAM, sham operated; CLP, cecal ligation and puncture; RAPA, rapamycin.

3.2. Rapamycin Alleviates CLP-Induced Cardiac Dysfunction in Rats. To explore the effects of rapamycin on CLP-induced cardiac dysfunction in rats, the rats were subjected to a noninvasive transthoracic echocardiography. As shown in Figure 2, LVEF and FS were measured at 18 h after treatment. Compared with the SHAM group, cardiac functions as indicated by LVEF (CLP 0.49 ± 0.08 versus SHAM 0.77 ± 0.08, $p < 0.0001$) and FS (CLP 0.32 ± 0.05 versus SHAM 0.50 ± 0.08, $p < 0.001$) were significantly reduced in the CLP group, and rapamycin partially, but significantly, reversed the reduced cardiac dysfunction caused by CLP (LVEF: CLP + RAPA 0.61 ± 0.06 versus CLP 0.49 ± 0.08, $p < 0.05$; FS: CLP + RAPA 0.42 ± 0.05 versus CLP 0.32 ± 0.05, $p < 0.05$).

3.3. Rapamycin Reduces Expression of HIF-1a during Septic Cardiomyopathy. As shown in Figure 3, HIF-1a expression was significantly increased in CLP rats compared with sham-operated rats ($p < 0.0001$). Interestingly, rapamycin pretreatment of sham-operated rats reduced the expression of HIF-1a compared with that of CLP rats ($p < 0.05$), indicating that rapamycin alleviated myocardial anoxia in septic cardiomyopathy.

3.4. mTOR Pathway Activity in the Myocardial Tissue of Model Rats. As expected, the mTOR pathway in the myocardium was significantly inhibited by rapamycin. Interestingly, the activity of the mTOR pathway in the myocardium was dramatically suppressed in CLP rats compared with SHAM rats. The level of p-mTOR (phosphorylation at Ser2448) was decreased in the myocardium of CLP rats ($p < 0.001$) and activation of p70s6 kinase (phosphorylation at Thr389), a direct downstream target of mTOR, was highly suppressed in CLP rats compared with sham-operated rats ($p < 0.01$) (Figure 4). These results indicated that the mTOR pathway might play vital roles in septic myocardial dysfunction.

3.5. Relationship between the mTOR Pathway and Autophagy Proteins (LC3-II and p62) in Septic Cardiomyopathy. LC3II/LC3I in the left ventricle was significantly increased at 18 h after CLP compared with sham-operated rats ($p < 0.05$). Rapamycin treatment further increased the expression of LC3II in the left ventricle compared with CLP rats without rapamycin treatment ($p < 0.05$) (Figure 5(b)). We also evaluated LC3II in the left ventricle by immunohistochemical staining. As shown in Figure 5(a), the left ventricle sections from CLP rats showed an increase in LC3II expression compared with that from sham-operated rats, and LC3II expression was further increased in CLP + RAPA rats compared with CLP rats. Consistent with the change in LC3II expression of the myocardium, p62 expression in CLP rats was decreased compared with that in sham-operated rats ($p < 0.001$). As shown in Figure 5(c), p62 expression in CLP + RAPA rats was lower than that in CLP rats ($p < 0.05$).

3.6. Rapamycin Increases Autophagic Vacuoles in the Myocardium during Septic Cardiomyopathy. As shown in Figure 6, LV tissues from sham-operated rats showed a normal structure, whereas CLP rats had cellular disorganization and myofibrillar disarray. Autophagic processes were observed by transmission electron microscopy. We found more autophagic vacuoles in the myocardium of CLP rats compared with sham-operated rats. We also found that rapamycin further promoted autophagic processes because more autophagic vacuoles were found in CLP + RAPA rats than in CLP rats.

4. Discussion

mTOR is a master sensor of energy status and promotes autophagy upon energy depletion [11]. Energy depletion is a major cause of myocardial dysfunction during sepsis [12, 13]. Therefore, the mTOR pathway might play a major role in cardiac dysfunction induced by sepsis. In the present study, we used rapamycin, an inhibitor of the mTOR pathway, to explore the role of the mTOR pathway and the relationship between autophagy and the mTOR pathway in cardiac dysfunction caused by sepsis. We found that the mTOR pathway was inhibited in CLP rats compared with sham-operated rats, and rapamycin significantly alleviated pathological injury and cardiac dysfunction induced by CLP and improved myocardial anoxia in septic cardiomyopathy. We also found that autophagy was activated in CLP

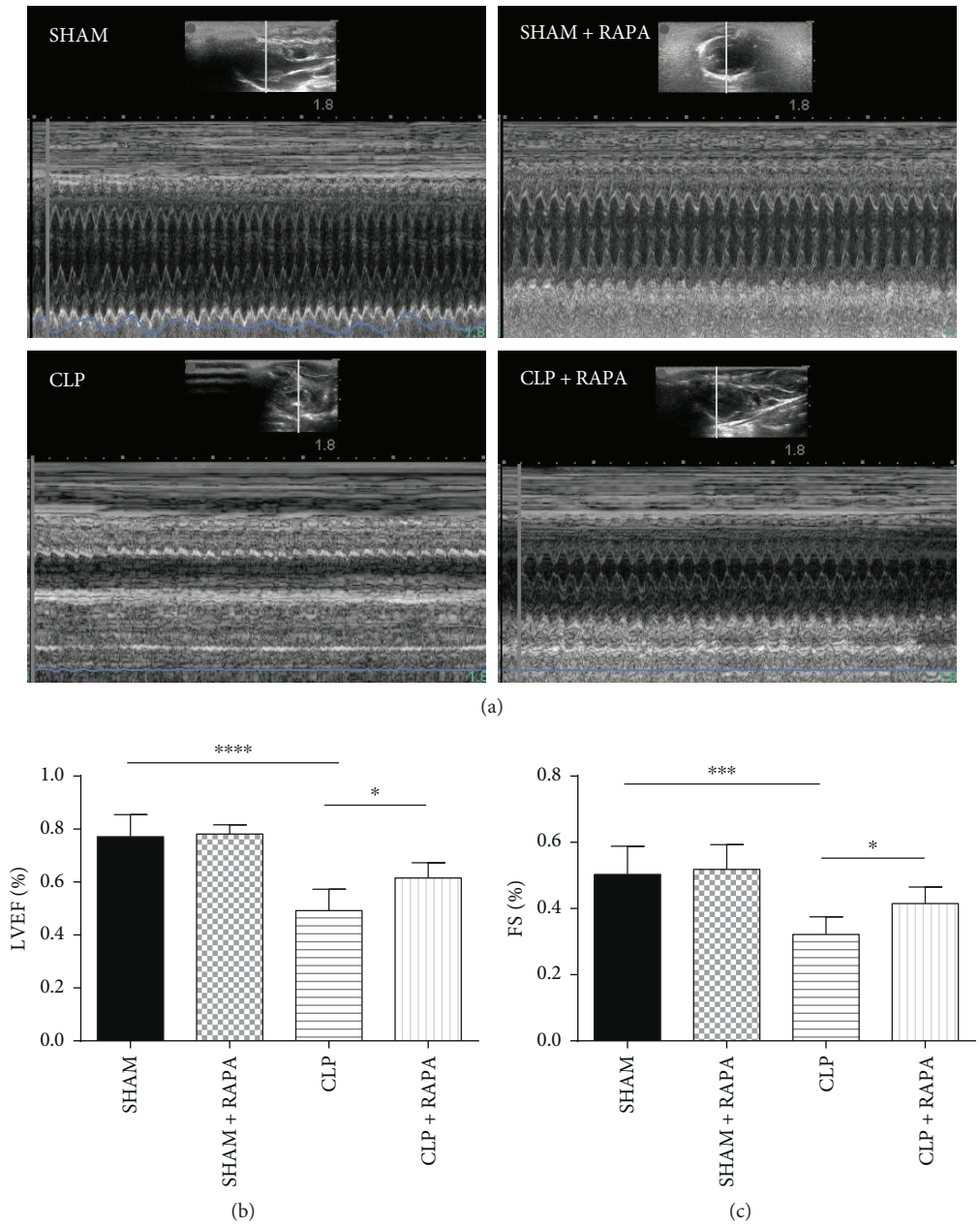

Figure 2: Cardiac functions examined by echocardiography. Representative echocardiographic recordings from the four groups (a). LVEF and FS were measured (b). Mean ± SD, six rats per group, $^{*}p < 0.05$; $^{***}p < 0.001$; $^{****}p < 0.0001$. LVEF, left ventricle ejection fraction; FS, fraction shortening.

rats compared with sham-operated rats, and rapamycin further promoted the autophagic process by affecting the mTOR pathway.

The heart is a high energy-demanding organ because it is required to constantly generate ATP to support the contraction/relaxation cycle. Energy depletion may cause cardiac dysfunction accompanied by changes in nutrient-sensing molecules. For example, in myocardial ischemia, the mTOR signaling pathway is inhibited by AMP-activated protein kinase (AMPK) that is activated by a reduction in cellular ATP levels [18]. Energy depletion also plays a major role in septic cardiac dysfunction induced by mitochondrial dysfunction and reduced cardiac fatty acid oxidation [19]. Our previous studies have found that the mTOR pathway in CD8 (+) T-cell was changed during the sepsis [20]; however, there is little evidence to prove the relevance of mTOR in sepsis-induced cardiac dysfunction [10, 14]. In our study, the mTOR pathway was significantly inhibited at 18 h after CLP. Phosphorylation of both mTOR and pS6K1, downstream targets of mTORC1, was significantly suppressed following CLP challenge. This result is consistent with a study by Li et al. Their study showed that the mTORC1 pathway was inhibited at 12 h after lipopolysaccharide (LPS) (20 mg/kg) injection [14],

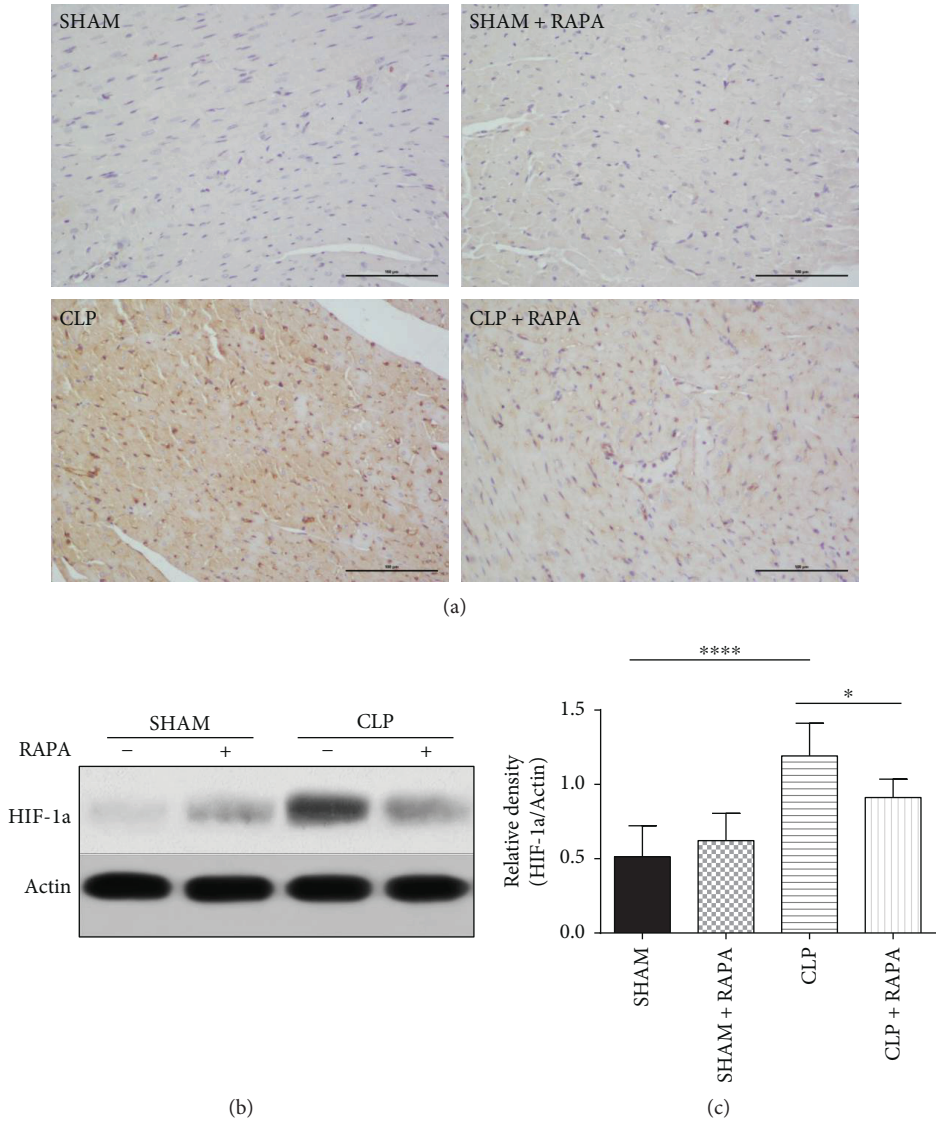

Figure 3: Effects of rapamycin on HIF-1a in the left ventricle 18 h after CLP. (a) The left ventricle sections stained with an anti-HIF-1a antibody. Magnification, ×200. Bar, 100 μm. (b, c) Expression of HIF-1a in the left ventricle. The left ventricle was harvested at 18 h after CLP, and HIF-1a protein levels were quantified by western blotting. Mean ± SD, six rats per group, $^{*}p < 0.05$; $^{****}p < 0.0001$.

whereas a recent study indicated that a small dose of LPS (4 mg/kg) overtly suppressed phosphorylation of AMPK and promoted phosphorylation of mTORC1 and S6 in the early stage of sepsis [10]. The reason for the different outcomes may be that in different stages of sepsis, the myocardium has specific energy states which needs to be further explored.

Inhibition of the mTOR signaling pathway has been reported to protect the heart against pathological damage including myocardial infarction and hypertrophy [21–23]. Recently, Li et al. showed that the inhibition of mTORC1 results in cardiac protection against LPS-induced sepsis [14]. However, few studies have supported their results. To explore the role of the mTOR pathway in sepsis-induced cardiac dysfunction, we used rapamycin to inhibit the mTOR signaling pathway. We found that rapamycin significantly alleviated CLP-induced pathological injury and cardiac dysfunction in rats. We also found that CLP rats treated with rapamycin had lower expression of HIF-1a in their myocardium, indicating that rapamycin improved myocardial anoxia in the sepsis model. These results suggest that rapamycin plays a protective role in CLP-induced sepsis cardiomyopathy. Combined with our results showing that CLP inhibited the mTOR signaling pathway in cardiomyocytes, we believe that CLP-induced inhibition of mTOR signaling is beneficial for cardiomyocyte survival, leading to improvement of cardiac functions under sepsis.

We further explored the mechanism by which rapamycin attenuated cardiac dysfunction induced by sepsis. Many studies have shown that the mTOR signaling pathway

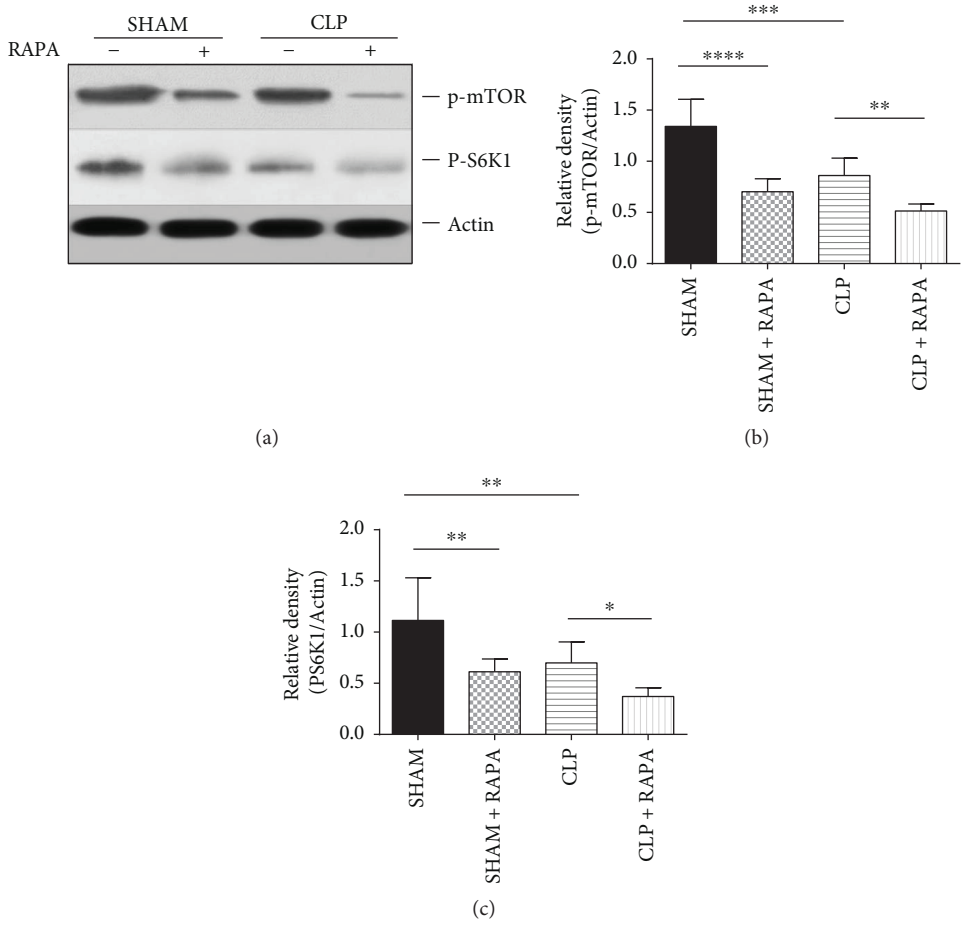

Figure 4: p-mTOR and PS6K1 expression in the left ventricle. The left ventricle was harvested 18 h after CLP, and p-mTOR and PS6K1 protein levels were quantified by western blotting. Mean ± SD, six rats per group, $^{*}p < 0.05$; $^{**}p < 0.01$; $^{***}p < 0.001$; $^{****}p < 0.0001$.

negatively regulates autophagy. Under nutrient-rich conditions, the mTOR pathway is activated and suppresses autophagy. Conversely, in response to energy depletion, the mTOR pathway is inhibited and autophagy is induced to provide an energy source [11]. As a housekeeping process, autophagy is vital for the normal structure and functions of the heart [7]. Additionally, autophagy plays a critical role in the maintenance of cardiac functions by removing damaged proteins and subcellular organelles under stress conditions [24]. It also plays an important role in the modulation of I/R injury. Evidence suggests that autophagy protects against I/R injury [8]. A recent study has shown that the process of autophagy in cardiomyocytes changes during sepsis, indicating that autophagy might play a major role in septic cardiac dysfunction [9].

In our study, we further explored changes of the autophagy process induced by CLP challenge and the relationship between the mTOR pathway and autophagy. We found that autophagy was activated at 18 h after CLP. The ratio of LC3II/LC3I was increased significantly, indicating that autophagosomal formation was improved at 18 h after CLP. We also found that p62, which inversely correlates with autophagic activity, was decreased significantly, indicating autophagy activation. This finding was confirmed by investigating the ultrastructure of the myocardial cells and finding more autophagic vacuoles in CLP rats. However, in a study by Hsieh et al. [9], they found that the process of autophagy in myocardial cells was not complete at 24 h after CLP. Despite both of our studies revealing elevation of LC3-II, they found that colocalization of LC3 and LAMP1 (a lysosome marker) was decreased at 24 h after CLP. They also observed increased numbers of large autophagosomes containing mitochondria in CLP mice, but few autolysosomes. The reason for the different experimental results may be obtaining myocardial tissues at different stages of sepsis. A recent study demonstrated that autophagy was activated initially in sepsis, followed by a subsequent phase of incompletion in the liver [25], which may be similar in the heart. Even though the time point that we chose was almost the same as that in the study by Hsieh et al., we ligated the cecum at half the distance between the distal pole and base of the cecum to establish the mid-grade sepsis model, whereas they ligated the cecum just below the ileocecal junction for high-grade sepsis. As a result, the myocardial tissue

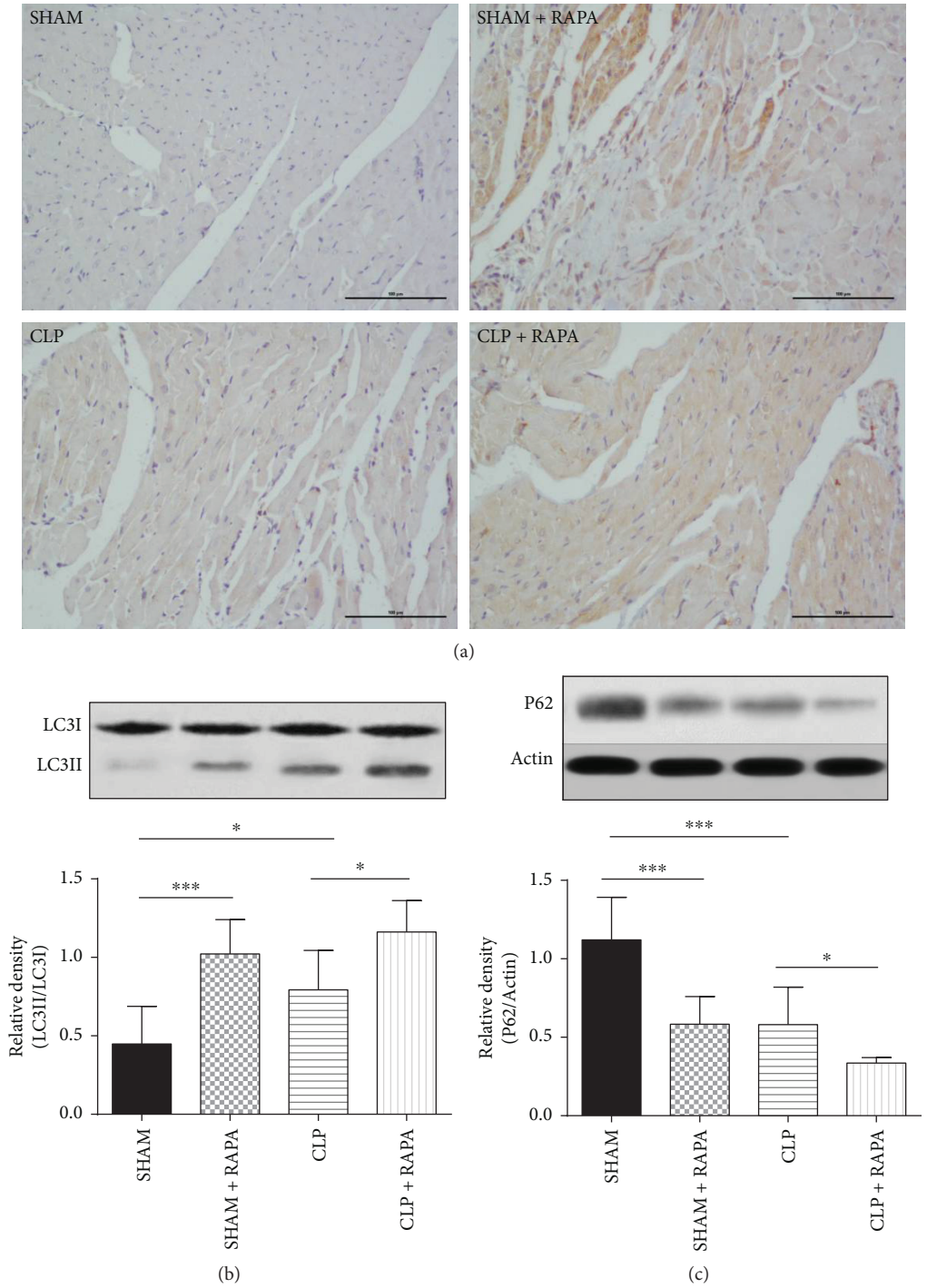

Figure 5: Effects of rapamycin on LC3-II and P62 expression in the left ventricle 18 h after CLP. (a) The left ventricle sections stained with an anti-LC3 antibody. Magnification, ×200. Bar, 100 μm. (b, c) LC3II and p62 expression in the left ventricle. The left ventricle was harvested at 18 h after CLP, and LC3II and P62 protein levels were quantified by western blotting. Mean ± SD, six rats per group, $^{*}p < 0.05$; $^{***}p < 0.001$.

in our study may indicate the condition of autophagy in the early stage of sepsis. We also found that rapamycin further activated autophagy in CLP rats, which was consistent with the improvement of cardiac functions and decreased HIF-1a, indicating that the cardioprotective effect of rapamycin in septic myocardial dysfunction may be mediated by acceleration of autophagy.

In conclusion, inhibition of the mTOR pathway plays a cardioprotective role in septic myocardial dysfunction, and this effect may be mediated by the acceleration of autophagy.

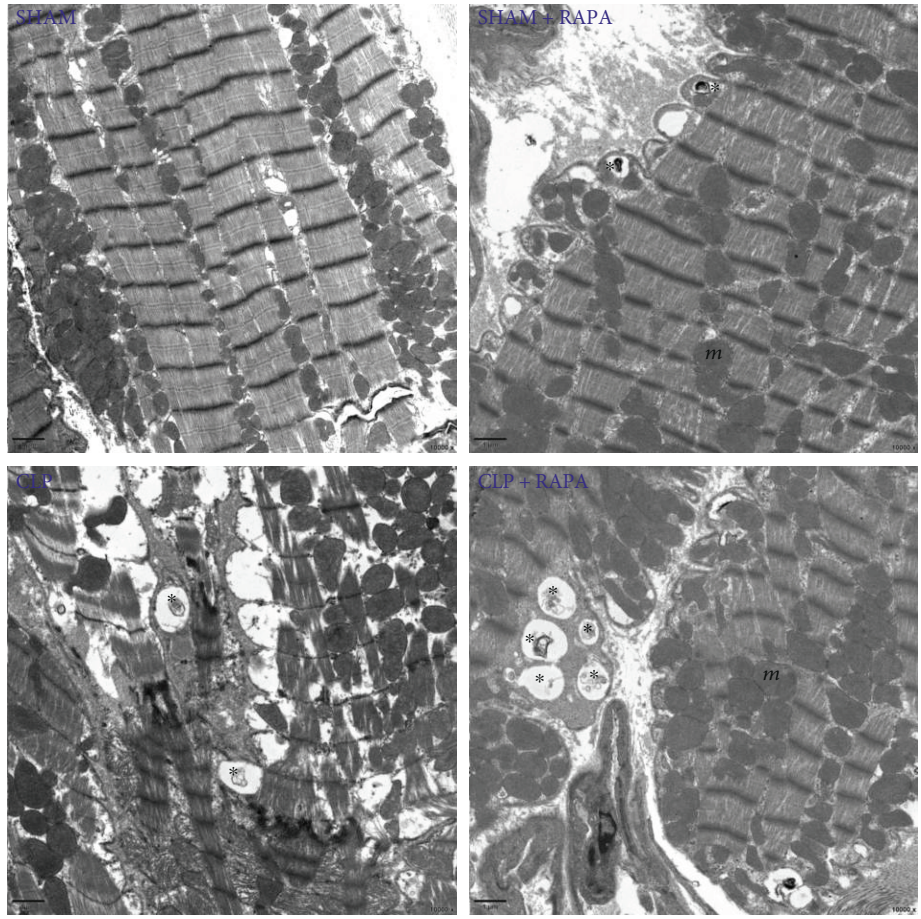

Figure 6: Ultrastructural features of autophagic vacuoles in the left ventricle harvested 18 h after CLP. The myocardium was normal in appearance with a proper mitochondria distribution in sham-operated rats. Myofibrillar disarray was seen in CLP rats. There were more autophagic vacuoles (asterisk) in CLP + RAPA rats compared with CLP rats. Mitochondria (*m*) were seen throughout the cytoplasm. Magnification ×10,000.

Data Availability

The details including all figures and raw data used to support the findings of this study are available from the corresponding author upon request.

Conflicts of Interest

All authors declare that they have no conflicts of interest.

Acknowledgments

The work was supported by the National Natural Science Foundation of China (no. 81601657).

References

[1] G. Kumar, N. Kumar, A. Taneja et al., "Nationwide trends of severe sepsis in the 21st century (2000-2007)," *Chest*, vol. 140, no. 5, pp. 1223–1231, 2011.

[2] V. Y. Dombrovskiy, A. A. Martin, J. Sunderram, and H. L. Paz, "Rapid increase in hospitalization and mortality rates for severe sepsis in the United States: a trend analysis from 1993 to 2003," *Critical Care Medicine*, vol. 35, no. 5, pp. 1244–1250, 2007.

[3] T. Shintani and D. J. Klionsky, "Autophagy in health and disease: a double-edged sword," *Science*, vol. 306, no. 5698, pp. 990–995, 2004.

[4] T. Shpilka, H. Weidberg, S. Pietrokovski, and Z. Elazar, "Atg 8: an autophagy-related ubiquitin-like protein family," *Genome Biology*, vol. 12, no. 7, p. 226, 2011.

[5] D. J. Klionsky, K. Abdelmohsen, A. Abe et al., "Guidelines for the use and interpretation of assays for monitoring autophagy (3rd edition)," *Autophagy*, vol. 12, no. 1, pp. 1–222, 2016.

[6] M. Komatsu and Y. Ichimura, "Physiological significance of selective degradation of p62 by autophagy," *FEBS Letters*, vol. 584, no. 7, pp. 1374–1378, 2010.

[7] Z. Giricz, R. M. Mentzer Jr., and R. A. Gottlieb, "Autophagy, myocardial protection, and the metabolic syndrome," *Journal of Cardiovascular Pharmacology*, vol. 60, no. 2, pp. 125–132, 2012.

[8] S. Sciarretta, N. Hariharan, Y. Monden, D. Zablocki, and J. Sadoshima, "Is autophagy in response to ischemia and reperfusion protective or detrimental for the heart?," *Pediatric Cardiology*, vol. 32, no. 3, pp. 275–281, 2011.

[9] C. H. Hsieh, P. Y. Pai, H. W. Hsueh, S. S. Yuan, and Y. C. Hsieh, "Complete induction of autophagy is essential for cardioprotection in sepsis," *Annals of Surgery*, vol. 253, no. 6, pp. 1190–1200, 2011.

[10] J. Zhang, P. Zhao, N. Quan et al., "The endotoxemia cardiac dysfunction is attenuated by AMPK/mTOR signaling pathway regulating autophagy," *Biochemical and Biophysical Research Communications*, vol. 492, no. 3, pp. 520–527, 2017.

[11] V. P. Tan and S. Miyamoto, "Nutrient-sensing mTORC1: integration of metabolic and autophagic signals," *Journal of Molecular and Cellular Cardiology*, vol. 95, pp. 31–41, 2016.

[12] J. A. Watts, J. A. Kline, L. R. Thornton, R. M. Grattan, and S. S. Brar, "Metabolic dysfunction and depletion of mitochondria in hearts of septic rats," *Journal of Molecular and Cellular Cardiology*, vol. 36, no. 1, pp. 141–150, 2004.

[13] E. Antonucci, E. Fiaccadori, K. Donadello, F. S. Taccone, F. Franchi, and S. Scolletta, "Myocardial depression in sepsis: from pathogenesis to clinical manifestations and treatment," *Journal of Critical Care*, vol. 29, no. 4, pp. 500–511, 2014.

[14] X. Li, L. Jiang, S. Lin et al., "Inhibition of mTORC1 renders cardiac protection against lipopolysaccharide," *International Journal of Clinical and Experimental Pathology*, vol. 7, no. 12, pp. 8432–8442, 2014.

[15] D. Rittirsch, M. S. Huber-Lang, M. A. Flierl, and P. A. Ward, "Immunodesign of experimental sepsis by cecal ligation and puncture," *Nature Protocols*, vol. 4, no. 1, pp. 31–36, 2009.

[16] G. Q. Wang, T. Tang, Z. S. Wang et al., "Overexpression of hypo-phosphorylated Ikappa Bbeta at Ser313 protects the heart against Sepsis," *PLoS One*, vol. 11, no. 8, article e0160860, 2016.

[17] K. Unuma, T. Aki, T. Funakoshi, K. I. Yoshida, and K. Uemura, "Cobalt protoporphyrin accelerates TFEB activation and lysosome reformation during LPS-induced septic insults in the rat heart," *PLoS One*, vol. 8, no. 2, article e56526, 2013.

[18] H. Takagi, Y. Matsui, S. Hirotani, H. Sakoda, T. Asano, and J. Sadoshima, "AMPK mediates autophagy during myocardial ischemia in vivo," *Autophagy*, vol. 3, no. 4, pp. 405–407, 2007.

[19] K. Drosatos, A. Lymperopoulos, P. J. Kennel, N. Pollak, P. C. Schulze, and I. J. Goldberg, "Pathophysiology of sepsis-related cardiac dysfunction: driven by inflammation, energy mismanagement, or both?," *Current Heart Failure Reports*, vol. 12, no. 2, pp. 130–140, 2015.

[20] N. Cui, H. Wang, L. X. Su, J. H. Zhang, Y. Long, and D. W. Liu, "Role of triggering receptor expressed on myeloid cell-1 expression in mammalian target of rapamycin modulation of $CD8^+$ T-cell differentiation during the immune response to invasive pulmonary aspergillosis," *Chinese Medical Journal*, vol. 130, no. 10, pp. 1211–1217, 2017.

[21] S. M. Filippone, A. Samidurai, S. K. Roh et al., "Reperfusion therapy with rapamycin attenuates myocardial infarction through activation of AKT and ERK," *Oxidative Medicine and Cellular Longevity*, vol. 2017, Article ID 4619720, 16 pages, 2017.

[22] Y. Baba, J. K. Higa, B. K. Shimada et al., "Protective effects of the mechanistic target of rapamycin against excess iron and ferroptosis in cardiomyocytes," *American Journal of Physiology-Heart and Circulatory Physiology*, vol. 314, no. 3, pp. H659–H668, 2018.

[23] A. Pena, A. Kobir, D. Goncharov et al., "Pharmacological inhibition of mTOR kinase reverses right ventricle remodeling and improves right ventricle structure and function in rats," *American Journal of Respiratory Cell and Molecular Biology*, vol. 57, no. 5, pp. 615–625, 2017.

[24] S. Sciarretta, P. Zhai, M. Volpe, and J. Sadoshima, "Pharmacological modulation of autophagy during cardiac stress," *Journal of Cardiovascular Pharmacology*, vol. 60, no. 3, pp. 235–241, 2012.

[25] C. W. Lin, S. Lo, D. S. Perng et al., "Complete activation of autophagic process attenuates liver injury and improves survival in septic mice," *Shock*, vol. 41, no. 3, pp. 241–249, 2014.

Hindawi
Mediators of Inflammation
Volume 2018, Article ID 1625414, 16 pages
https://doi.org/10.1155/2018/1625414

Research Article

Selenoprotein S Attenuates Tumor Necrosis Factor-α-Induced Dysfunction in Endothelial Cells

Siyuan Cui,[1] Lili Men,[1] Yu Li,[1] Yingshuo Zhong,[1] Shanshan Yu,[1] Fang Li,[2] and Jianling Du[1]

[1]*Department of Endocrinology, The First Affiliated Hospital of Dalian Medical University, Dalian, Liaoning 116011, China*
[2]*Department of Immunology, Dalian Medical University, Dalian, Liaoning 116044, China*

Correspondence should be addressed to Jianling Du; dujianlingcn@163.com

Received 30 September 2017; Revised 22 December 2017; Accepted 8 January 2018; Published 1 April 2018

Academic Editor: Adrian Doroszko

Endothelial dysfunction, partly induced by inflammatory mediators, is known to initiate and promote several cardiovascular diseases. Selenoprotein S (SelS) has been identified in endothelial cells and is associated with inflammation; however, its function in inflammation-induced endothelial dysfunction has not been described. We first demonstrated that the upregulation of SelS enhances the levels of nitric oxide and endothelial nitric oxide synthase in tumor necrosis factor- (TNF-) α-treated human umbilical vein endothelial cells (HUVECs). The levels of TNF-α-induced endothelin-1 and reactive oxygen species are also reduced by the upregulation of SelS. Furthermore, SelS overexpression blocks the TNF-α-induced adhesion of THP-1 cells to HUVECs and inhibits the increase in intercellular adhesion molecule-1 and vascular cell adhesion molecule-1. Moreover, SelS overexpression regulates TNF-α-induced inflammatory factors including interleukin-1β, interleukin-6, interleukin-8, and monocyte chemotactic protein-1 and attenuates the TNF-α-induced activation of p38 mitogen-activated protein kinase (MAPK) and nuclear factor-κB (NF-κB) pathways. Conversely, the knockdown of SelS with siRNA results in an enhancement of TNF-α-induced injury in HUVECs. These findings suggest that SelS protects endothelial cells against TNF-α-induced dysfunction by inhibiting the activation of p38 MAPK and NF-κB pathways and implicates it as a possible modulator of vascular inflammatory diseases.

1. Introduction

The vascular endothelium is regarded as a dynamic organ between blood vessels and circulating blood and plays a crucial role in the cardiovascular system, including the control of fibrinolysis and coagulation, regulation of vascular tone, inflammatory responses and angiogenesis processes, and synthesis and secretion of vasoactive substances [1]. In the healthy state, vascular equilibrium is regulated by a strict balance between agonist and antagonist substances secreted by the endothelium. One of the major vasodilatory substances produced by the endothelium is nitric oxide (NO). NO is a potent relaxing factor that plays a fundamental role in the maintenance of vasomotor function. In addition, it inhibits leukocyte adhesion, platelet aggregation, vascular smooth muscle cells (VSMCs) proliferation, and extracellular matrix secretion [2]. Reduced NO and an imbalance between NO and constriction factors such as endothelin-1 (ET-1) and angiotensin have been implicated in impaired endothelial function [3]. When abnormal vascular homeostasis occurs, injured endothelial cells synthesize and release various kinds of proinflammatory factors and adhesion molecules, such as interleukin-6 (IL-6), interleukin-1β (IL-1β), interleukin-8 (IL-8), monocyte chemotactic protein-1 (MCP-1), intercellular adhesion molecule-1 (ICAM-1), and vascular cell adhesion molecule-1 (VCAM-1), which facilitate the recruitment, adhesion, and migration of circulating leukocytes to vascular endothelial surfaces and exacerbate inflammatory damage to the endothelium [4].

Several studies have reported a strong relationship between inflammation and the development of endothelial dysfunction [4, 5]. Tumor necrosis factor-α (TNF-α), one of the prototype proinflammatory cytokines, is highly expressed during a variety of inflammatory conditions and is elevated in the arteries and plasma of humans and animals with vascular complications [6, 7]. Previous studies have also

shown that a high level of TNF-α could increase endothelium permeability, disrupt endothelium integrity, and induce cytokine secretion, all of which lead to the progression of vascular damage [8].

There is increasing evidence that endothelial dysfunction is crucial for the initiation and progression of primitive atherosclerosis and other forms of cardiovascular diseases including peripheral artery disease, chronic heart failure, hypertension, and coronary artery disease [9]. In this sense, endothelial function is considered as an important predictor of future cardiovascular events for individuals with cardiovascular diseases [10]. Thus, the treatment of endothelial dysfunction is imperative as it promises to reduce cardiovascular risk.

Selenoprotein S (SelS), a member of the selenoprotein family, is located on the endoplasmic reticulum and cell membranes and is expressed in various organs and cells [11]. SelS is involved in the reduction of endoplasmic reticulum stress, resistance to oxidative stress, regulation of inflammation, and glycolipid metabolism [12–15]. SelS has been reported as a receptor for serum amyloid A (SAA), which is an acute inflammatory response protein [16]. Accordingly, the inhibition of SelS is accompanied with increased SAA in lipopolysaccharide- (LPS-) induced HepG2 cells [17]. Fradejas et al. [18] have reported that SelS is markedly increased by the induction of inflammatory stimuli in the brain tissue of C57BL/6 mice, while its inhibition further increases the expression of IL-1β and IL-6 in LPS-induced human and mouse astrocytes. These reports indicate that SelS is strongly associated with the regulation of inflammation. However, the molecular mechanisms and effects of SelS on inflammation-induced endothelial damage remain unclear. To address this issue, this study was designed to clarify the biological effects of SelS on TNF-α-induced endothelial injury and illustrate the intercellular signaling cascades. We reveal, for the first time, that SelS could regulate TNF-α-induced endothelial dysfunction, suggesting that SelS might be a new biomarker for preventing vascular inflammatory disease.

2. Materials and Methods

2.1. Cell Culture. Human umbilical vein endothelial cells (HUVECs) and THP-1 monocytes were obtained from the American Type Culture Collection. The cells were separately cultured in RPMI-1640 medium containing 10% fetal bovine serum (Hyclone, USA), 100 U/ml penicillin, and 100 μg/ml streptomycin at 37°C and 5% CO_2. The medium was changed every two days, and the cells were ready for use when they reached 80–90% confluence. The endothelial cells were seeded into 6-well plates and treated with or without TNF-α (10 ng/ml, Sigma, USA) at different time points. In some experiments, the cells were pretreated with an inhibitor of the p38 MAPK pathway (SB203580, Selleckchem, USA) or an inhibitor of the NF-κB pathway (S2882, Selleckchem, USA) for 1 h.

2.2. Animals. Six-week-old male low-density lipoprotein receptor (LDLR) knockout (KO) mice were purchased from Ireland Matt Technology Co. Ltd. (Suzhou Industrial Park, China) and housed in a specific pathogen-free facility at the Animal Center of Dalian Medical University, China. All animal experiments were approved by the ethical committee of animal experiments in Dalian Medical University (Dalian, China) and followed the Care and Use of Laboratory Animals guidelines sanctioned by the National Institutes of Health. The LDLR-KO mice were randomly divided into control and treatment groups (six mice per group). The control group was given a regular chow (RC) diet, whereas the treatment group was provided with a high-fat diet (HFD, including 10% lard and 2% cholesterol). The mice were fed for 16 weeks during which their food intake, water intake, and body weight were recorded. After the feeding period, sodium pentobarbital solution was administered via an intraperitoneal injection. The LDLR-KO mice were then sacrificed and their thoracic aorta segments were harvested and fixed in neutral formalin. The tissues were then embedded in paraffin and prepared for staining.

2.3. Identification of pcDNA3.1-SelS Recombinant Plasmid. A segment of the human SelS gene (GenBank: NM_018445.5) containing 1102 bp (from 104 bp to 1205 bp) was synthesized by Sangon Biotech Co. Ltd. (Shanghai, China). A BamHI cleavage site and a His-tag protein coding sequence were added to the 5′ end, and an EcoRI cleavage site was added to the 3′ end. After EcoRI and BamHI cleavage, the SelS segment was combined with a pcDNA3.1 (+) expression vector by a T4 DNA ligase. The pcDNA3.1-SelS recombinant plasmid was then constructed, and its identification has been previously completed by our study group [19].

2.4. Transfection with pcDNA3.1-SelS Recombinant Plasmid or SelS siRNAs. HUVECs were seeded into 6-well plates and prepared for transfection using Lipofectamine 3000 reagent (Invitrogen, USA). Briefly, 2 μg of empty vector plasmid or pcDNA3.1-SelS recombinant plasmid was mixed with 5 μl of Lipofectamine 3000 in serum-free medium. The mixture was dispensed into the wells for incubation. After a 6 h incubation, the cells were cultured in fresh medium for another 24 h and used for the subsequent assays. SelS siRNAs and negative siRNA (the base sequences are provided in Supplementary Table 1) were designed and synthesized by GenePharma Co. Ltd. (Shanghai, China). The steps for the transfection of the SelS siRNAs were the same as for the transfection of the pcDNA3.1-SelS plasmid, and the negative siRNA (Neg.RNA) served as a negative control.

2.5. Cell Viability Measurement. The viability of endothelial cells was assessed with a cell counting kit-8 (CCK-8) according to manufacturer's instructions (Dojindo, Kumamoto, Japan). Briefly, the transfected HUVECs were seeded into 96-well plates and treated with TNF-α. The CCK-8 solution was added into the cells and incubated at 37°C for 2 h. The absorbance at 490 nm was measured using a microplate reader (NanoDrop, USA). The results were expressed as the percentage of cell viability with respect to control absorbance.

2.6. Nitric Oxide Assays. The nitrite concentrations in the medium of different treatment groups which represent NO levels were analyzed using the nitric oxide assay kit according to manufacturer's instructions (KeyGen Biotech, Nanjing, China). The absorbance of the samples was measured using a microplate reader (NanoDrop, USA) at a 550 nm wavelength, and concentration of the samples was determined.

2.7. Oxygen-Free Radical Test. HUVECs in different groups were stimulated with TNF-α and then incubated with 2′, 7′-dichlorodihydrofluorescein diacetate (2′, 7′-DCFH-DA, Sigma, USA) for 30 min. After washing twice with phosphate-buffered saline (PBS), the levels of cellular reactive oxygen species (ROS) were evaluated using a fluorescence microscope (Leica, Germany). To quantify the results, the photographs were observed under the same exposure condition, and the fluorescence mean densities were estimated using the Image Pro Plus 6.0 software (Microsoft Media Cybernetics, Bethesda, MD, USA).

2.8. Cell Adhesion Test. Monocyte adhesion to endothelial cells was determined using fluorescence-labeled THP-1 cells as described in previous studies [20, 21]. In brief, the transfected HUVECs were grown to confluence in 96-well plates and treated with TNF-α. The cells were gently washed with serum-free medium, and calcein AM-labeled THP-1 cells (5×10^4/ml DMEM medium) (Sigma, USA) were then added to the endothelial cells. After a 1 h incubation, the endothelial cell monolayer was gently rinsed twice to remove unbound monocytes. The adhesion of THP-1 cells in each group was observed with a fluorescence microscope (Leica, Germany). Under the same exposure condition, the values of fluorescence intensity were measured using the Image Pro Plus 6.0 software (Microsoft Media Cybernetics, Bethesda, MD, USA) and normalized to the control.

2.9. Real-Time Quantitative PCR. The total RNA of the samples was extracted using the TRIzol reagent (Takara Bio Inc., Dalian, China). Reverse transcription of the total RNA was then performed using a PrimeScript^{TM} cDNA kit (Takara Bio Inc., Dalian, China) according to manufacturer's directions. Real-time quantitative PCR (RT-qPCR) reactions were incubated initially at 95°C for 30 sec, 95°C for 5 sec, and 60°C for 30 sec of 35 cycles using a SYBR Green PCR Master Mix (Takara Bio Inc., Dalian, China) and were carried out with a PCR System 9700 (Applied Biosystems, USA). Three samples of each group were randomly selected for the RT-qPCR experiment. The samples were analyzed in triplicates, and the relative expression of mRNA was determined using glyceraldehyde-3-phosphatedehydrogenase (GAPDH) as an internal control. The relative gene expression was analyzed using the $2^{-\Delta\Delta Ct}$ method. The specific primers are listed in Supplementary Table 2 and the curves of amplification and dissolution of all RT-qPCR experiments are shown in Supplementary Figure 1.

2.10. ELISA. The levels of ICAM-1 and VCAM-1 in the supernatants of cells with different treatments were measured using a commercially available kit (Senbeijia Bio Inc., Nanjing, China) according to manufacturer's instructions. The absorbance of the samples was read on a microplate reader (NanoDrop, USA) at 450 nm.

2.11. Western Blot. The lysates of treated cells were reconstituted with loading buffer and run by sodium dodecyl sulfate polyacrylamide gel electrophoresis. Nitrocellulose membranes (Millipore, USA) containing the transferred proteins were soaked in blocking buffer for 2 h and then separately incubated at 4°C overnight with the following primary antibodies: SelS (Sigma, USA), endothelial nitric oxide synthase (eNOS; Proteintech, Wuhan, China), p-c-jun (Proteintech, Wuhan, China), c-jun (Proteintech, Wuhan, China), p-p38 MAPK (Abcam, USA), p38 MAPK (Abcam, USA), inhibitory kappa B α kinase β (IKKβ, CST, USA), p-IKKβ (CST, USA), inhibitory kappa B α (IκBα, CST, USA), p-IκBα (CST, USA), NF-κB p65 (Bioworld, USA), Lamin B (Proteintech, Wuhan, China), and GAPDH (Proteintech, Wuhan, China). After washing for 30 min, the nitrocellulose membranes were then incubated with horseradish peroxidase-conjugated secondary antibody for 1 h at room temperature. The membranes were subsequently treated with enhanced chemiluminescence (ECL, Thermo Scientific, USA) to develop the protein bands, and images were captured using the ChemiDoc MP Imaging System (Bio-Rad, USA). Quantitative analysis of the band intensities was performed with the Quantity One 4.52 software program (Bio-Rad, USA). Lamin B and GAPDH were used as internal controls.

2.12. Immunohistochemistry. The sections were dewaxed, hydrated, and microwaved to boiling point in citrate buffer to restore the tissue antigens. Each section was treated with 3% H_2O_2 to block endogenous peroxidase activity. After rinsing in PBS, the sections were incubated with bull serum albumin (Beyotime, Shanghai, China) to remove nonspecific antigens. The specimens were then treated with the primary antibody of SelS (1 : 200, Sigma, USA) and incubated at 4°C overnight. Subsequently, the specimens were treated with secondary antibody for 30 min. After treating with freshly constituted diaminobenzidine (ZsBio, Beijing, China), each section was then stained with hematoxylin and rinsed three times. Finally, the sections were dehydrated, rendered transparent, mounted, and dried. The sections were observed and photographed under the same condition using an inverted microscope (Leica, Germany). The mean intensities of the targeted proteins were analyzed semiquantitatively using the Image Pro Plus 6.0 software program (Microsoft Media Cybernetics, Bethesda, MD, USA).

2.13. Statistical Analysis. The data were analyzed using SPSS 19.0 (IBM, Armonk, NY, USA) and expressed as mean ± standard deviation (SD). The difference between groups was analyzed with one-way analysis of variance (ANOVA) or the unpaired Student's t-test, and p values less than 0.05 were considered statistically significant.

3. Results

3.1. HFD and TNF-α Induce Elevated SelS Expression in LDLR-KO Mice and HUVECs, Respectively. To investigate the relationship between SelS and endothelial dysfunction,

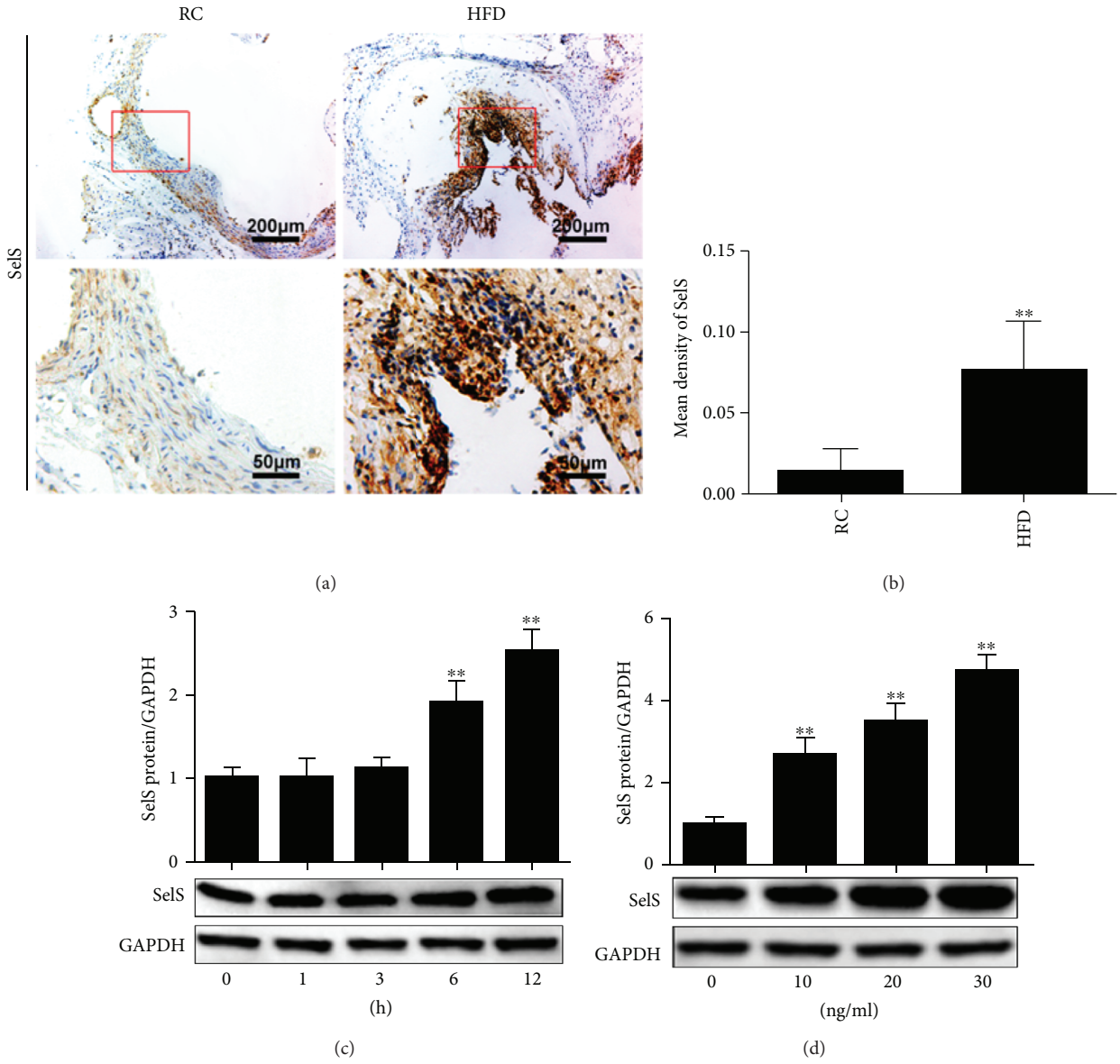

Figure 1: Induction and detection of SelS in LDLR-KO mice and TNF-α-treated HUVECs. (a) Representative images of SelS expression detected by immunohistochemistry, and representative images captured at 10x and 40x magnifications. (b) Mean density of SelS analyzed in different groups with the semiquantitative method using the Image Pro Plus 6.0 software. The sections from six mice of each group were observed and three different fields of each slice were randomly selected. (c) Expression of SelS tested in HUVECs at different time points with TNF-α (10 ng/ml) stimulation. (d) SelS expression determined in HUVECs with different concentrations of TNF-α treatment (for 6 h of incubation). The results are representative of triplicate independent experiments and are presented as mean ± SD, ($n = 3$). $^{**}p < 0.01$ versus control. LDLR: low-density lipoprotein receptor; KO: knockout; HUVECs: human umbilical vein endothelial cells; RC: regular chow; HFD: high-fat diet.

we first explored the levels of SelS in the intima of the thoracic aorta of LDLR-KO mice. As shown in Figures 1(a) and 1(b), the immunohistochemistry staining revealed a significant increase in SelS expression in the aortic intima of LDLR-KO mice fed with HFD. Conversely, LDLR-KO mice fed with RC expressed relatively low levels of SelS (Figures 1(a) and 1(b)). In an *in vitro* study, we investigated the expression levels of SelS after treating HUVECs with TNF-α. It was observed that TNF-α significantly induced SelS expression in both a time- and dosage-dependent manner (Figures 1(c) and 1(d)). These findings suggest the involvement of SelS in aortic intima damage, and the induction of SelS may be associated with endothelium injury caused by TNF-α stimulation.

3.2. Transfection of HUVECs with pcDNA3.1-SelS Plasmid or SelS siRNAs and Selection of Transfectant. The transfection technique was employed to explore the functional role of SelS. HUVECs were transfected with either pcDNA3.1-SelS plasmid or SelS siRNAs. The successful overexpression or inhibition of SelS was confirmed by the RT-qPCR and western blot techniques. Both mRNA and

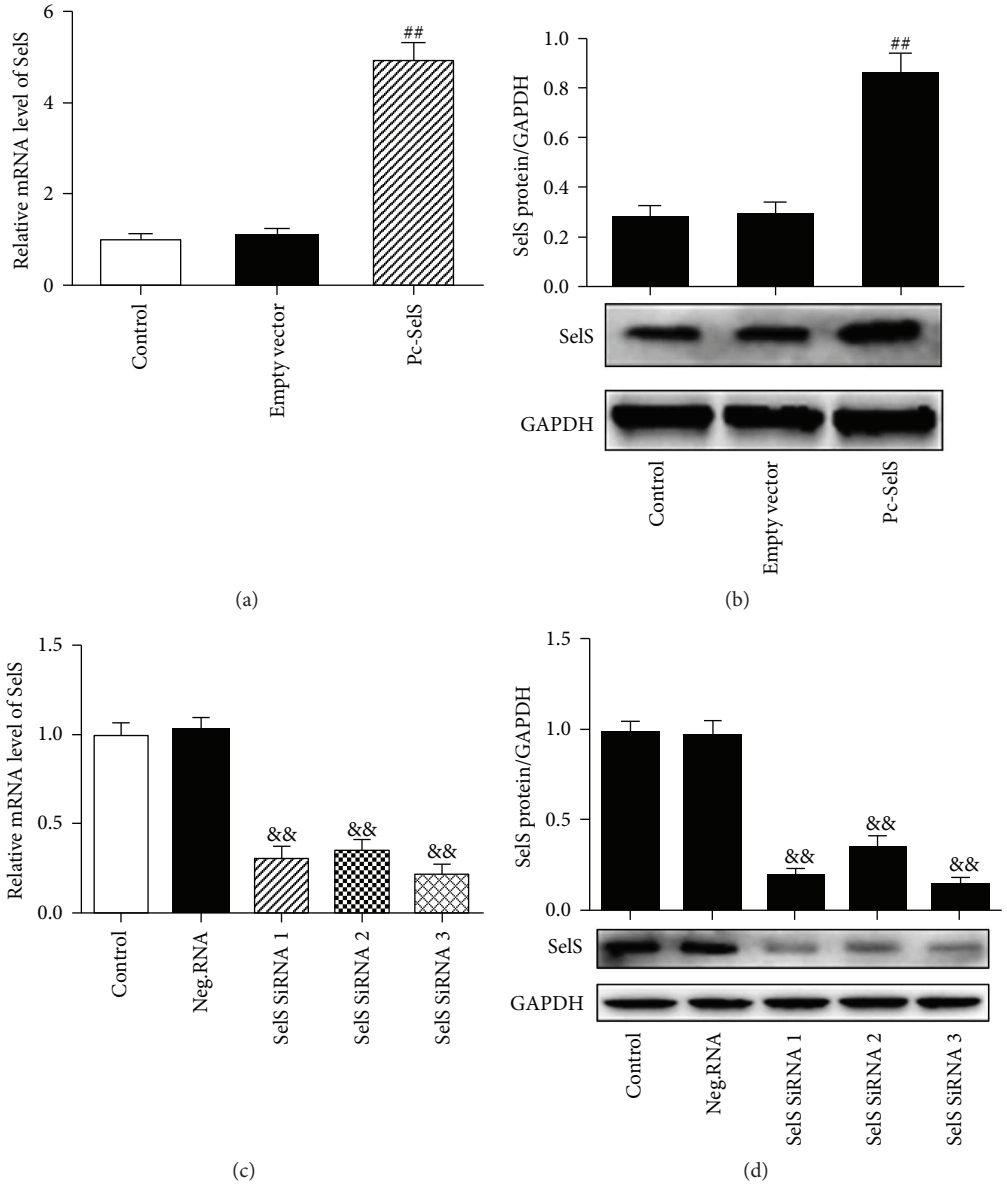

Figure 2: Upregulation and knockdown of SelS in HUVECs. HUVECs with pcDNA3.1-SelS plasmid transfection confirmed by RT-qPCR (a) and by the western blot (b). The mRNA levels (c) and protein expression (d) of SelS determined following the transfection with SelS siRNAs or negative siRNA in HUVECs. The cells were transfected with pcDNA3.1-SelS recombinant plasmid or SelS siRNAs for 30 h. The results are representative of six independent experiments and are presented as mean ± SD ($n = 6$). $^{\#\#}p < 0.01$ versus empty vector; $^{\&\&}p < 0.01$ versus negative siRNA. E-vector: empty vector; Pc-SelS: pcDNA3.1-SelS plasmid; Neg.RNA: negative siRNA.

protein levels of SelS were, respectively, increased by approximately 4.94-fold and 3.12-fold, respectively, in HUVECs transfected with the pcDNA3.1-SelS plasmid (Figures 2(a) and 2(b)). In contrast, HUVECs transfected with SelS siRNAs demonstrated an inhibition of both mRNA and protein expressions of SelS by SelS siRNA 3, with a reduction of 80% and 88%, respectively (Figures 2(c) and 2(d)). Consequently, SelS siRNA 3 transfection was selected for subsequent experiments.

3.3. SelS Enhances Endothelial Cell Viability after TNF-α Treatment. Increasing evidence has demonstrated that TNF-α reduces endothelium viability and promotes its apoptosis, which contributes to the development of cardiovascular diseases. To investigate the role of SelS in endothelial cells viability, we treated the HUVECs with 100 ng/ml TNF-α and assessed their viability with CCK-8. The expression of SelS was determined in the experiment and shown in Supplementary Figure 2. The viability of TNF-α-treated HUVECs was strongly enhanced in SelS plasmid transfection compared with transfection with an empty vector plasmid (Figure 3(a)). However, SelS siRNA transfection further reduced endothelial cell viability after TNF-α treatment (Figure 3(a)). This observation reveals the protective role of SelS in TNF-α-associated endothelial damage.

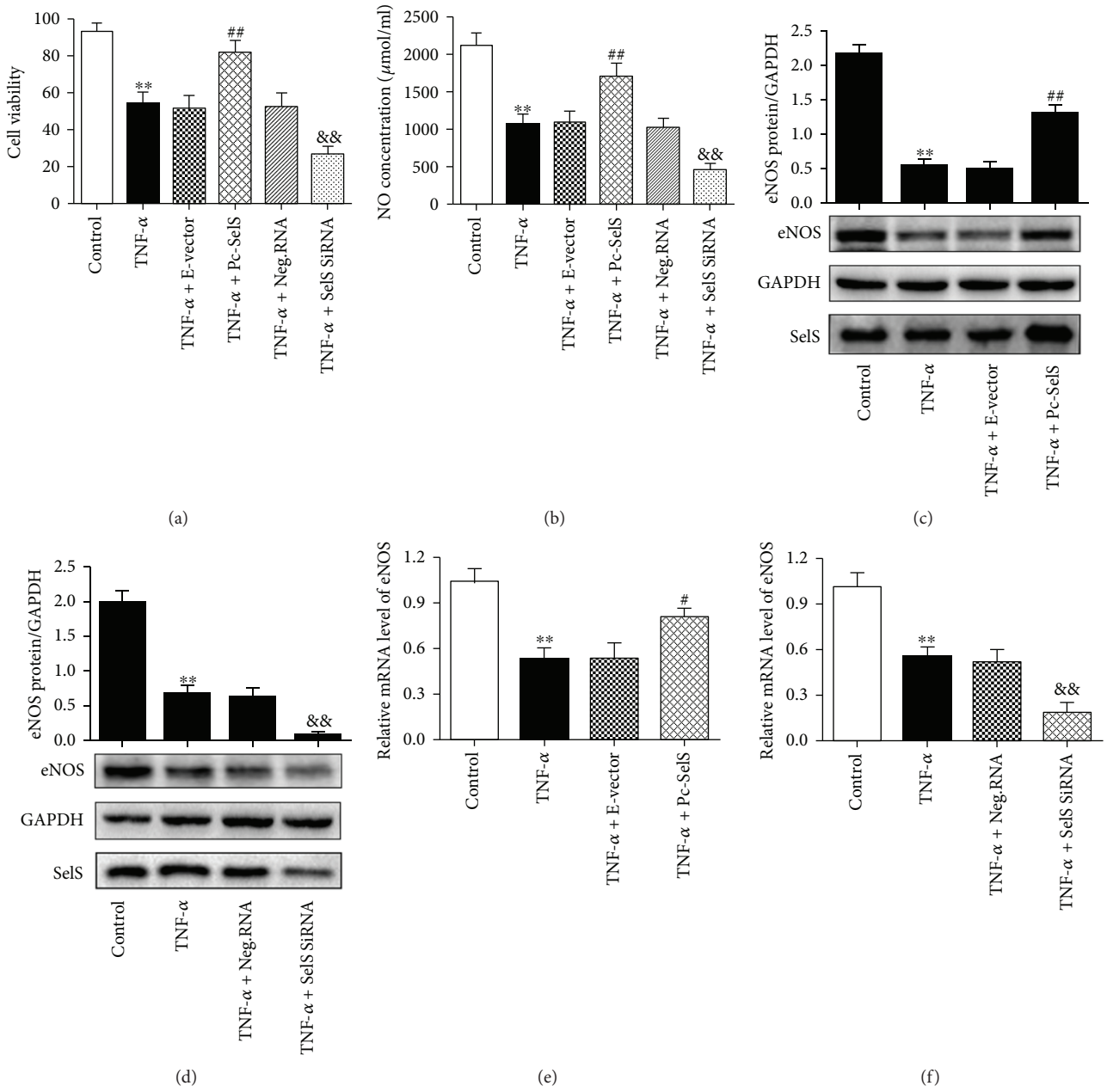

Figure 3: Effect of SelS on the viability of HUVECs and NO and eNOS expressions. (a) Viability of the transfected HUVECs after a 12 h stimulation with TNF-α (100 ng/ml), tested using the CCK-8 method. (b) The concentrations of NO in transfected HUVECs with 6 h TNF-α (10 ng/ml) treatment, determined using the nitrate reductase assay. The protein expression of eNOS in 10 ng/ml TNF-α-induced HUVECs after transfection with SelS plasmid (c) or SelS siRNA (d) examined by the western blot. The mRNA levels of eNOS in 10 ng/ml TNF-α-induced HUVECs after transfection with SelS plasmid (e) or SelS siRNA (f). The cells were transfected with pcDNA3.1-SelS recombinant plasmid or SelS siRNAs for 30 h. The eNOS expression was tested after 6 h TNF-α treatment. The results are representative of triplicate independent experiments and are presented as mean ± SD, ($n = 3$). $^{**}p < 0.01$ versus control; $^{\#}p < 0.05$ versus empty vector; $^{\#\#}p < 0.01$ versus empty vector; $^{\&\&}p < 0.01$ versus negative siRNA. CCK-8: cell counting kit-8; NO: nitric oxide; eNOS: endothelial nitric oxide synthase; E-vector: empty vector; Pc-SelS: pcDNA3.1-SelS plasmid; Neg.RNA: negative siRNA.

3.4. SelS Increases NO and eNOS Levels in TNF-α-Treated HUVECs. In order to further observe the effects of SelS on endothelium relaxation, we determined the levels of NO and eNOS in the HUVECs using different treatments. SelS expression was tested in the experiments and shown in Supplementary Figure 2. It was observed that the upregulation of SelS relieved TNF-α-induced reduction in NO production (Figure 3(b)). In contrast, the knockdown of SelS in the endothelial cells further reduced TNF-α-induced NO level (Figure 3(b)). At the protein level, eNOS was significantly enhanced by SelS overexpression, but the inhibition of SelS further reduced the level of

eNOS in the TNF-α-treated endothelial cells (Figures 3(c) and 3(d)). Additionally, compared with transfection with the empty vector plasmid, the mRNA expression of eNOS was significantly increased in SelS plasmid transfection (Figure 3(e)). However, SelS siRNA transfection significantly reduced the level of TNF-α-induced eNOS in the HUVECs (Figure 3(f)). These results suggest that SelS enhances the levels of NO and eNOS in TNF-α-treated endothelial cells.

3.5. SelS Reduces Elevated ET-1 and ROS Levels Caused by TNF-α Induction. ET-1 is a potent vasoconstrictor, and regulating its level of expression is crucial to maintaining endothelial function. Similarly, ROS is highly expressed in the endothelium under the stressed condition and facilitates vascular endothelium damage. We, therefore, investigated the effect of SelS on ET-1 and ROS with RT-qPCR and fluorescence staining, respectively. In the transcription state, transfection with SelS plasmid reduced TNF-α-induced ET-1 expression in HUVECs, compared with empty vector transfection (Figure 4(a)). HUVECs transfected with SelS siRNA had an increased mRNA expression of ET-1 (Figure 4(b)). Similarly, our fluorescence staining revealed that intracellular ROS levels were largely increased in HUVECs after TNF-α treatment (Figures 4(c) and 4(d)). However, the upregulation of SelS inhibited the increase in TNF-α-induced ROS production. In contrast, the knockdown of SelS in the endothelial cells further elevated the production of ROS induced by TNF-α (Figures 4(c) and 4(d)). Collectively, these outcomes indicate that SelS protects the endothelium by regulating ET-1 and ROS expressions in TNF-α-induced endothelial damage.

3.6. SelS Suppresses TNF-α-Induced Adhesion Molecules and the Adhesion of THP-1 Cells to Endothelial Cells. In trauma, the trafficking of leukocytes to the endothelium is among the initial stages in endothelial injury. Therefore, we examined the effect of SelS on the TNF-α-induced adhesion of THP-1 cells to endothelial cells. We observed via fluorescence staining that SelS plasmid transfection significantly suppressed the TNF-α-induced adhesion of THP-1 cells (Figures 5(a) and 5(b)). However, the reverse was noticed in SelS siRNA transfection, where a significant increase in the adhesion of THP-1 cells to HUVECs was noted (Figures 5(a) and 5(b)). Because several molecules mediate leukocyte adhesion to endothelial cells, we examined the effects of SelS on ICAM-1 and VCAM-1 expressions with ELISA and RT-qPCR, respectively. TNF-α generally augmented the levels of ICAM-1 and VCAM-1 compared with the control group (Figures 5(c)–5(h)). However, SelS overexpression significantly reduced TNF-α-induced increase in the production of ICAM-1 and VCAM-1, while the inhibition of SelS notably enhanced the TNF-α-induced expression of ICAM-1 and VCAM-1 (Figures 5(c)–5(h)). These results indicate that SelS has the potential to reduce leukocyte adhesion by inhibiting adhesion molecules.

3.7. SelS Reduces the Expression of Chemokines and Cytokines Induced by TNF-α. Chemokines, such as MCP-1 and IL-8, are responsible for recruiting leukocytes and for their migration to the subintimal layer of injured endothelium. The influence of SelS on TNF-α was, therefore, investigated by measuring the expression levels of MCP-1 and IL-8 using RT-qPCR. At the transcription stage, mRNA levels of MCP-1 and IL-8 were significantly enhanced by TNF-α stimulation but were reduced in SelS overexpression (Figures 6(a) and 6(c)). Compared with negative siRNA transfection, the levels of MCP-1 and IL-8 were elevated in SelS knockdown cells (Figures 6(b) and 6(d)). In addition, we investigated the effects of SelS on the proinflammatory cytokines, IL-6 and IL-1β, which exacerbate endothelial damage, and they were elevated by TNF-α (Figures 6(e)–6(h)). Similar to the observation made in MCP-1 and IL-8 production, the upregulation of SelS reduced the mRNA expression of IL-6 and IL-1β in TNF-α-treated HUVECs. However, the expression of these cytokines was enhanced in SelS knockdown cells (Figures 6(e)–6(h)). The inhibition of these molecules by SelS suggests its antagonizing effect against proinflammatory chemokines and cytokines.

3.8. SelS Inhibits the Activation of the TNF-α-Induced p38 MAPK Pathway. As shown in Figures 7(a)–7(d), when HUVECs were treated with SB203580 (a p38 MAPK pathway inhibitor) or S2882 (a NF-κB pathway inhibitor), the elevation of ICAM-1, VCAM-1, IL-6, and IL-1β by TNF-α induction was significantly inhibited, suggesting that the production of these adhesion molecules and proinflammatory factors partly depends on the activation of the NF-κB and p38 MAPK signaling pathways. Consequently, we first evaluated the role of SelS in the activation of p38 MAPK signaling pathways. The levels of phosphorylated p38 MAPK were upregulated after treatment with TNF-α for 30 min (Figures 7(e) and 7(f)). Subsequently, there was an increase in its downstream phosphorylated c-jun (a subunit of activator protein-1) in endothelial cells treated with TNF-α for 1 h (Figures 7(g) and 7(h)). Conversely, the upregulation of SelS significantly reduced the TNF-α-induced activation of phosphorylated p38 MAPK and phosphorylated c-jun, while SelS knockdown further increased TNF-α-induced phosphorylated proteins in HUVECs (Figures 7(e)–7(h)).

3.9. SelS Inhibits the Activation of the TNF-α-Induced NF-κB Pathway. The translocation of NF-κB from the cytoplasm to the nucleus is an essential step for the activation of inflammatory factors. HUVECs pretreated with SelS plasmid or SelS siRNA were incubated with TNF-α within a range of indicated time points. Cytoplasmic and nuclear lysates were western blotted for NF-κB p65 to determine the translocation of NF-κB. TNF-α treatment increased nuclear NF-κB p65 levels and reduced cytoplasmic NF-κB p65 levels compared with the control group (Figures 8(a)–8(d)). However, SelS overexpression reduced the levels of nuclear NF-κB p65 and enhanced the expression of cytoplasmic NF-κB p65, but the inhibition of SelS further enhanced the expression of TNF-α-induced nuclear NF-κB p65 and decreased the levels of cytoplasmic NF-κB p65 (Figures 8(a)–8(d)), indicating that SelS inhibits the translocation of NF-κB from the cytoplasm to the nucleus in HUVECs.

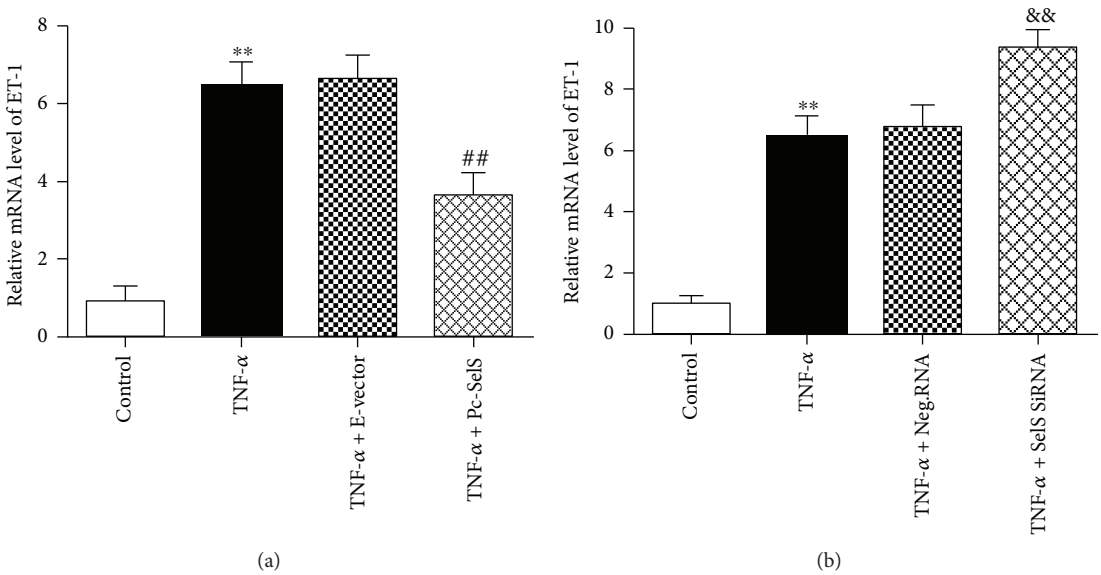

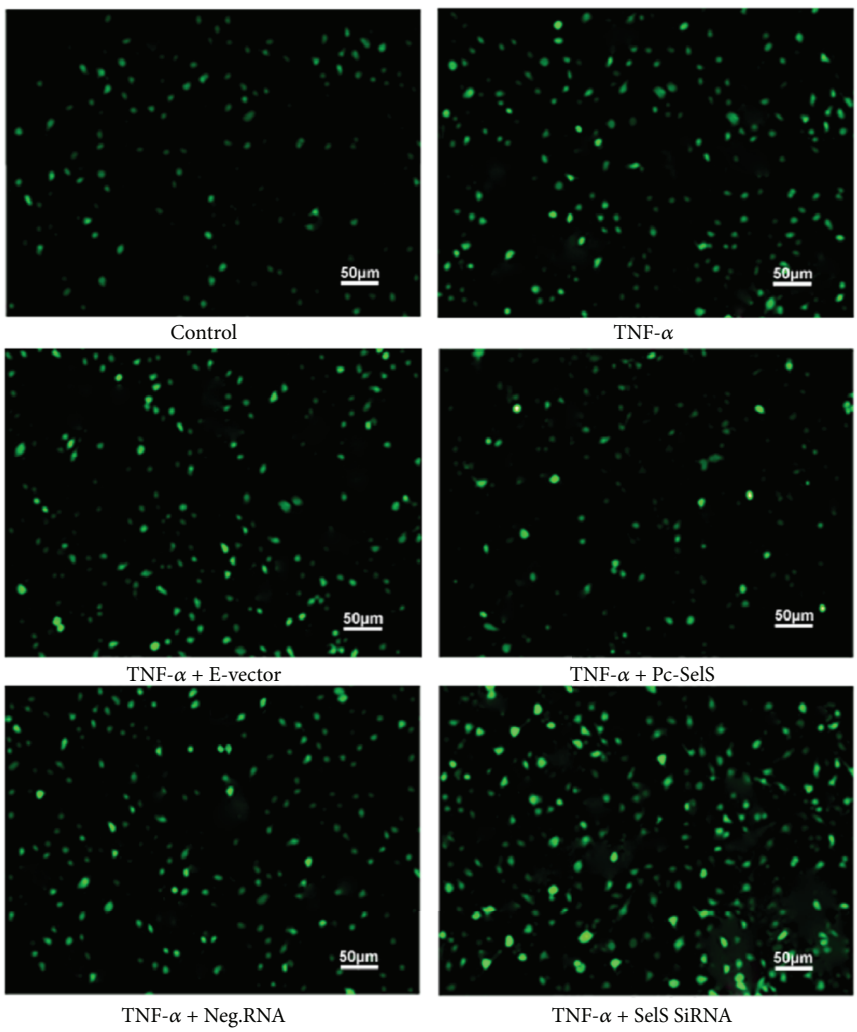

Figure 4: Continued.

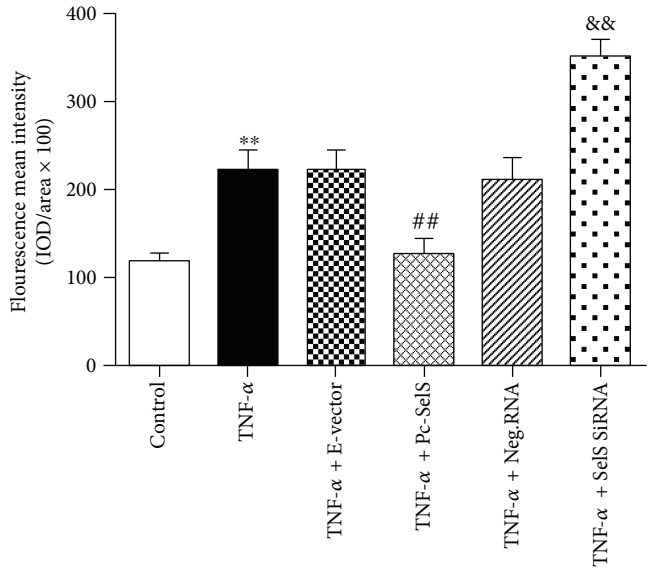

(d)

Figure 4: Effect of SelS on the levels of ET-1 and ROS in TNF-α-treated HUVECs. The mRNA levels of ET-1 detected in HUVECs transfected with SelS plasmid (a) or SelS siRNA (b) after 10 ng/ml TNF-α induction. (c) The levels of cellular ROS measured in different groups with 10 ng/ml TNF-α treatment using fluorescent probe method and (d) the corresponding fluorescent mean intensity evaluated by the Image Pro Plus 6.0 software. The cells were transfected with pcDNA3.1-SelS recombinant plasmid or SelS siRNAs for 30 h. The levels of ET-1 and ROS were tested after 6 h TNF-α treatment. The results are representative of triplicate independent experiments and are presented as mean ± SD, ($n = 3$). $^{**}p < 0.01$ versus control; $^{\#\#}p < 0.01$ versus empty vector; $^{\&\&}p < 0.01$ versus negative siRNA. ROS: reactive oxygen species; ET-1: endothelin-1; E-vector: empty vector; Pc-SelS: pcDNA3.1-SelS plasmid; Neg.RNA: negative siRNA.

To further explore the mechanisms by which SelS inhibits NF-κB activation, we studied its upstream pathways by investigating the effects of SelS on IKKβ/IκBα. We observed that TNF-α treatment rapidly led to the phosphorylation of IκBα, degradation of IκBα, and phosphorylation of IKKβ in HUVECs in a time-dependent manner (Figures 8(e)–8(h)). Moreover, the upregulation of SelS markedly inhibited the TNF-α-induced phosphorylation of IκBα and suppressed the degradation of IκBα induced by TNF-α (Figures 8(e) and 8(f)). There was no significant difference in the expression of IKKβ in SelS plasmid transfection or SelS siRNA transfection (Figure 8(g)). However, the phosphorylation of IKKβ was significantly reduced in cells transfected with the SelS plasmid and was further increased in cells transfected with SelS siRNA (Figure 8(h)), suggesting SelS as a negative regulator of IKKβ/IκBα signaling via the inhibition of IκBα and IKKβ phosphorylation and via the degradation of IκBα in endothelial inflammation.

4. Discussion

As a biological barrier between the vessel wall and circulating blood, the vascular endothelium is especially crucial for the maintenance of vascular homeostasis [1]. Many risk factors such as smoking, hyperglycemia, and hyperlipidemia may promote the pathogenesis of endothelial dysfunction through the modulation of inflammatory pathways [9]. SelS has been reported to be strongly associated with inflammation [14]. In our *in vivo* study, we observed a significant increase in SelS expression in the aortic intima of LDLR-KO mice fed with HFD, indicating that SelS is closely associated with the formation of arteriosclerosis (AS). However, endothelial dysfunction has been established as a foundation in the initiation and progression of AS, and SelS is highly expressed during endothelial injury. The upregulation of SelS could, therefore, be viewed as a defensive response against AS formation and seems to play a mediatory role in endothelial dysfunction. HUVECs are usually employed to explore the biology of vascular endothelial cells, inflammation, and the onset mechanisms of multiple diseases. We found that TNF-α increased SelS expression in HUVECs in a time- and dose-dependent manner (Figure 1), indicating that TNF-α regulates SelS expression, and suggesting that SelS plays a critical role in endothelial inflammation.

In order to better understand the molecular mechanisms underlying inflammatory endothelial dysfunction, we examined the effects of SelS on TNF-α-induced HUVECs dysfunction. The hallmark of endothelial dysfunction is impaired NO bioavailability. NO is synthesized by eNOS during the conversion of L-arginine to L-citrulline within endothelial cells, and eNOS, a dimeric enzyme, is mainly expressed by vascular endothelial cells [22]. We found that SelS overexpression improved TNF-α-induced NO reduction by increasing the level of eNOS (Figure 3). Under normal conditions, inactive eNOS binds to caveolin-1 (Cav-1) and remains in cytoplasmic caveolae. When the concentration of cytoplasmic Ca^{2+} increases, caldesmon (CAM) replaces Cav-1 and binds to eNOS to activate it [23]. However, the upregulation of Cav-1 led to an interruption in the activation of eNOS in the liver of mice [24]. Our previous study

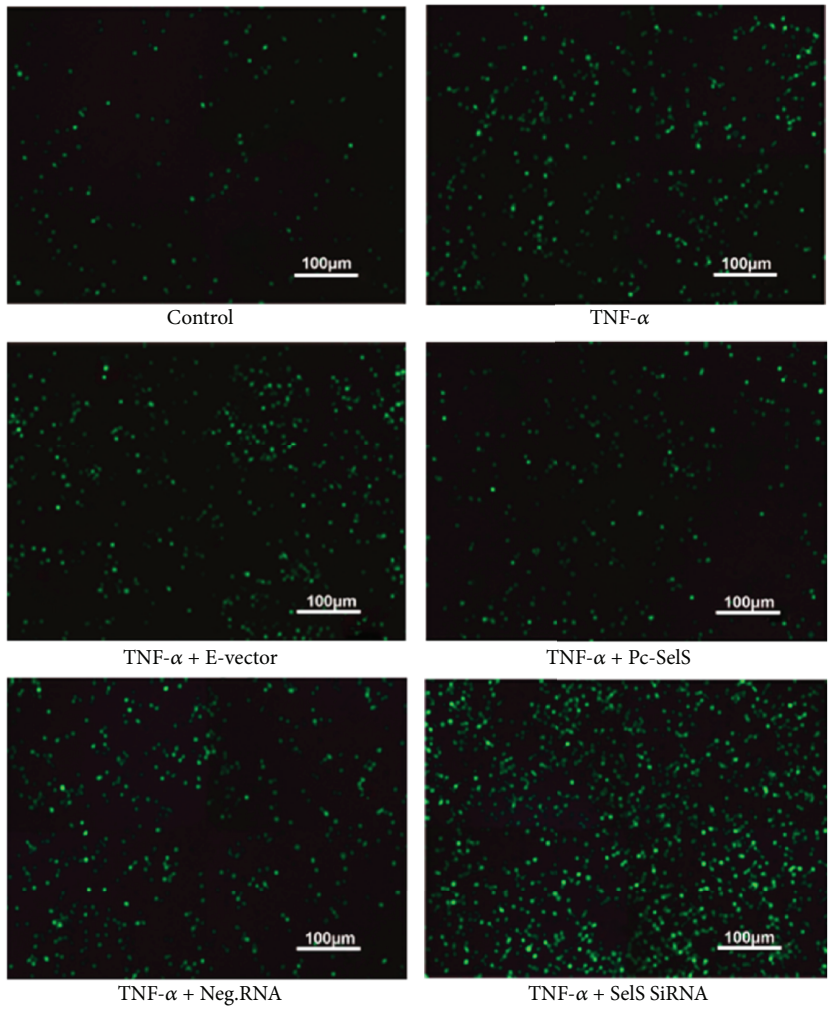

(a)

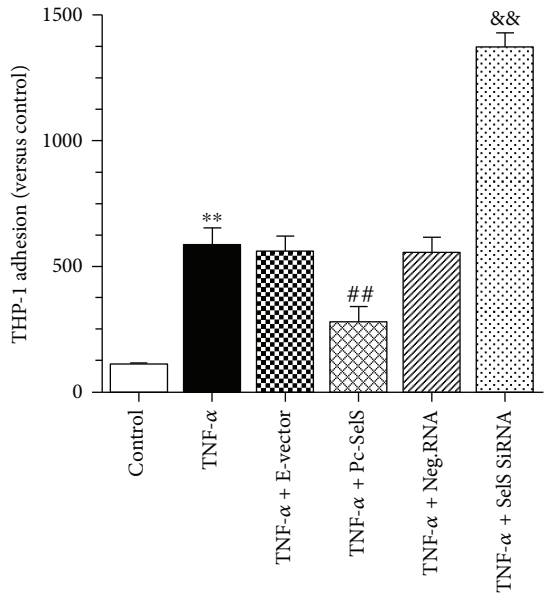

(b)

Figure 5: Continued.

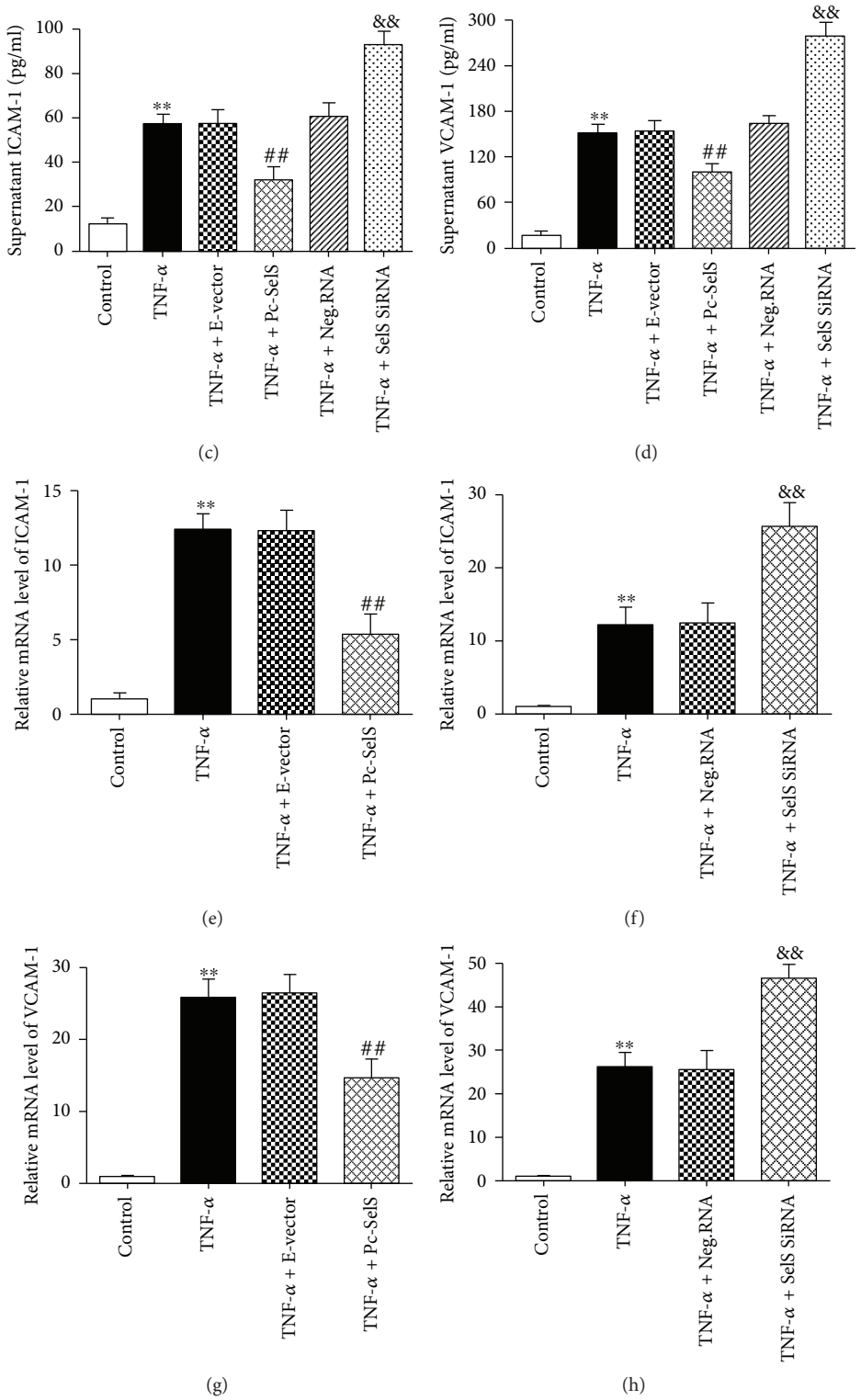

Figure 5: Effect of SelS on THP-1 cells adhesion and adhesion factors. (a) Adhesion of THP-1 cells to HUVECs shown by the fluorescent probe method and (b) the corresponding fluorescence intensity analyzed using Image Pro Plus 6.0 software. The production of ICAM-1 (c) and VCAM-1 (d) detected in the supernatant of cultures with 10 ng/ml TNF-α treatment by ELISA. The mRNA levels of ICAM-1 estimated in 10 ng/ml TNF-α-induced cells after transfection with SelS plasmid (e) or SelS siRNA (f). The mRNA levels of VCAM-1 determined in SelS plasmid (g) or SelS siRNA (h) transfected cells after 10 ng/ml TNF-α induction (for 6 h). The cells were transfected with pcDNA3.1-SelS recombinant plasmid or SelS siRNAs for 30 h. The results are representative of triplicate independent experiments and are presented as mean ± SD, ($n = 3$). $^{**}p < 0.01$ versus control; $^{\#\#}p < 0.01$ versus empty vector; $^{\&\&}p < 0.01$ versus negative siRNA. ICAM-1: intercellular adhesion molecule-1; VCAM-1: vascular cell adhesion molecule-1; E-vector: empty vector; Pc-SelS: pcDNA3.1-SelS plasmid; Neg.RNA: negative siRNA.

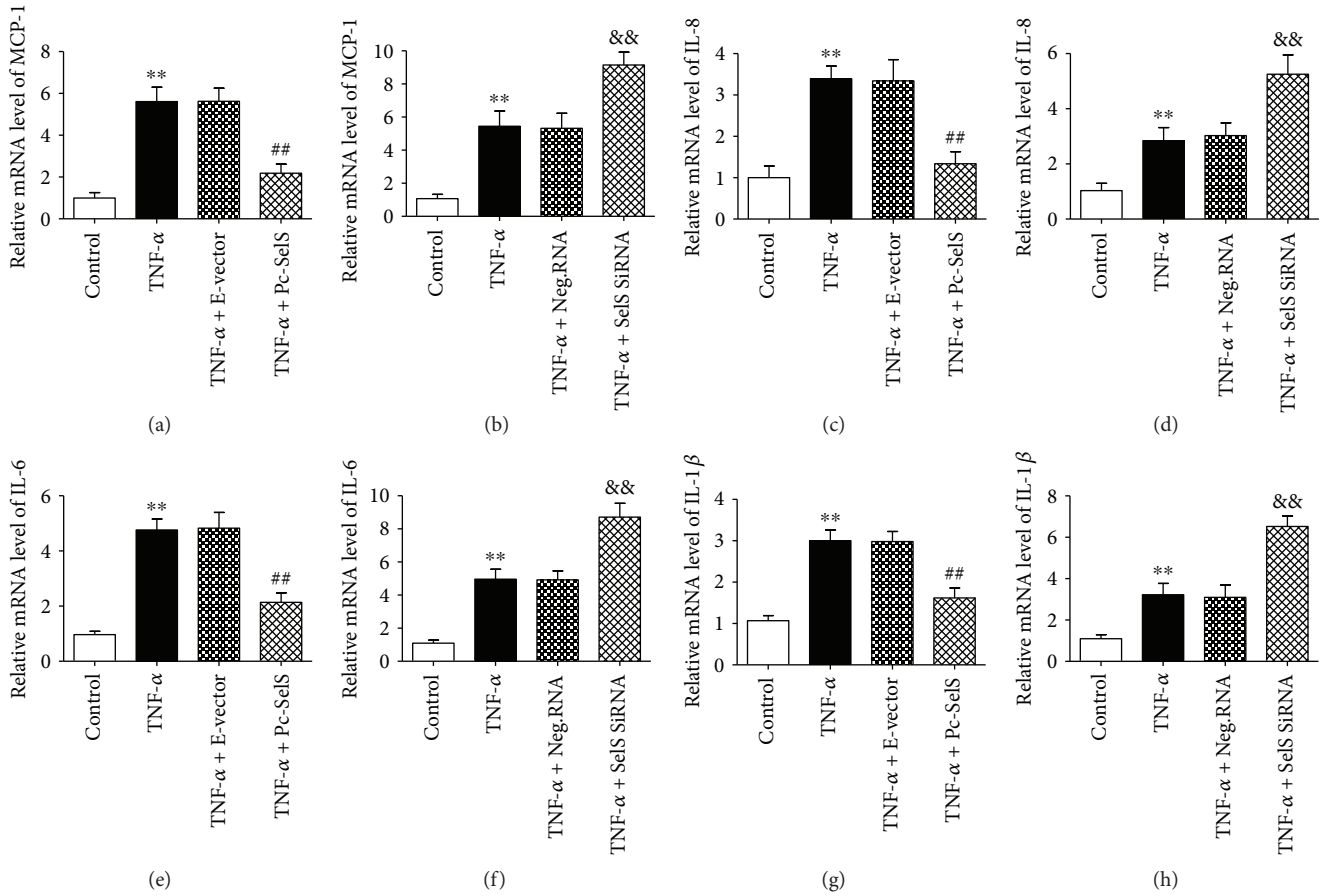

Figure 6: Influence of SelS on inflammatory factors. The effect of SelS on the mRNA level of MCP-1 (a), IL-8 (c), IL-6 (e), and IL-1β (g) was determined in TNF-α-treated cells (10 ng/ml) by means of SelS transfection. The mRNA levels of MCP-1 (b), IL-8 (d), IL-6 (f), and IL-1β (h) in transfected cells with 10 ng/ml TNF-α treatment (for 6 h), estimated via RT-qPCR. The cells were transfected with pcDNA3.1-SelS recombinant plasmid or SelS siRNAs for 30 h. The results are representative of triplicate independent experiments and are presented as mean ± SD, ($n = 3$). $^{**}p < 0.01$ versus control; $^{\#\#}p < 0.01$ versus empty vector; $^{\&\&}p < 0.01$ versus negative siRNA. MCP-1: monocyte chemoattractant protein-1; IL-8: interleukin-8; IL-6: interleukin-6; IL-1β: interleukin-1β; E-vector: empty vector; Pc-SelS: pcDNA3.1-SelS plasmid; Neg.RNA: negative siRNA.

found that transfection with SelS plasmid inhibited H_2O_2-induced Cav-1 expression in HUVECs [25]. As such, SelS may influence the levels of eNOS by regulating Cav-1 in HUVECs; however, this hypothesis requires more research for verification.

In the vascular system, excessive ROS facilitates the production of superoxide anions ($O_2^{\bullet-}$) in endothelial cells. $O_2^{\bullet-}$ easily binds to NO and forms peroxynitrite, compromising vasorelaxation [26]. However, we observed, in this study, that the upregulation of SelS significantly reduced TNF-α-induced production of ROS in the endothelial cells (as shown in Figure 4). Our findings suggest that the elevated expression of SelS increases NO levels not only by increasing the levels of eNOS but also by reducing ROS production and indicate that the free radical scavenging effect of SelS contributes to its anti-inflammatory effects. ET-1 is a potent vasoconstrictor peptide that exhibits both prooxidant and proinflammatory properties and accelerates the development of endothelial dysfunction [27]. TNF-α induces the excessive production of ET-1 in the endothelium, and excessive ET-1 reduces eNOS expression by influencing the distribution of eNOS between the membrane and mitochondria [28]. Additionally, the characteristic manifestation of endothelial injury is a dysfunctional vasorelaxation caused by a severe imbalance between NO and ET-1. We demonstrated in this study that the elevation of TNF-α-induced ET-1 expression in HUVECs is suppressed by SelS overexpression (Figure 4). Optimizing and controlling SelS expression could be explored in endothelial dysfunction to enhance the level of eNOS via inhibition of ET-1 expression and also to modulate ET-1 and NO communication.

Endothelial dysfunction is also characterized by leukocyte accumulation and increased adhesions. When endothelial cells undergo inflammatory activation, an increase in MCP-1 and IL-8 promotes the recruitment of leukocytes, with a corresponding increase in ICAM-1 and VCAM-1, which promotes the adherence of leukocyte to the endothelium and aggravates endothelial damage. Our model confirmed that TNF-α mediates the production of ICAM-1, VCAM-1, MCP-1, and IL-8 and enhances leukocyte

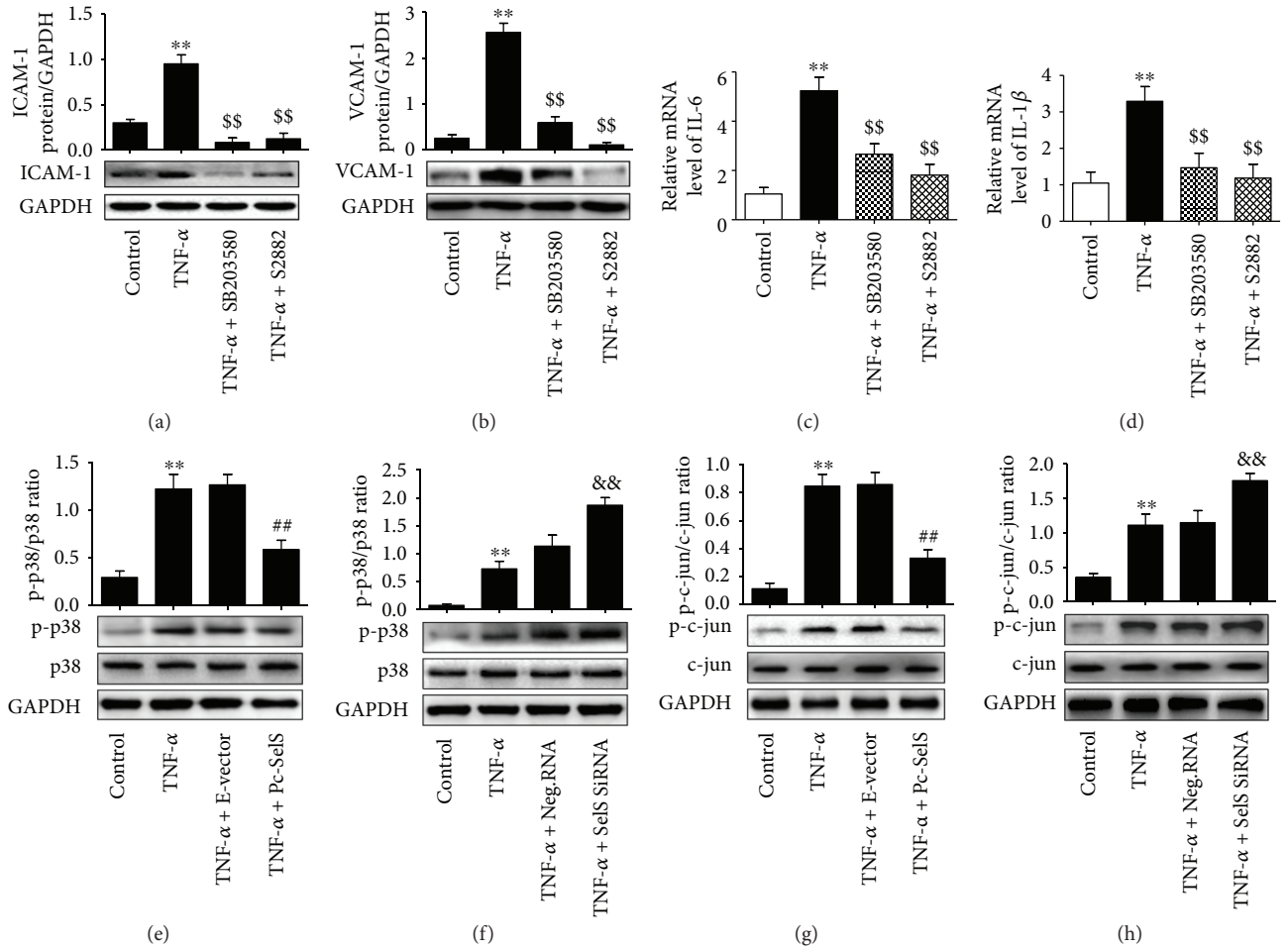

Figure 7: Effect of SelS on the p38 MAPK pathway. The expression of ICAM-1 (a) and VCAM-1 (b) in cells treated with SB203580 (an inhibitor of the p38/MAPK pathway) or S2882 (an inhibitor of the NF-κB pathway), prior to 10 ng/ml TNF-α treatment, detected by the western blot. The mRNA levels of IL-6 (c) and IL-1β (d) in HUVECs treated with SB203580 or S2882 before 10 ng/ml TNF-α induction. (e) and (f) The levels of phosphorylated p38 MAPK and p38 MAPK tested in the transfected cells after 10 ng/ml TNF-α stimulation. The expression of phosphorylated c-jun and c-jun in SelS plasmid (g) or SelS siRNA (h) transfection following 10 ng/ml TNF-α treatment and determined by the western blot. The cells were transfected with pcDNA3.1-SelS recombinant plasmid or SelS siRNAs for 30 h. The dosage used for inhibitors SB203580 and S2882 was 20 μM and 10 μM, respectively. The results are representative of triplicate independent experiments and are presented as mean ± SD, ($n = 3$). $^{**}p < 0.01$ versus control; $^{\#\#}p < 0.01$ versus empty vector; $^{\&\&}p < 0.01$ versus negative siRNA; $^{\$\$}p < 0.01$ versus TNF-α treatment. E-vector: empty vector; Pc-SelS: pcDNA3.1-SelS plasmid; Neg.RNA: negative siRNA.

adhesion to the endothelium (Figures 5 and 6). Notably, these effects were downregulated after SelS overexpression, demonstrating that SelS overexpression reduces leukocyte adhesion by possibly inhibiting its chemotaxis and adhesive molecules during inflammation. It has been established that the elevation of inflammatory cytokines such as IL-1β and IL-6 has adverse consequences and could worsen endothelial damage and that limiting their expression implies the reduction of the associated cellular insult. Our study shows that the upregulation of SelS expression attenuates the deleterious effects of IL-1β and IL-6 during endothelial inflammation. By extension, SelS appears to regulate the expression of several proinflammatory genes associated with endothelial dysfunction.

We deduced from our study that the expression of targeted cytokines and adhesion factors following endothelial injury induced by TNF-α is mediated by the activation of the p38 MAPK pathway. Activator protein-1 (AP-1), a transcription factor, regulates a variety of cytokine expressions and consists of the jun and fos proteins [29]. In most cells, the AP-1 dimer consists of c-jun and c-fos [29]. When TNF-α binds to its receptors on the endothelium, p38 MAPK is activated which leads to the phosphorylation of c-jun and c-fos and the subsequent activation of AP-1 [30]. In this study, HUVECs transfected with SelS plasmid inhibited TNF-α-induced phosphorylated p38 MAPK and phosphorylated c-jun activation (Figure 7). This suggests that the elevated expression of SelS attenuates TNF-α-induced inflammation in endothelial cells by inhibiting the activation of p38 MAPK pathways.

Similarly, treating HUVECs with the NF-κB inhibitor S2882 downregulated ICAM-1, VCAM-1, IL-6, and IL-1β

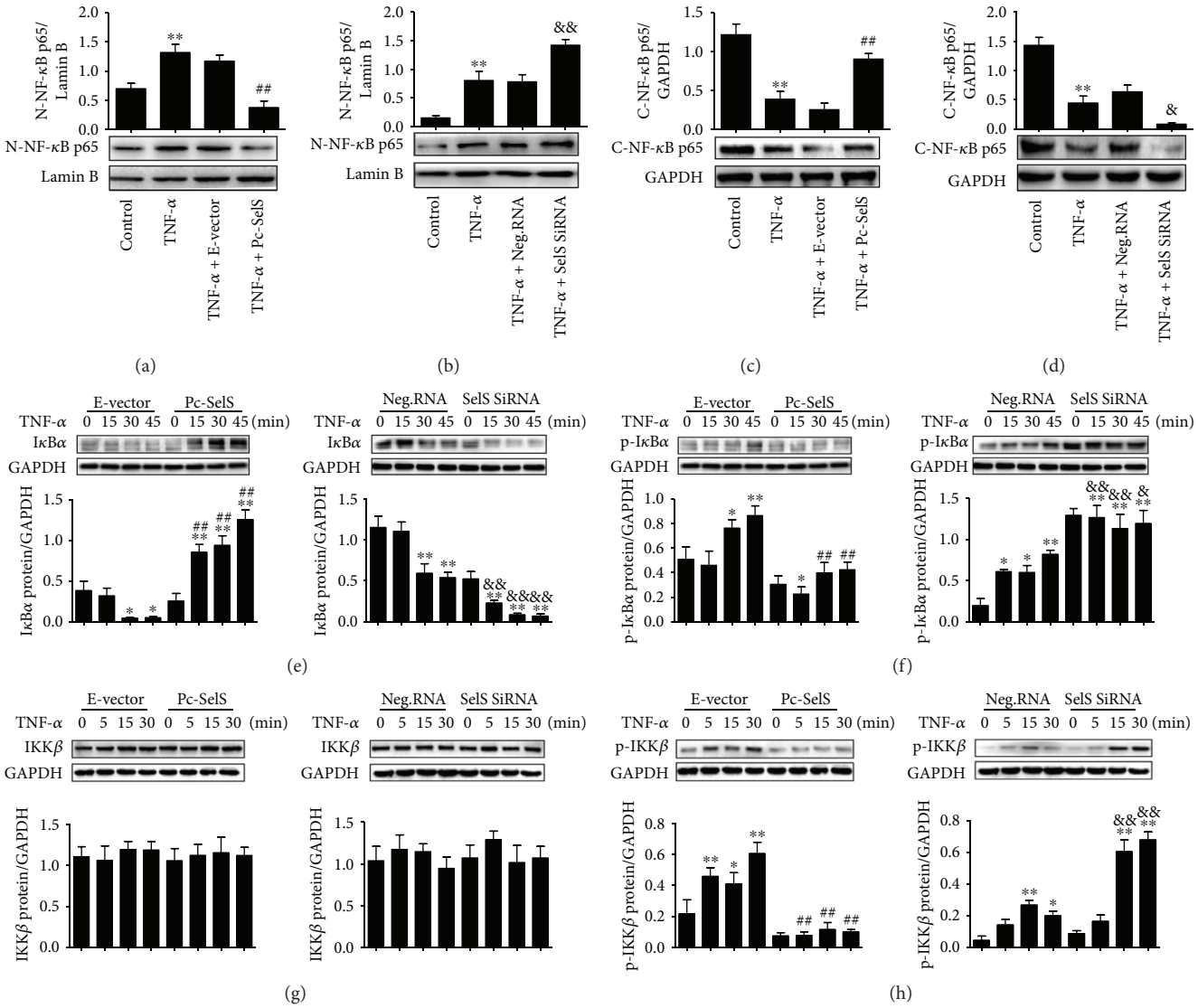

Figure 8: Effect of SelS on the NF-κB pathway. Levels of nuclear NF-κB p65 in SelS plasmid (a) or SelS siRNA (b) transfected HUVECs after 10 ng/ml TNF-α treatment, determined by the western blot. The expression of cytoplasmic NF-κB p65 in HUVECs transfected with SelS plasmid (c) or SelS siRNA (d) and treated with 10 ng/ml TNF-α. Expression of IκBα (e) and phosphorylated IκBα (f) detected in different groups at indicated time points after 10 ng/ml TNF-α induction. Levels of IKKβ (g) and phosphorylated IKKβ (h) detected in HUVECs with different treatments after 10 ng/ml TNF-α induction. The cells were transfected with pcDNA3.1-SelS recombinant plasmid or SelS siRNAs for 30 h. The results are representative of triplicate independent experiments and are presented as mean ± SD, ($n = 3$). $^{*}p < 0.05$ and $^{**}p < 0.01$ versus control; $^{\#\#}p < 0.01$ versus empty vector at corresponding time point; $^{\&}p < 0.05$ and $^{\&\&}p < 0.01$ versus negative siRNA at corresponding time points. IκBα: inhibitory kappa B α; IKKβ: inhibitor of nuclear factor kappa-B kinase β; N-NF-κB p65: nuclear NF-κB p65; C-NF-κB p65: cytoplasmic NF-κB p65; E-vector: empty vector; Pc-SelS: pcDNA3.1-SelS plasmid; Neg.RNA: negative siRNA.

in TNF-α-treated cells, revealing that TNF-α induces dysfunction through activating the NF-κB pathway. In NF-κB signaling, the p50-p65 heterodimer contributes to the regulation of the transcription of inflammatory-related factors [31]. When endothelial cells are inactive, NF-κB remains in the cell cytoplasm and the p65 subunit binds to the protein IκBα, covering the p50 subunit, which serves as the nuclear localization signal. However, when endothelial cells are stimulated by TNF-α, the phosphorylated inhibitor of IKKβ causes the phosphorylation of IκBα and detachment from NF-κB. NF-κB then migrates from the cytoplasm to the nucleus to regulate gene transcription [31]. This study demonstrated that the upregulation of SelS inhibited TNF-α-induced p65 migration from the cytoplasm to the nucleus (Figure 8). In addition, SelS reduced the levels of phosphorylated IkBα and phosphorylated IKKβ in HUVECs in a time-dependent manner, following TNF-α treatment, suggesting that SelS suppressed NF-κB translocation by regulating IKKβ/IkBα signaling pathways. Other study revealed that there are two loci bound by NF-κB in the SelS promoter region in HepG2 cells [14], which suggest that NF-κB regulates SelS genes transcription. However, in our study, SelS

overexpression regulated NF-κB translocation. By inference, we hypothesize that a feedback loop exists between SelS and NF-κB, in which NF-κB increases SelS transcription, and that conversely elevated SelS expression inhibits the excessive activation of NF-κB.

This is the first study to demonstrate that SelS could protect HUVECs from inflammatory damage by inhibiting the p38 MAPK and NF-κB pathways. Our previous studies have shown that SelS overexpression protects the endothelium from oxidative stress injury by the inhibition of H_2O_2-induced Cav-1 [25]. Another study has indicated that SelS overexpression increases the resistance of VSMCs to oxidative stress damage [13]. In addition, SelS may be associated with the pathogenesis and development of diabetic macroangiopathy [19]. In the present study, we have demonstrated that SelS attenuates endothelial dysfunction via the inhibition of inflammatory responses. These results elucidate the mechanism of SelS function in vascular protection. SelS may be considered as a clinical predictive biomarker or a therapeutic option for vascular diseases associated with endothelial dysfunction.

5. Conclusion

In summary, we have shown that the upregulation of SelS improves the viability of endothelial cells, enhances the levels of NO and eNOS, reduces the production of ET-1 and ROS, and inhibits the adhesion of TNF-α-induced THP-1 cells to endothelial cells. SelS overexpression also reduces the expression of ICAM-1, VCAM-1, MCP-1, IL-8, IL-6, and IL-1β mediated by TNF-α. In addition, the upregulation of SelS inactivates TNF-α-induced NF-κB and p38 MAPK pathways, while the knockdown of SelS leads to an enhancement of inflammatory damage to endothelial cells. Moreover, a feedback signaling may exist between SelS and NF-κB, and the overexpression of SelS attenuates TNF-α-induced endothelial dysfunction by inhibiting the p38 MAPK and NF-κB pathways in HUVECs.

Abbreviations

AS: Atherosclerosis
AP-1: Activator protein-1
CCK-8: Cell count kit-8
Cav-1: Caveolin-1
CAM: Caldesmon
ET-1: Endothelin-1
eNOS: Endothelial nitric oxide synthase
IL-1β: Interleukin-1β
IL-6: Interleukin-6
IL-8: Interleukin-8
ICAM-1: Intercellular adhesion molecule-1
IκBα: Inhibitory kappa B α
IKKβ: Inhibitory kappa B kinase β
NO: Nitric oxide
NF-κB: Nuclear factor-κB
p38 MAPK: p38 mitogen-activated protein kinase
ROS: Reactive oxygen species
SelS: Selenoprotein S
SNP: Single nucleotide polymorphism
siRNA: Small interfering RNA
TNF-α: Tumour necrosis factor-alpha
VSMCs: Vascular smooth muscle cells
VCAM-1: Vascular cell adhesion molecule-1.

Conflicts of Interest

The authors declare that they have no competing interests.

Authors' Contributions

Jianling Du and Siyuan Cui designed the project. Siyuan Cui and Lili Men performed all experiments. Yingshuo Zhong and Fang Li analyzed the data. Siyuan Cui, Yu Li, and Shanshan Yu wrote the manuscript. Jianling Du and Fang Li instructed the experiments and improved the manuscript. All authors read and approved the final manuscript. Siyuan Cui and Lili Men contributed equally to this work.

Acknowledgments

This work was supported by two grants from the National Natural Science Foundation of China (NSFC) (nos. 30970841 and 81570727) and one grant from the Natural Science Foundation of Liaoning Province (no. 2015020290).

Supplementary Materials

Table S1: the sequences of SelS siRNAs and negative siRNA are shown. The sequences of SelS siRNA 1, SelS siRNA 2, SelS siRNA 3, and negative siRNA are listed in Table S1. The SelS siRNAs were used for SelS knockdown and the negative siRNA was used as a control in liposome transfection experiments. Table S2: the specific primers for RT-qPCR are shown. The sequences of specific primers such as SelS, GAPDH, eNOS, ET-1, ICAM-1, VCAM-1, IL-6, IL-1β, MCP-1, and IL-8 are listed in Table S2. The primers were used for RT-qPCR experiments to test gene mRNA levels. The reactions were incubated initially at 95°C for 30 sec, 95°C for 5 sec, and 60°C for 30 sec of 35 cycles and were carried out with a PCR System 9700 (Applied Biosystems, USA). The relative expression of mRNA was determined using GAPDH as an internal control. Figure S1: the dissolve and amplification curves are shown in RT-qPCR experiments. The dissolve and amplification curves of RT-qPCR experiments are listed in Figure S1. The left part of the figure is shown as amplification curves and the right part of the figure is shown as dissolve curves in the RT-qPCR experiments. The curves could reflect the accuracy, credibility, and authenticity of the results. Figure S2: the transfection with pcDNA3.1-SelS recombinant plasmid or SelS siRNA is identified in Figure 3 listed experiments. (a) pcDNA3.1-SelS plasmid transfection and (b) SelS siRNA transfection using in cell viability experiment were determined by western blot. (c) The transfection with pc-SelS plasmid and (d) transfection with SelS siRNA using in NO measurement were tested by western blot. (e) The pc-SelS plasmid transfection or (f) SelS siRNA transfection in eNOS mRNA testing was determined by RT-qPCR. *(Supplementary Materials)*

References

[1] M. A. Gimbrone Jr and G. García-Cardeña, "Endothelial cell dysfunction and the pathobiology of atherosclerosis," *Circulation Research*, vol. 118, no. 4, pp. 620–636, 2016.

[2] C. M. Sena, A. M. Pereira, and R. Seiça, "Endothelial dysfunction—a major mediator of diabetic vascular disease," *Biochimica et Biophysica Acta (BBA) - Molecular Basis of Disease*, vol. 1832, no. 12, pp. 2216–2231, 2013.

[3] M. Butt, G. Dwivedi, A. Blann, O. Khair, and G. Y. H. Lip, "Endothelial dysfunction: methods of assessment & implications for cardiovascular diseases," *Current Pharmaceutical Design*, vol. 16, no. 31, pp. 3442–3454, 2010.

[4] G. Favero, C. Paganelli, B. Buffoli, L. F. Rodella, and R. Rezzani, "Endothelium and its alterations in cardiovascular diseases: life style intervention," *BioMed Research International*, vol. 2014, Article ID 801896, 28 pages, 2014.

[5] C. M. Steyers 3rd and F. J. Miller Jr, "Endothelial dysfunction in chronic inflammatory diseases," *International Journal of Molecular Sciences*, vol. 15, no. 12, pp. 11324–11349, 2014.

[6] M. Naya, T. Tsukamoto, K. Morita et al., "Plasma interleukin-6 and tumor necrosis factor-α can predict coronary endothelial dysfunction in hypertensive patients," *Hypertension Research*, vol. 30, no. 6, pp. 541–548, 2007.

[7] L. Brånén, L. Hovgaard, M. Nitulescu, E. Bengtsson, J. Nilsson, and S. Jovinge, "Inhibition of tumor necrosis factor-α reduces atherosclerosis in apolipoprotein E knockout mice," *Arteriosclerosis, Thrombosis, and Vascular Biology*, vol. 24, no. 11, pp. 2137–2142, 2004.

[8] H. Zhang, Y. Park, J. Wu et al., "Role of TNF-α in vascular dysfunction," *Clinical Science*, vol. 116, no. 3, pp. 219–230, 2009.

[9] F. Grover-Páez and A. B. Zavalza-Gómez, "Endothelial dysfunction and cardiovascular risk factors," *Diabetes Research and Clinical Practice*, vol. 84, no. 1, pp. 1–10, 2009.

[10] Y. Matsuzawa, R. R. Guddeti, T. G. Kwon, L. O. Lerman, and A. Lerman, "Treating coronary disease and the impact of endothelial dysfunction," *Progress in Cardiovascular Diseases*, vol. 57, no. 5, pp. 431–442, 2015.

[11] Y. Ye, Y. Shibata, C. Yun, D. Ron, and T. A. Rapoport, "A membrane protein complex mediates retro-translocation from the ER lumen into the cytosol," *Nature*, vol. 429, no. 6994, pp. 841–847, 2004.

[12] S. Du, H. Liu, and K. Huang, "Influence of SelS gene silence on β-mercaptoethanol-mediated endoplasmic reticulum stress and cell apoptosis in HepG2 cells," *Biochimica et Biophysica Acta (BBA) - General Subjects*, vol. 1800, no. 5, pp. 511–517, 2010.

[13] Y. Ye, F. Fu, X. Li, J. Yang, and H. Liu, "Selenoprotein S is highly expressed in the blood vessels and prevents vascular smooth muscle cells from apoptosis," *Journal of Cellular Biochemistry*, vol. 117, no. 1, pp. 106–117, 2016.

[14] Y. Gao, N. R. F. Hannan, S. Wanyonyi et al., "Activation of the selenoprotein SEPS1 gene expression by pro-inflammatory cytokines in HepG2 cells," *Cytokine*, vol. 33, no. 5, pp. 246–251, 2006.

[15] Y. Gao, K. Walder, T. Sunderland et al., "Elevation in Tanis expression alters glucose metabolism and insulin sensitivity in H4IIE cells," *Diabetes*, vol. 52, no. 4, pp. 929–934, 2003.

[16] K. Walder, L. Kantham, J. S. McMillan et al., "Tanis: a link between type 2 diabetes and inflammation?," *Diabetes*, vol. 51, no. 6, pp. 1859–1866, 2002.

[17] J. Zeng, S. Du, J. Zhou, and K. Huang, "Role of SelS in lipopolysaccharide-induced inflammatory response in hepatoma HepG2 cells," *Archives of Biochemistry and Biophysics*, vol. 478, no. 1, pp. 1–6, 2008.

[18] N. Fradejas, C. del Carmen Serrano-Pérez, P. Tranque, and S. Calvo, "Selenoprotein S expression in reactive astrocytes following brain injury," *Glia*, vol. 59, no. 6, pp. 959–972, 2011.

[19] S. Yu, L. Men, J. Wu et al., "The source of circulating selenoprotein S and its association with type 2 diabetes mellitus and atherosclerosis: a preliminary study," *Cardiovascular Diabetology*, vol. 15, no. 1, p. 70, 2016.

[20] T. Bian, H. Li, Q. Zhou, C. Ni, Y. Zhang, and F. Yan, "Human β-defensin 3 reduces TNF-α-induced inflammation and monocyte adhesion in human umbilical vein endothelial cells," *Mediators of Inflammation*, vol. 2017, Article ID 8529542, 11 pages, 2017.

[21] H.-J. Wang, Y.-L. Huang, Y.-Y. Shih, H.-Y. Wu, C.-T. Peng, and W.-Y. Lo, "MicroRNA-146a decreases high glucose/thrombin-induced endothelial inflammation by inhibiting NAPDH oxidase 4 expression," *Mediators of Inflammation*, vol. 2014, Article ID 379537, 12 pages, 2014.

[22] M. Siragusa and I. Fleming, "The eNOS signalosome and its link to endothelial dysfunction," *Pflügers Archiv*, vol. 468, no. 7, pp. 1125–1137, 2016.

[23] C. Dessy, O. Feron, and J. L. Balligand, "The regulation of endothelial nitric oxide synthase by caveolin: a paradigm validated in vivo and shared by the 'endothelium-derived hyperpolarizing factor'," *Pflügers Archiv*, vol. 459, no. 6, pp. 817–827, 2010.

[24] W. Kwok and M. G. Clemens, "Targeted mutation of Cav-1 alleviates the effect of endotoxin in the inhibition of ET-1-mediated eNOS activation in the liver," *Shock*, vol. 33, no. 4, pp. 392–398, 2010.

[25] Y. Zhao, H. Li, L. L. Men et al., "Effects of selenoprotein S on oxidative injury in human endothelial cells," *Journal of Translational Medicine*, vol. 11, no. 1, p. 287, 2013.

[26] H. N. Siti, Y. Kamisah, and J. Kamsiah, "The role of oxidative stress, antioxidants and vascular inflammation in cardiovascular disease (a review)," *Vascular Pharmacology*, vol. 71, pp. 40–56, 2015.

[27] F. Böhm and J. Pernow, "The importance of endothelin-1 for vascular dysfunction in cardiovascular disease," *Cardiovascular Research*, vol. 76, no. 1, pp. 8–18, 2007.

[28] X. Sun, S. Kumar, S. Sharma et al., "Endothelin-1 induces a glycolytic switch in pulmonary arterial endothelial cells via the mitochondrial translocation of endothelial nitric oxide synthase," *American Journal of Respiratory Cell and Molecular Biology*, vol. 50, no. 6, pp. 1084–1095, 2014.

[29] R. Zenz, R. Eferl, C. Scheinecker et al., "Activator protein 1 (Fos/Jun) functions in inflammatory bone and skin disease," *Arthritis Research & Therapy*, vol. 10, no. 1, p. 201, 2008.

[30] J. F. Schindler, J. B. Monahan, and W. G. Smith, "p38 pathway kinases as anti-inflammatory drug targets," *Journal of Dental Research*, vol. 86, no. 9, pp. 800–811, 2007.

[31] I. Pateras, C. Giaginis, C. Tsigris, E. Patsouris, and S. Theocharis, "NF-κB signaling at the crossroads of inflammation and atherogenesis: searching for new therapeutic links," *Expert Opinion on Therapeutic Targets*, vol. 18, no. 9, pp. 1089–1101, 2014.

Hindawi
Mediators of Inflammation
Volume 2018, Article ID 2784701, 9 pages
https://doi.org/10.1155/2018/2784701

Research Article

Oxysterols Increase Inflammation, Lipid Marker Levels and Reflect Accelerated Endothelial Dysfunction in Experimental Animals

Tomasz Wielkoszyński,[1] **Jolanta Zalejska-Fiolka**,[1] **Joanna K. Strzelczyk**,[2] **Aleksander J. Owczarek**,[3] **Armand Cholewka**,[4] **Marcin Furmański**,[1] **and Agata Stanek**[5]

[1]*Department of Biochemistry, School of Medicine with the Division of Dentistry in Zabrze, Medical University of Silesia, Jordana 19, 41-808 Zabrze, Poland*
[2]*Department of Medical and Molecular Biology, School of Medicine with the Division of Dentistry in Zabrze, Medical University of Silesia, Jordana 19, 41-808 Zabrze, Poland*
[3]*Department of Statistics, Department of Instrumental Analysis, School of Pharmacy with the Division of Laboratory Medicine, Medical University of Silesia, Ostrogórska 30, Sosnowiec 41-209, Poland*
[4]*Department of Medical Physics, Chelkowski Institute of Physics, University of Silesia, Uniwersytecka 4, 40-007 Katowice, Poland*
[5]*Department of Internal Medicine, Angiology and Physical Medicine, School of Medicine with the Division of Dentistry in Zabrze, Medical University of Silesia, Batorego 15, 41-902 Bytom, Poland*

Correspondence should be addressed to Agata Stanek; astanek@tlen.pl

Received 17 December 2017; Accepted 15 January 2018; Published 11 March 2018

Academic Editor: Adrian Doroszko

Objective. Oxidized cholesterol derivatives are thought to exert atherogenic effect thus adversely affecting vascular endothelium. The aim of the study was to assess the effect of 5*α*,6*α*-epoxycholesterol on experimentally induced hypercholesterolemia in rabbits, and the levels of homocysteine (HCY), asymmetric dimethylarginine (ADMA), paraoxonase-1 (PON-1), and inflammatory parameters (IL-6, TNF-*α*, CRP). *Material and methods*. The rabbits were divided into 3 groups, 8 animals each, and fed with basic fodder (C), basic fodder plus cholesterol (Ch) or basic fodder plus 5*α*,6*α*-epoxycholesterol, and unoxidized cholesterol (ECh). Serum concentrations of studied parameters were determined at 45-day intervals. The study was continued for six months. *Results*. We demonstrated that adding 5*α*,6*α*-epoxycholesterol to basic fodder significantly affected lipid status of the experimental animals, increasing total cholesterol and LDL cholesterol levels, as well as HCY and ADMA levels, whilst leaving the PON-1 activity unaffected. Additionally, the ECh group presented with significantly higher concentrations of inflammatory biomarkers (IL-6, TNF-*α*, and CRP). In the Ch group, lower yet significant (as compared to the C group) changes of levels of studied parameters were observed. *Conclusion*. Exposure of animals with experimentally induced hypercholesterolemia to 5*α*,6*α*-epoxycholesterol increases dyslipidaemia, endothelial dysfunction, and inflammatory response.

1. Introduction

Cardiovascular disease (CVD) is the leading cause of death in Europe and the United States. Heart disease, stroke, and hypertension are currently recognized to be caused, in part, by arterial endothelial dysfunction. Endothelial dysfunction may occur much earlier than the clinical manifestation of cardiovascular diseases [1].

A healthy vascular endothelium remains in a tightly regulated balance between pro and antioxidants, vasodilators and vasoconstrictors, pro and anti-inflammatory molecules, and pro and antithrombotic signals. Dysfunctional endothelium, though, displays prooxidant, vasoconstrictor, proinflammatory, and prothrombotic properties [1–3].

Oxysterols are cholesterol oxidation products formed through enzymatic or autoxidation mechanisms. They

may be originally present in food containing animal fat, but they are chiefly generated during food storing and cooking. These compounds show a biochemical reactivity that is one or even two orders of magnitude higher than that of the parent compound. Furthermore, unlike cholesterol, oxysterols are able to permeate through lipophilic membranes [4, 5].

Oxysterols can affect many cellular functions and influence various physiological processes (e.g., cholesterol metabolism, membrane fluidity regulation, and intracellular signaling pathways). They are implicated in a number of pathologies, including type 2 diabetes mellitus, neurodegenerative diseases, inflammatory bowel disease, or degenerative changes within the retina. It has also been suggested that oxysterols may play a role in malignancies such as breast, prostate, colon, and bile duct cancer [5–7]. Furthermore, it has been postulated that oxysterols may play a role in atherosclerosis [8, 9].

In light of such findings, the primary aim of the study was to assess the effect of dietary oxysterols on vascular endothelium.

2. Material and Methods

2.1. Animals. The protocol was approved by the Bioethical Committee for Animal Experimentation of the Medical University of Silesia in Katowice, Poland (approval number 27/2007, dated April 17th 2007). All animals received humane care in compliance with the 8th edition of the *Guide for the Care and Use of Laboratory Animals* published by the National Institute of Health [10].

Twenty-four male Chinchilla rabbits (b.m. 2870 ± 20 g) were obtained from the Center for Experimental Medicine, Medical University of Silesia in Katowice. The animals were housed individually in stainless steel metabolic cages under a 12-hour light/dark cycle. The rabbits were fed proper fodder (80 g/kg) once a day, allowed unlimited access to water, and weighed at 45-day intervals.

The rabbits were divided into three groups of eight animals each, according to the following scheme:

(1) Control group (C): rabbits fed only a basal diet (BD)

(2) Cholesterol group (Ch): rabbits fed BD with 0.5% cholesterol, 5% sunflower oil, and 2% porcine lard

(3) Oxidized cholesterol group (ECh): rabbits fed BD with 5α,6α-epoxycholesterol acetate equal to 250 mg free 5α,6α-epoxycholesterol/kg BD, 0.5% cholesterol, 5% sunflower oil and 2% porcine lard. Daily estimated dose of oxysterol in ECh group was about 10–15 mg/kg

The specific diets for each group were prepared weekly and stored in a freezer at −20°C. The BD was composed of 24% protein, 69% carbohydrate, and 7% fat of the total energy content of the diet. Groups fed BD with cholesterol (Ch group) and 5α,6α-epoxycholesterol (ECh group) received 19% of energy from proteins, 42% from carbohydrates, and 39% from fat, respectively. The current study was continued for six months.

2.2. Synthesis of 5α,6α-Epoxycholesterol Acetate. 5α,6α-Epoxycholesterol acetate was synthetized from cholesterol acetate (Sigma-Aldrich, USA) by oxidation with m-chloroperoxybenzoic acid (Sigma-Aldrich, USA) as described by McCarthy [11]. Next, oxidation product mixture was purified by column chromatography on silica gel with the use of chloroform-acetone (4 : 1, *v*/*v*) as mobile phase. Fractions containing pure ester were controlled by TLC technique (silica gel plates, solvent as above), pooled, and dried under vacuum.

2.3. Blood Sample Collection. At the beginning of experiment (following the acclimatization period) and at 45-day intervals thereafter, 10 mL blood samples were collected from ear veins of each animal to plain and EDTA tubes (Sarstedt, S-Monovette) in a total of six samplings. For serum preparation, samples were allowed to clot and centrifuge (15 min, 1500 *g*). The serum was analyzed instantly (lipid parameters and PON-1 activity) or stored deep frozen at −75°C (other assays). Plasma from EDTA tubes was separated immediately after sampling (15 min, 1500 g, 4°C) and stored at −75°C.

2.4. Biochemical Analyses

2.4.1. Lipid Profile Parameters Concentrations. Total cholesterol and triacylglycerol concentrations were assayed using a standard enzymatic method (Emapol, Poland). HDL cholesterol was determined using an enzymatic method after precipitation of other lipoproteins with phosphotungstic acid (Emapol, Poland). For LDL cholesterol assay, QUANTOLIP LDL kit (Technoclone, Austria) was used. All analyses were performed using the EM280 biochemical analyzer (Emapol, Poland). Interassay and intra-assay coefficients of variation (CV) were below 3% and 5%, respectively, for all parameters.

2.4.2. Endothelial Dysfunction Markers

(1) Total Homocysteine Concentration. Total homocysteine (tHCY) plasma concentration was estimated using the HPLC method with spectrofluorimetric detection according to Kuo et al. [12] and Minniti et al. [13]. HPLC separations were conducted on LC-10ATVP chromatograph (Shimadzu, Japan) equipped with RF-10AXL detector (Shimadzu, Japan) and SUPELCOSIL RP-18 column (4.6 x 150 mm, 5 μm, Supelco, USA). Inter and intra-assay coefficients (CV) of variation were 7.7% and 11.2%, respectively.

(2) Asymmetric Dimethylarginine Concentration. Asymmetric dimethylarginine (ADMA) plasma concentration was determined using the HPLC method as described previously [14, 15]. Assays were performed on Nucleosil Phenyl column (25×4.6 mm; 7 μm; Supelco, USA) and Shimadzu chromatograph with spectrofluorimetric detector (as described above). Inter and intra-assay coefficients (CV) of variation were 7.2% and 10.9%, respectively.

(3) Paraoxonase-1 Activity. Paraoxonase-1 (PON-1) serum activity was assayed using the kinetic method with paraoxon (*o*,*o*-diethyl-*o*-(*p*-nitrophenyl)-phosphate; Sigma, USA) as a substrate [16]. Determinations were performed at 37°C on TECHNICON RA-XT™ analyzer (Technicon Instruments

Corporation, USA). For cholinesterase inactivation, physostigmine salicylate (eserine) was added to serum samples prior to the assay. One unit (1 IU) of PON-1 is the amount of enzyme sufficient to decompose 1 micromole of substrate per minute under testing conditions. Inter and intra-assay coefficients (CV) of variation were 2.6% and 4.4%, respectively.

2.4.3. Inflammatory Markers

(1) C-Reactive Protein Concentration. C-reactive protein (CRP) serum concentration was determined using ELISA assay with use the immunoaffinity purified, hen antirabbit CRP antibody as a capture antibody, rabbit CRP reference serum as a standard, and biotinylated CCRP-15A-Z antibody (all reagents were from Immunology Consultants Laboratory Inc., USA) along with streptavidin-horseradish peroxidase conjugate (DakoCytomation, Denmark) for the immunocomplex detection. Inter and intra-assay coefficients of variation were 5% and 7.6%, respectively.

(2) Tumor Necrosis Factor α Concentration. The concentration of rabbit tumor necrosis factor α (TNF-α) in serum was measured using ELISA method with goat antirabbit TNF-α antibody as a capture antibody, biotinylated, monoclonal antirabbit TNF-α antibody (both from BD PharMingen, USA), and streptavidin-horseradish peroxidase conjugate (DakoCytomation, Denmark) as a tracer. The assay was performed according to the manufacturer's instruction and calibrated with the use of rabbit TNF-α (BD PharMingen, USA). Results were presented as pg of TNF-α per mL of serum [pg/mL]. Inter and intra-assay coefficients of variation were 6.4% and 8.9%, respectively.

2.5. Statistical Analyses. Statistical analysis was performed using STATISTICA 10.0 PL (StatSoft, Poland, Cracow) and StataSE 12.0 (StataCorp LP, TX, U.S.) bundles and R software. p value below 0.05 was considered as statistically significant. All tests were two tailed. Imputations were not done for missing data. Nominal and ordinal data were expressed as percentages, whilst interval data were expressed as mean value ± standard deviation if normally distributed or as median/interquartile range if the distribution was skewed or nonnormal. Distribution of variables was evaluated by the Shapiro–Wilk test and homogeneity of variances was assessed using the Levene test. The comparisons were made using one-way parametric ANOVA with Tukey's posthoc test and one-way repeated measures ANOVA with contrast analysis as a posthoc test.

3. Results

3.1. Animal Body Weight. The analysis of animal body weight during the experiment demonstrated a statistically significant growth inhibition in a group fed with 5α,6α-epoxycholesterol acetate (ECh group) as compared to the control group. There were no significant profile differences between the C and Ch groups. Figure 1 shows measurement results, and Table 1 shows the result of statistical analyses for the studied variables.

3.2. Lipid Profile Parameters. Changes in total cholesterol and LDL cholesterol during the experimental exposure to oxysterols and cholesterol demonstrated significant differences in concentration increase rates between the groups of experimental animals. The fastest concentration increase was seen in the group fed with both 5α,6α-epoxycholesterol and cholesterol (ECh group). Total cholesterol and LDL cholesterol levels in this group reached the plateau on day 90 and remained unchanged thereafter. In a group fed with BD and cholesterol only (Ch group), the concentration of the markers in question increased at a slower rate to eventually settle at a lower level. The total cholesterol and LDL cholesterol concentration profiles in ECh group differed significantly from those of the Ch group (see Figure 1 and Table 1). Together, ECh and Ch groups had significantly higher levels of total cholesterol and LDL cholesterol as compared to the control group (C), where there was no change in these parameters throughout the entire experiment.

The HDL cholesterol levels tended to increase in both cholesterol-fed groups (ECh and Ch groups). The highest increase of HDL cholesterol levels was noted in a group fed with cholesterol-rich diet without oxysterols (Ch group). Furthermore, there was a significant difference in HDL cholesterol profile between ECh and Ch groups. The analysis of HDL cholesterol concentration as a percentage of total cholesterol did not demonstrate changes between the group exposed to oxysterols and cholesterol versus the group exposed to native cholesterol only (Figure 1 and Table 1).

Triacylglycerol levels varied in a nonspecific way with no significant differences between the groups. There was a significant variability between the individual time points (collections). In a control group, triacylglycerol level at the end of the experiment was significantly lower than the baseline value, whereas in the two remaining groups, there were no significant differences between the baseline and final levels (Figure 1 and Table 1).

3.3. Endothelial Dysfunction Markers. The analysis of changes in total plasma tHCY concentration in rabbits demonstrated an increase tendency in a control group and a marked significant increase in both cholesterol-fed groups. The highest increase was observed in a group exposed additionally to 5α,6α-epoxycholesterol. The tHCY levels in this group differed significantly from the only cholesterol-fed group (Ch group) or the control group (Figure 2, Table 1).

Similar observations were made for plasma ADMA in rabbits. The highest rate of ADMA concentration increase was seen in ECh (Figure 2, Table 1).

Serum PON-1 activity in rabbits dropped significantly as a result of exposure to dietary cholesterol. However, there was no additional modulation of its activity by oxysterols, as PON-1 levels decreased in the same manner in both ECh group, exposed to oxycholesterol, and Ch group, exposed to cholesterol. Figure 2 shows PON-1 activity at subsequent time points, and Table 1 shows statistical analysis of these results.

3.4. Inflammatory Markers. The analysis of changes in inflammatory marker concentrations during experimental

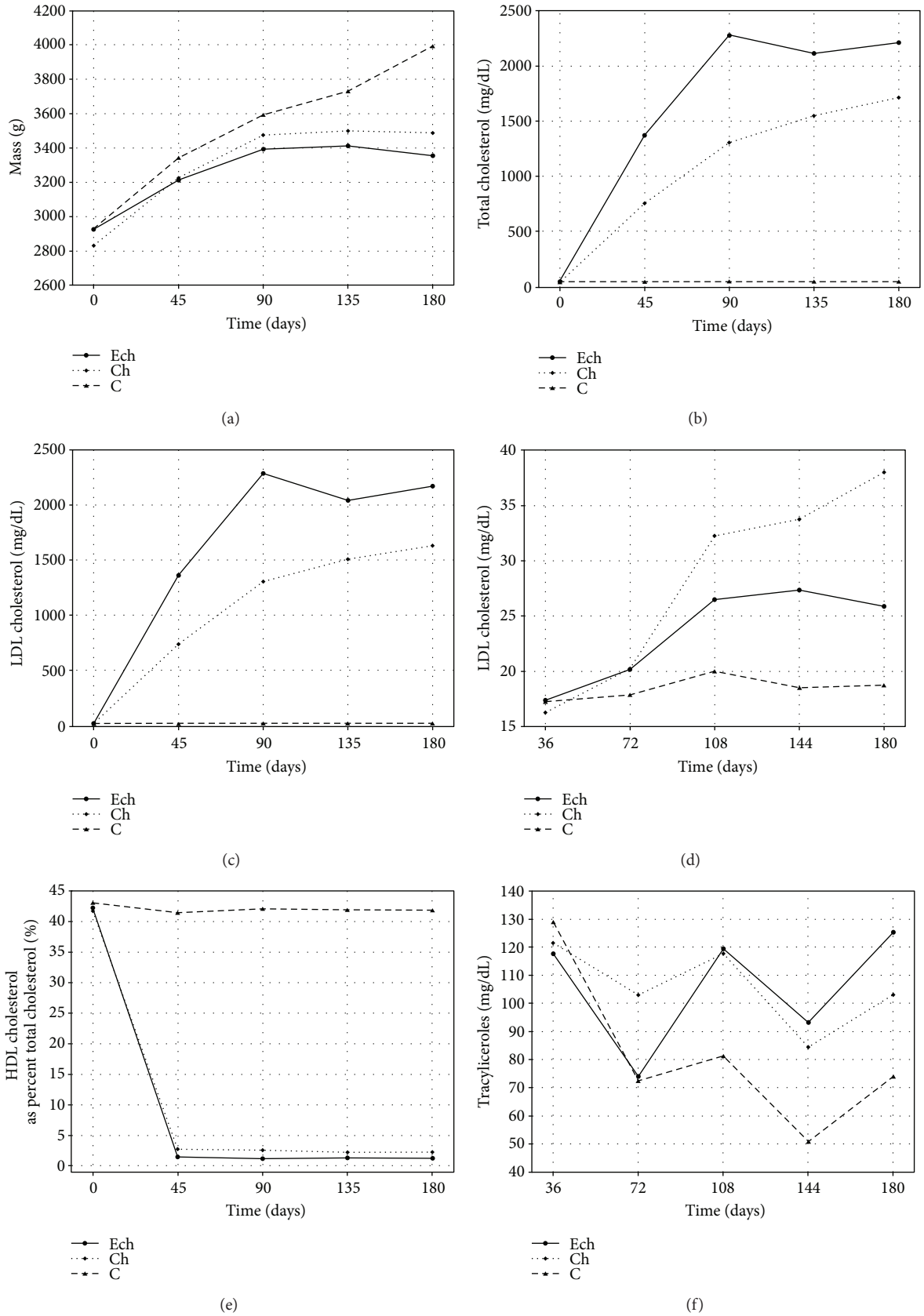

Figure 1: Time's profile of body weight and concentrations of total cholesterol, LDL cholesterol, HDL cholesterol, HDL cholesterol as a percentage of total cholesterol (% HDL), and triacylglycerols in rabbits exposed to 5α,6α-epoxycholesterol and cholesterol (ECh group), cholesterol (Ch group), and fed with basal diet (C group).

Table 1: Results of ANOVA analysis of parameters between groups and inside each group (between first and last sampling).

Parameter	Body mass	Total cholesterol	LDL cholesterol	HDL cholesterol	HDL cholesterol as percent of total cholesterol	Triacylglycerols	tHCY	ADMA	PON-1	IL-6	TNF-α	CRP
Differences between groups for all sampling (*p values)*												
C–ECh	<0.05	<0.001	<0.001	<0.01	<0.001	<0.05	<0.001	<0.001	NS	<0.001	<0.001	<0.001
C–Ch	NS	<0.001	<0.001	<0.001	<0.001	<0.05	<0.05	<0001	<0.01	<0.001	<0.001	<0.001
ECh–Ch	NS	<0.001	<0.001	<0.01	NS	NS	<0.01	<0.001	NS	<0.001	<0.001	NS
Differences inside each group between 0 day and 180 day (*p values)*												
Ech	<0.001	<0.001	<0.001	<0.01	<0.001	NS	<0.001	<0.001	<0.001	<0.001	<0.001	<0.001
Ch	<0.001	<0.001	<0.001	<0.001	<0.001	NS	<0.001	<0.001	<0.001	<0.05	<0.001	<0.001
C	<0.001	NS	NS	NS	NS	<0.001	NS	NS	NS	NS	NS	NS

NS: nonstatistically significant.

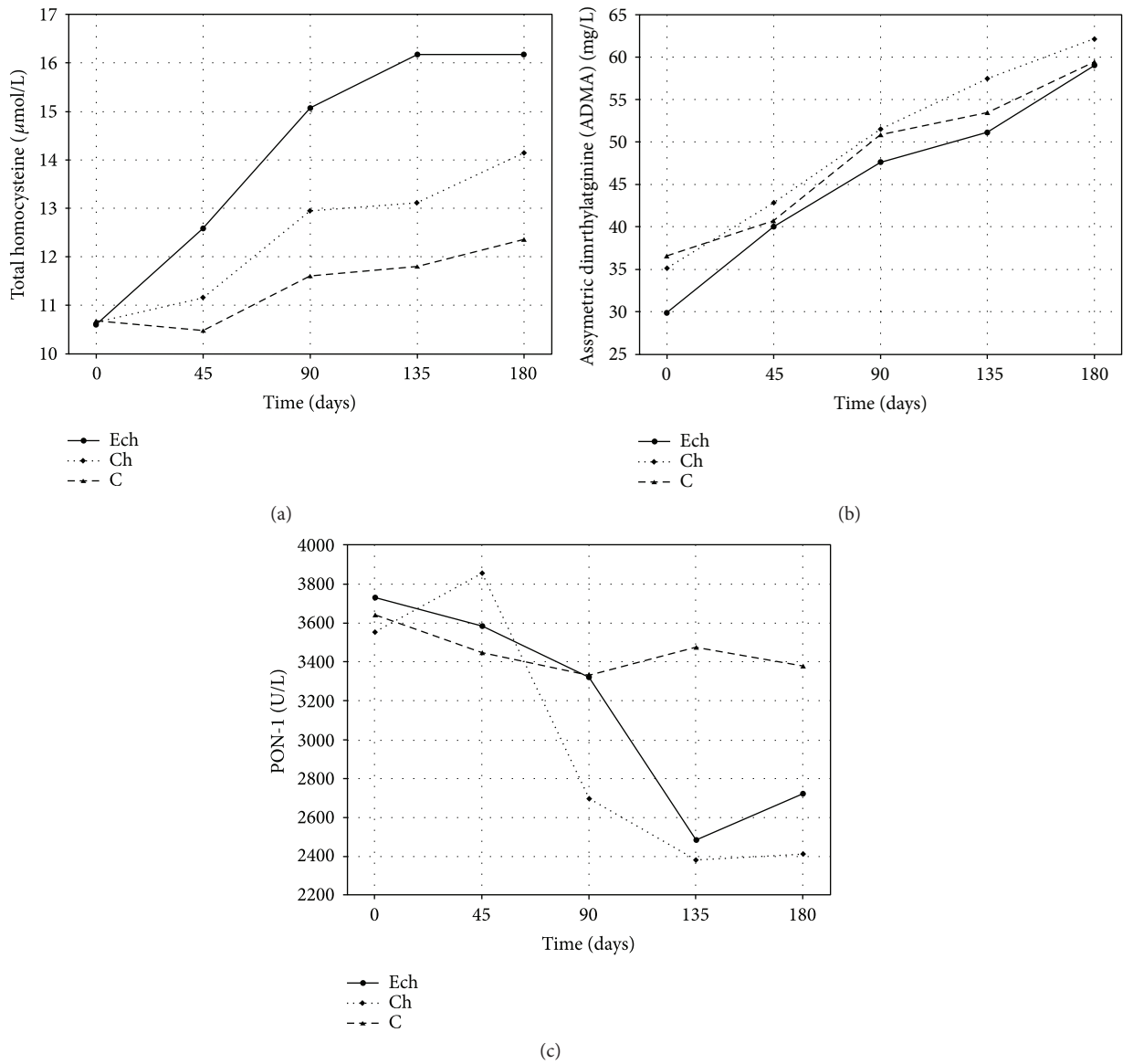

Figure 2: Time's profile of concentrations of total homocysteine (tHCY), asymmetric dimethylarginine (ADMA), and paraoxonase-1 (PON-1) activity in rabbits exposed to 5α,6α-epoxycholesterol and cholesterol (ECh group), cholesterol (Ch group), and fed with basal diet (C group).

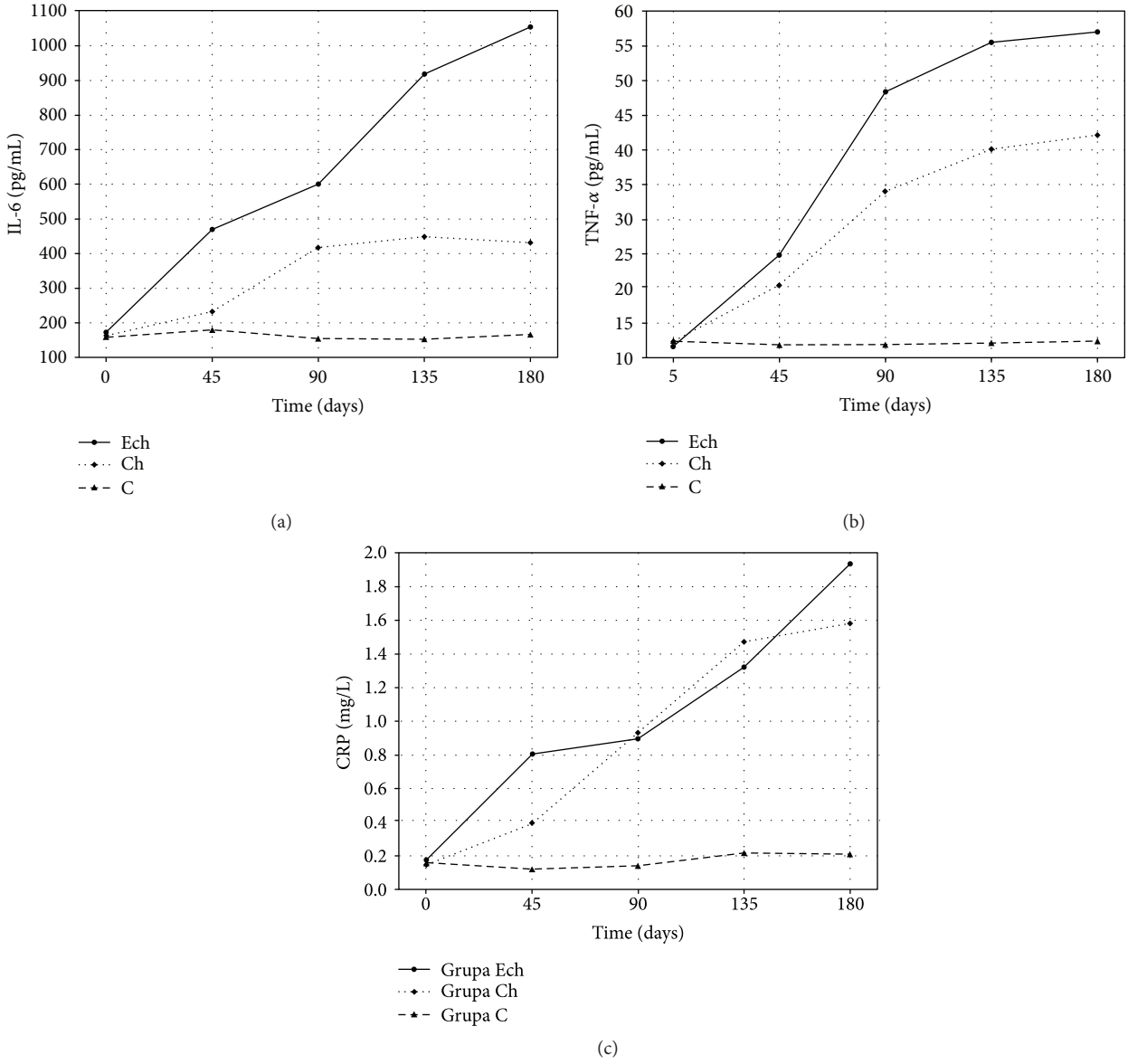

Figure 3: Time's profile of concentrations of IL-6, TNF-α, and C-reactive protein (CRP) in rabbits exposed to 5α,6α-epoxycholesterol and cholesterol (ECh group), cholesterol (Ch group), and fed with basal diet (C group).

rabbit exposure to cholesterol and its epoxy derivatives demonstrated activation of acute phase response in studied animals (see Figure 3 and Table 1). Changes in IL-6 levels demonstrated a significant increase in its production following an exposure to 5α,6α-epoxycholesterol as compared to exposure to native cholesterol or basal diet. Its increase rate and the ultimate level achieved in month 6 in the ECh group were significantly higher than in the Ch and C groups, respectively.

A similar pattern was observed for the serum TNF-α concentration during the experimental exposure to epoxycholesterol. The highest concentrations were achieved in animals exposed to 5α,6α-epoxycholesterol and cholesterol-rich fodder. The TNF-α profile in the ECh group significantly differed to the one of the control group and the group receiving cholesterol-rich fodder (Ch). Although the cytokine in question was also biosynthesized in the Ch group, the increase rate and the ultimate TNF-α level were significantly lower than in the ECh group.

The serum CRP concentration increased in a similar manner in both groups exposed to cholesterol. The CRP profiles of ECh and Ch groups were significantly different to the one of the control group. There was no significant difference in CRP profiles between the ECh and Ch groups (see Figure 3 and Table 1).

4. Discussion

The results achieved during the current study demonstrated changes in the lipid parameters, endothelial dysfunction

markers (tHCY, ADMA, and PON-1), and selected inflammatory markers in rabbits fed with cholesterol-rich diet with added oxidized cholesterol derivatives for 6 months. The concentrations of all these markers were assessed several times at 45-day interval, which undoubtedly adds value to the current study, as the experiments reported so far provided only baseline and end concentrations of these parameters. Having reviewed the available literature, we failed to identify a study to assess changes in serum biochemical markers during exposure to cholesterol-rich diet and oxysterols.

In our research, we found total cholesterol and LDL cholesterol levels in rabbits fed with cholesterol-rich diet increased several dozenfold, with the highest increase observed in a group of animals fed with both cholesterol and 5α,6α-epoxycholesterols. Both total cholesterol and LDL cholesterol levels in this group of animals were significantly higher than in those fed with unoxidized cholesterol. Therefore, adding 5α,6α-epoxycholesterols to the fodder increased plasma levels of total cholesterol and LDL cholesterol. The study by Mahfouz et al. [17] did not confirm that replacing native cholesterol with autooxidized cholesterol leads to changes in the plasma lipid profile. The mechanisms leading to these observable changes in plasma cholesterol levels are difficult to explain, especially that most published data support inhibition by oxysterols of HMG-CoA reductase activity, which should be reflected in decreased biosynthesis of endogenous cholesterol. On the other hand, it can be hypothesized that endogenous cholesterol in plasma of rabbits with experimentally induced hypercholesterolemia constitutes only a small share of total amount of cholesterol, so it is bioavailability (intestinal absorption and excretion) of exogenous, dietary cholesterol, which mainly affects the blood concentration. Another possible explanation is that 5α,6α-epoxycholesterols exert their effect at the stage of intestinal absorption, as with the unchanged plasma levels of biliary acids (unpublished data), slowing of cholesterol metabolite elimination appears less likely mechanism contributing to increasing hypercholesterolaemia [18].

The analysis of changes in HDL cholesterol levels in rabbit serum demonstrated that absolute concentrations of this fraction increased heterogeneously in the groups exposed to cholesterol, with the highest increase observed in the Ch group. The difference between the ECh and Ch groups, though, was nonsignificant when the comparison was made between HDL cholesterol levels expressed as a percentage of total cholesterol in a given group. This finding indicates the increased HDL production in the liver in response to increased dietary cholesterol intake, which is in keeping with published data [19].

Analysing the results of tHCY and ADMA assays in a rabbit model, it becomes clear that the exposure to oxidized cholesterol derivatives and cholesterol leads to their gradual plasma level elevation and increases endothelial dysfunction as compared to the controls. The plasma levels of both tHCY and ADMA were elevated following the exposure to oxysterols and cholesterol. However, exposure to cholesterol only also resulted in a significant elevation of these biomarkers. Significant elevation of HCY and ADMA levels in a group fed with fodder containing 5α,6α-epoxycholesterols, as compared to the groups C and Ch, indirectly confirms additional effect of epoxycholesterols on tHCY and ADMA levels. The HCY and ADMA levels in the ECh group were significantly higher than in the Ch group. In the ECh group, plasma ADMA levels tended to start increasing earlier and more markedly, which can be attributed to the angiotoxic effect of oxysterols on vascular endothelium or abnormal renal ADMA elimination.

The analysis of IL-6 concentrations in our experimental animals seems to suggest that IL-6 biosynthesis is regulated by exogenous epoxycholesterols, as IL-6 concentrations increased significantly faster to settle at a higher level in animals exposed to oxycholesterol as compared to the groups Ch and C. In the group Ch, the IL-6 level in month 6 was twice as low as in the ECh group. In the control group, it remained unchanged throughout the experiment. The above findings are comparable to those published previously [20–22]. However, the values reported in individual papers tend to differ markedly, potentially due to different assay methods used. Due to the well-established role of IL-6 in promoting atherosclerosis in humans, its increased biosynthesis seen in a rabbit model (particularly marked in a group exposed to oxysterols) appears to be a significant biomarker suggestive of chronic vascular wall inflammation.

In our experiment, the TNF-α concentration in rabbits exposed to unoxidized cholesterol significantly increased over the first four months to stabilise over the subsequent two months. In the group fed additionally with 5α,6α-epoxycholesterol, the rate and extent of increase were significantly higher with higher TNF-α levels in month 6.

Rabbits with experimentally induced hypercholesterolemia presented with elevated levels of TNF-α, IL-6, IL-1, and selected endothelial dysfunction markers, as it was seen in a rat model [23]. Direct exposure of HUVEC cells to 7-keto-, 7β-hydroxycholesterol, and 7α-hydroxycholesterol resulted in an increased TNF-α production [24]. This can explain elevated TNF-α levels in animals exposed to oxysterols. However, the available literature lacks data on the effect of 5α,6α-epoxycholesterol on biosynthesis of inflammatory cytokines.

The elevated levels of CRP in animals with experimentally induced hypercholesterolemia, demonstrated in the current study, are consistent with the available published data [20, 23, 25]. Additional intake of dietary 5,6-epoxycholesterol did not affect CRP levels. There is data to confirm extrahepatic origin of CRP in rabbits with experimentally induced hypercholesterolemia, as its synthesis in adipocytes was shown to be inhibited by administering atorvastatin [26]. Perhaps, then, animal adipose tissue constitutes an alternative source of this protein in the plasma, which is true for some proinflammatory cytokines, such as TNF-α. This hypothesis, though, appears unlikely due to decreased weight gain observed in animals exposed to oxysterols as compared to animals in the groups C and Ch.

The current study has some limitations. Extrapolating the findings of experimental research in animal models to the risk of oxysterol intake by humans, it should be noted that the intake of cholesterol derivatives in experimental

animals ranged between 2.5 to approx. 10 mg/kg per day [27, 28], which translates into the intake of 175–700 mg of oxysterols per day in an adult and amounts to at least 100% of typical cholesterol daily intake. Therefore, it is highly unlikely that a diet of a modern individual can comply with these assumptions. Another issue is interspecies differences between experimental animals (usually rabbits, rodents, or birds) and humans. A limitation of the current study is also a relatively low number of experimental animals in each group, which was guided by ethical considerations relevant to animal research experiments.

5. Conclusions

Based on our findings, we conclude that having been absorbed from the gastrointestinal tract and incorporated in lipoprotein structures, oxidized cholesterol derivatives exert cytotoxic effect on vascular endothelial cells, causing endothelial dysfunction, the severity of which depends on the duration of exposure. Combined administration of oxysterols and cholesterol is likely to increase their angiotoxic effect. At the same time, the inflammatory response and dyslipidaemia increase in severity.

Conflicts of Interest

The authors declare that there are no conflicts of interest regarding the publication of this paper.

Acknowledgments

This work was support by the grants from the Medical University of Silesia (KNW-2-156/09 and KNW-1-053/N/7/Z).

References

[1] A. J. Donato, R. G. Morgan, A. E. Walker, and L. A. Lesniewski, "Cellular and molecular biology of aging endothelial cells," *Journal of Molecular and Cellular Cardiology*, vol. 89, no. Part B, pp. 122–135, 2015.

[2] H. A. Hadi, C. S. Carr, and J. Al Suwaidi, "Endothelial dysfunction: cardiovascular risk factors, therapy, and outcome," *Vascular Health and Risk Management*, vol. 1, no. 3, pp. 183–198, 2005.

[3] M. R. Khaddaj, J. C. Mathew, D. J. Kendrick, and A. P. Braun, "The vascular endothelium: a regulator of arterial tone and interface for the immune system," *Critical Reviews in Clinical Laboratory Sciences*, vol. 54, no. 7-8, pp. 458–470, 2017.

[4] S. Meaney, K. Bodin, U. Diczfalusy, and I. Björkhem, "On the rate of translocation in vitro and kinetics in vivo of the major oxysterols in human circulation," *Journal of Lipid Research*, vol. 43, no. 12, pp. 2130–2135, 2002.

[5] G. Poli, G. F. Biasi, and G. Leonarduzzi, "Oxysterols in the pathogenesis of major chronic diseases," *Redox Biology*, vol. 1, no. 1, pp. 125–130, 2013.

[6] W. J. Griffiths, J. Abdel-Khalik, T. Hearn, E. Yutuc, A. H. Morgan, and Y. Wang, "Current trends in oxysterol research," *Biochemical Society Transactions*, vol. 44, no. 2, pp. 652–658, 2016.

[7] A. Kloudova, F. P. Guengerich, and P. Soucek, "The role of oxysterols in human cancer," *Trends in Endocrinology and Metabolism*, vol. 28, no. 7, pp. 485–496, 2017.

[8] M. Brzeska, K. Szymczyk, and A. Szterk, "Current knowledge about oxysterols: a review," *Journal of Food Science*, vol. 81, no. 10, pp. R2299–R2308, 2016.

[9] V. W. Virginio, V. S. Nunes, F. A. Moura et al., "Arterial tissue and plasma concentration of enzymatic-driven oxysterols are associated with severe peripheral atherosclerotic disease and systemic inflammatory activity," *Free Radical Research*, vol. 49, no. 2, pp. 199–203, 2015.

[10] "Guide for the Care and Use of Laboratory Animals," in *National Research Council (US) Committee for the Update of the Guide for the Care and Use of Laboratory Animals*, National Academies Press (US), Washington (DC), USA, 8th edition, 2011, http://www.ncbi.nlm.nih.gov/books/NBK54050/.

[11] F. O. McCarthy, J. Chopra, A. Ford et al., "Synthesis, isolation and characterisation of β-sitosterol and β-sitosterol oxide derivatives," *Organic & Biomolecular Chemistry*, vol. 3, no. 16, pp. 3059–3065, 2005.

[12] K. Kuo, R. Still, S. Cale, and I. McDowell, "Standardization (external and internal) of HPLC assay for plasma homocysteine," *Clincal Chemistry*, vol. 43, no. 9, pp. 1653–1655, 1997.

[13] G. Minniti, A. Piana, U. Armani, and R. Cerone, "Determination of plasma and serum homocysteine by high-performance liquid chromatography with fluorescence detection," *Journal of Chromatography A*, vol. 828, no. 1-2, pp. 401–405, 1998.

[14] R. H. Böger, S. M. Bode-Böger, S. Kienke, A. C. Stan, R. Nafe, and J. C. Frölich, "Dietary L-arginine decreases myointimal cell proliferation and vascular monocyte accumulation in cholesterol-fed rabbits," *Atherosclerosis*, vol. 136, no. 1, pp. 67–77, 1998.

[15] T. Teerlink, "HPLC analysis of ADMA and other methylated L-arginine analogs in biological fluids," *Journal of Chromatography. B, Analytical Technologies in the Biomedical and Life Sciences*, vol. 851, no. 1-2, pp. 21–29, 2007.

[16] M. I. Mackness, D. Harty, and D. Bhatnagar, "Serum paraoxonase activity in familial hypercholesterolaemia and insulin-dependent diabetes mellitus," *Atherosclerosis*, vol. 86, no. 2-3, pp. 193–199, 1991.

[17] M. M. Mahfouz, H. Kawano, and F. A. Kummerow, "Effect of cholesterol-rich diets with and without added vitamins E and C on the severity of atherosclerosis in rabbits," *The American Journal of Clinical Nutrition*, vol. 66, no. 5, pp. 1240–1249, 1997.

[18] J. Bełtowski, "Liver X receptors (LXR) as therapeutic targets in dyslipidemia," *Cardiovascular Therapeutics*, vol. 26, no. 4, pp. 297–316, 2008.

[19] N. Duverger, H. Kruth, F. Emmanuel et al., "Inhibition of atherosclerosis development in cholesterol-feed human apolipoprotein A-I transgenic rabbits," *Circulation*, vol. 94, no. 4, pp. 713–717, 1996.

[20] R. Largo, O. Sánchez-Pernaute, M. E. Marcos et al., "Chronic arthritis aggravates vascular lesions in rabbits with atherosclerosis. a novel model of atherosclerosis associated with chronic inflammation," *Arthritis and Rheumatism*, vol. 58, no. 9, pp. 2723–2734, 2008.

[21] R. Takeda, E. Suzuki, H. Satonaka et al., "Blockade of endogenous cytokines mitigates neointimal formation in obese Zucker rats," *Circulation*, vol. 111, no. 11, pp. 1398–1406, 2005.

[22] S. Zhao and D. Zhang, "Atorvastatin reduces interleukin-6 plasma concentration and adipocyte secretion of hypercholesterolemic rabbits," *Clinica Chimica Acta*, vol. 336, no. 1-2, pp. 103–108, 2003.

[23] M. Hongbao and C. Shen, "Relationship of inflammation/thrombosis and C-reactive protein (CRP), plasminogen activator inhibitor 1 (PAI-1), Inteleukin-6 (IL-6), Inteleukin-1 (IL-1), tissue factor (TF), tumor necrosis factor-alpha (TNF-α), tTssue plasminogen activator (tPA), CD40," *Nature and Science*, vol. 5, no. 4, pp. 61–74, 2007.

[24] S. Lemaire, G. Lizard, S. Monier et al., "Different patterns of IL-1β secretion, adhesion molecule expression and apoptosis induction in human endothelial cells treated with 7α-, 7β-hydroxycholesterol, or 7-ketocholesterol," *Federation of European Biochemical Societies Letters*, vol. 440, no. 3, pp. 434–439, 1998.

[25] N. M. Rajamannan, M. Subramaniam, M. Springett et al., "Atorvastatin inhibits hypercholesterolemia-induced cellular proliferation and bone matrix production in the rabbit aortic valve," *Circulation*, vol. 105, no. 22, pp. 2660–2665, 2002.

[26] D. Zhang, D. Che, S. Zhao, and Y. Sun, "Effects of atorvastatin on C-reactive protein secretions by adipocytes in hypercholesterolemic rabbits," *Journal of Cardiovascular Pharmacology*, vol. 50, no. 3, pp. 281–285, 2007.

[27] A. J. Brown and W. Jessup, "Oxysterols and atherosclerosis," *Atherosclerosis*, vol. 142, no. 1, pp. 1–28, 1999.

[28] J. X. Rong, L. Shen, Y. H. Chang, A. Richters, H. N. Hodis, and A. Sevanian, "Cholesterol oxidation products induce vascular foam cell lesion formation in hypercholesterolemic New Zealand white rabbits," *Arteriosclerosis, Thrombosis, and Vascular Biology*, vol. 19, no. 9, pp. 2179–2188, 1999.

Hindawi
Mediators of Inflammation
Volume 2018, Article ID 8592532, 11 pages
https://doi.org/10.1155/2018/8592532

Research Article

Whole-Body Cryotherapy Decreases the Levels of Inflammatory, Oxidative Stress, and Atherosclerosis Plaque Markers in Male Patients with Active-Phase Ankylosing Spondylitis in the Absence of Classical Cardiovascular Risk Factors

Agata Stanek,[1] **Armand Cholewka**,[2] **Tomasz Wielkoszyński**,[3] **Ewa Romuk**,[3] **and Aleksander Sieroń**[1]

[1]*School of Medicine with the Division of Dentistry in Zabrze, Department of Internal Medicine, Angiology and Physical Medicine, Medical University of Silesia, Batorego Street 15, 41-902 Bytom, Poland*
[2]*Department of Medical Physics, Chełkowski Institute of Physics, University of Silesia, 4 Uniwersytecka St., 40-007 Katowice, Poland*
[3]*School of Medicine with the Division of Dentistry in Zabrze, Department of Biochemistry, Medical University of Silesia, Jordana 19 St., 41-808 Zabrze, Poland*

Correspondence should be addressed to Agata Stanek; astanek@tlen.pl

Received 26 August 2017; Accepted 19 October 2017; Published 1 February 2018

Academic Editor: Adrian Doroszko

Objective. The aim of the study was to estimate the impact of whole-body cryotherapy (WBC) on cardiovascular risk factors in patients with ankylosing spondylitis (AS). *Material and Methods*. We investigated the effect of WBC with subsequent kinesiotherapy on markers of inflammation, oxidative stress, lipid profile, and atherosclerosis plaque in male AS patients (WBC group). To assess the disease activity, the BASDAI and BASFI were also calculated. The results from the WBC group were compared with results from the kinesiotherapy (KT) group. *Results*. The results showed that in the WBC group, the plasma hsCRP level decreased without change to the IL-6 level. The ICAM-1 level showed a decreasing tendency. The CER concentration, as well as the BASDAI and BASFI, decreased in both groups, but the index changes of disease activity were higher in the WBC than KT patients. Additionally, in the WBC group, we observed a decrease in oxidative stress markers, changes in the activity of some antioxidant enzymes and nonenzymatic antioxidant parameters. In both groups, the total cholesterol and LDL cholesterol, triglycerides, sCD40L, PAPP-A, and PLGF levels decreased, but the parameter changes were higher in the WBC group. *Conclusion*. WBC appears to be a useful method of atherosclerosis prevention in AS patients.

1. Introduction

Patients with ankylosing spondylitis (AS) have a higher risk of cardiovascular morbidity and mortality in comparison to the general population, which may be connected with the disease's activity, the functional and mobility limitations, structural damage, and inflammation [1, 2]. Even AS patients without concomitant classical cardiovascular risk factors yet, but in an active phase of the disease, are characterized by increased levels of oxidative stress, inflammatory states, higher serum concentrations of soluble CD40 ligand (sCD40L), and increased carotid intima-media thickness (IMT) in comparison to the general population. These factors may accelerate atherosclerosis in this group of patients [3, 4].

Fortunately, over the last several years, a revolution in the treatment of AS has taken place through the introduction of biological and disease-modifying antirheumatic drugs (DMARDs). Despite these advances, exercise and physiotherapy still play a very important role [5, 6].

A relatively new physiotherapeutic method used in the rheumatic disease treatment is whole-body cryotherapy

(WBC), which is based on the therapeutic exposure of the entire human body to very low temperatures (below −100°C) for 120–180 seconds [7].

Recent studies have confirmed the anti-inflammatory, antianalgesic, and antioxidant effects of extremely low temperatures in athletes [8]. WBC procedures also have had a beneficial influence on lipid profiles in healthy subjects [9] and in obese people [10].

In addition, noticeably positive effects on the mental state [11] and antioxidant status of patients with multiple sclerosis [12] and seropositive rheumatoid arthritis [13] have been observed when low temperatures were applied to the entire body.

Little is still known about the role of WBC in the management of AS patients. So far, the studies have shown that WBC procedures in AS patients do not influence ejection fraction, late ventricular potentials, nor QT dispersion. However, they do have a beneficial effect on the adaptive processes of the vegetative nervous system in patients without a significant pathology in the circulatory system [14].

It has also been proved that in AS patients, WBC procedures with subsequent kinesiotherapy may improve BASDAI (Bath Ankylosing Spondylitis Diseases Activity Index) and BASFI (Bath Ankylosing Spondylitis Functional Index) and some spinal mobility parameters and help to decrease pain [15, 16].

In our preliminary study [17], we showed that WBC may also have a beneficial influence on some specific inflammatory parameters in AS patients.

In light of the above findings, the primary aim of the study was to assess the influence of WBC on cardiovascular risk factors in AS patients with active phase and without any concomitant classical cardiovascular risk factors.

2. Materials and Methods

2.1. Participants. The study protocol had been reviewed and approved by the Bioethical Committee of the Medical University of Silesia in Katowice (permission number: NN-6501-93/I/07), and all analyzed patients were informed about the trial and provided written consent for inclusion in the study. All clinical investigations were conducted according to the principles expressed in the Declaration of Helsinki (1964).

The study involved a total of 32 nonsmoking male patients with ankylosing spondylitis who were divided randomly by a physician into two groups with an allocation ratio 1 : 1. The first group consisted of 16 AS patients exposed to whole-body cryotherapy procedures with subsequent kinesiotherapy (WBC group, mean age 46.63 ± 1.5 years). The second group consisted of 16 AS patients exposed only to kinesiotherapy procedures (KT group, mean age 45.94 ± 1.24 years). There was no significant difference in the mean age, BMI, carotid IMT, BASDAI, BASFI, and comorbiding disorders and distribution of classical cardiovascular risk factors between these groups.

Computer-generated random numbers were sealed in sequentially numbered envelopes, and the group allocation was independent of the time and person delivering the treatment. The physician (main coordinator) who allocated the patients to groups had 32 envelopes, each containing a piece of paper marked with either group WBC or KT. The physician selected and opened each envelope in the presence of a physiotherapist to see the symbol and would then direct the subject to the corresponding group.

Male patients who successfully enrolled in the study had a definite diagnosis of AS, did not suffer from any other diseases, had no associated pathologies, and had an attending physician who did not apply disease-modifying antirheumatic drugs (DMARDs), biologic agents, or steroids. The AS patients were treated with doses of nonsteroidal anti-inflammatory drugs (NSAIDs), which were not altered within one month before the beginning of the study and during it. All the patients included in the trial fulfilled the modified New York Criteria for definite diagnosis of AS, which serves as the basis for the ASAS/EULAR recommendations [18]. The final selection for the study included only HLA B27-positive patients, who exhibited II and III radiographic grades of sacroiliac joint disease and attended a consulting unit in a health resort in the period of subsidence of acute clinical symptoms, in order to qualify for sanatorium treatment (physiotherapy). The demographic data of the subjects is shown in Table 1.

The patients from both groups were asked to abstain from alcohol, drugs and any immunomodulators, immunostimulators, hormones, vitamins, minerals, or other substances with antioxidant properties for 4 weeks before the study. All the patients were also asked to refrain from the consumption of caffeine 12 hours prior to laboratory analyses. The diet of the patients was not modified.

Before the study, each patient was examined by a physician to exclude any coexisting diseases as well as any contraindications for WBC procedures. Prior to the study, a resting electrocardiogram was performed on all the patients, and before each session of cryotherapy, the blood pressure was measured for each patient.

2.2. Whole-Body Cryotherapy and Kinesiotherapy Procedures. Depending on the group, the AS patients were exposed either to a cycle of WBC procedures lasting 3 minutes a day with a subsequent 60-minute session of kinesiotherapy or to a 60-minute session of kinesiotherapy only, for 10 consecutive days excluding the weekend.

The WBC procedures were performed in a cryochamber with cold retention and cooled by synthetic liquid air (produced by Metrum Cryoflex, Poland), which consists of two compartments: the antechamber and the proper chamber, which were connected by a door. In the trial, the temperature in the antechamber was −60°C, whereas in the proper chamber, it reached −120°C. After a 30-second adaptation process in the antechamber, the patients were exposed to cryogenic temperatures in the proper chamber for 3 minutes. During the WBC procedure, all the patients were dressed in swimsuits, cotton socks and gloves, and wooden shoes and their mouths and noses were protected by surgical masks and their ears by ear protectors. All jewelry, glasses, and contact lenses were removed before entry into the chamber. During the WBC procedure, the

Table 1: Demographic data of the study subjects.

Characteristic	WBC group ($n = 16$)	Kinesiotherapy group ($n = 16$)	P value
Age (years), mean (SD)	46.63 ± 1.5	45.94 ± 1.24	0.114
Sex (M/F)	16/0	16/0	—
BMI (kg/m^2), mean (SD)	24.24 ± 4.4	23.76 ± 6.8	0.880
BASDAI	5.43 ± 1.61	5.28 ± 1.71	0.720
BASFI	5.20 ± 2.29	5.01 ± 2.06	1.00
Carotid IMT (mm)	1.1 ± 0.13	1.0 ± 0.14	0.925
Smoking (yes/no)	0/16	0/16	—
	Medication		
NSAID (yes/no)	16/0	16/0	—
DMARD (yes/no)	0/16	0/16	—
Biological agents (yes/no)	0/16	0/16	—

SD: standard deviation; BMI: body mass index; BASDAI: the Bath Ankylosing Spondylitis Diseases Activity Index; BASFI: the Bath Ankylosing Spondylitis Functional Index; IMT: intima-media thickness; NSAID: nonsteroidal anti-inflammatory drug; DMARD: disease-modifying antirheumatic drug.

patients were walking round the chamber without touching each other.

Immediately after leaving the cryogenic chamber and changing into track suits and trainers, the AS patients underwent kinesiotherapy lasting one hour. The program of kinesiotherapy was the same for all the patients in both groups. Kinesiotherapy procedures included range-of-motion exercises of the spine and major joints (including the ankle, knee, hip, wrist, elbow, and shoulder). Chest expansion and breathing exercises were also included. Apart from range-of-motion exercise, the AS patients received strengthening exercises of the muscles of the major joints (including the ankle, knee, hip, wrist, elbow, shoulder, thoracolumbar spine, and cervical spine) as well as aerobic exercise (including cycling and fast walking). All the exercises were carried out under the supervision of physical therapists.

All the patients completed the study and no complications or side effects related to the WBC procedures were observed.

2.3. Blood Sample Collection. Blood samples of all the subjects were collected in the morning before the first meal. Samples of whole blood (5 ml) were drawn from the basilic vein of each subject and then collected into tubes containing ethylenediaminetetraacetic acid (Sarstedt, S-Monovette with 1.6 mg/ml EDTA-K_3) and into tubes with a clot activator (Sarstedt, S-Monovette). The blood samples were centrifuged (10 min, 900g at 4°C), and then the plasma and serum were immediately separated and stored at the temperature of −75°C, until biochemical analyses could be performed. In turn, the red blood cells retained from the removal of EDTA plasma were rinsed with isotonic salt solution and then 10% of the hemolysates were prepared for further analyses. The hemoglobin concentration in the hemolysates was determined by the standard cyanmethemoglobin method. The inter- and intra-assay coefficients of variations (CV) were 1.1% and 2.4%, respectively.

2.4. Biochemical Analyses

2.4.1. Determination of Inflammatory-State Parameters. High-sensitivity C-reactive protein (hs-CRP) concentration in the serum was determined by the latex immunoturbidimetric method (BioSystems, Spain) and expressed in mg/l. The inter- and intra-assay coefficients of variations (CV) were 2.3% and 5.5%, respectively.

The serum ceruloplasmin (CER) oxidase activity was measured using the p-phenylenediamine kinetic method by Richterich [19] and expressed in mg/dl after a calibration with pure ceruloplasmin isolated from a healthy donor serum pool. The inter- and intra-assay coefficients of variations (CV) were 3.1% and 6.1%, respectively.

The plasma interleukin 6 (IL-6) and soluble intercellular adhesion molecule-1 (sICAM-1) concentrations were determined using the ELISA method from R&D Systems (USA). The concentrations of IL-6 and sICAM-1 were expressed in pg/ml and ng/ml. The inter- and intra-assay coefficients of variations (CV) were 5.1% and 8.8%, respectively, for IL-6 and 4.8% and 9.1%, respectively, for sICAM-1.

2.4.2. Oxidative Stress Marker Analyses

(1) Determination of Lipid Peroxidation Products, Total Oxidative Status, and Oxidative Stress Index. The intensity of lipid peroxidation in the plasma and the erythrocytes was measured spectrofluorimetrically as thiobarbituric acid-reactive substances (TBARS) according to Ohkawa et al. [20]. The TBARS concentrations were expressed as malondialdehyde (MDA) equivalents in μmol/l in plasma or in nmol/gHb in erythrocytes. The inter- and intra-assay coefficients of variations (CV) were 2.1% and 8.3%, respectively.

The serum concentrations of oxidized low-density lipoprotein (ox-LDL) and antibodies to ox-LDL (ab-ox-LDL) were measured with the use of ELISA kits (Biomedica, Poland). The ox-LDL and the ab-ox-LDL concentrations were expressed in ng/ml and mU/ml, respectively. The inter- and intra-assay coefficients of variations (CV) for ox-LDL were 5.8% and 9.4%, respectively, and −4.1% and 8.7% for ab-ox-LDL, respectively.

The serum total oxidant status (TOS) was determined with the method described by Erel [21] and expressed in μmol/l. The inter- and intra-assay coefficients of variations (CV) were 2.2% and 6.4%, respectively.

The oxidative stress index (OSI), an indicator of the degree of oxidative stress, was expressed as the ratio of total oxidant status (TOS) to total antioxidant capacity (FRAP) in arbitrary units [22].

(2) Determination of Activity of Antioxidant Enzymes. The plasma and erythrocytes superoxide dismutase (SOD - E.C.1.15.1.1) activity was determined by the Oyanagui method [23]. Enzymatic activity was expressed in nitrite unit (NU) in each mg of hemoglobin (Hb) or ml of blood plasma. One nitrite unit (1 NU) means a 50% inhibition of nitrite ion production by SOD in this method. SOD isoenzymes (SOD-

Mn and SOD-ZnCu) were measured using potassium cyanide as the inhibitor of the SOD-ZnCu isoenzyme. The inter- and intra-assay coefficients of variations (CV) were 2.8% and 5.4%, respectively.

The catalase (CAT - E.C.1.11.1.6.) activity in erythrocytes was measured by the Aebi [24] kinetic method and expressed in IU/mgHb. The inter- and intra-assay coefficients of variations (CV) were 2.6% and 6.1%, respectively.

The erythrocyte glutathione peroxidase (GPx - E.C.1.11.1.9.) activity was assayed by Paglia and Valentine's kinetic method [25], with t-butyl peroxide as a substrate and expressed as micromoles of NADPH oxidized per minute and normalized to one gram of hemoglobin (IU/gHb). The inter- and intra-assay coefficients of variations (CV) were 3.4% and 7.5%, respectively.

The activity of glutathione reductase in erythrocytes (GR - E.C.1.6.4.2) was assayed by Richterich's kinetic method [19], expressed as micromoles of NADPH utilized per minute and normalized to one gram of hemoglobin (IU/gHb). The inter- and intra-assay coefficients of variations (CV) were 2.1% and 5.8%, respectively.

(3) Determination of Nonenzymatic Antioxidant Status. The total antioxidant capacity of plasma was measured as the ferric-reducing ability of plasma (FRAP) according to Benzie and Strain [26] and calibrated using Trolox and expressed in (μmol/l). The inter- and intra-assay coefficients of variations (CV) were 1.1% and 3.8%, respectively.

The serum concentration of protein sulfhydryl (PSH) was determined by Koster's method [27], using dithionitrobenzoic acid (DTNB) and expressed in (μmol/l). The inter- and intra-assay coefficients of variations (CV) were 2.6% and 5.4%, respectively.

The serum concentration of uric acid (UA) was determined by a uricase-peroxidase method [28] on the Cobas Integra 400 plus analyzer and expressed as (mg/dl). The inter- and intra-assay coefficients of variations (CV) were 1.4% and 4.4%, respectively.

2.4.3. Determination of Lipid Profile. The total, HDL, and LDL cholesterol (T-Chol, HDL-Chol, and LDL-Chol, resp.) and triglyceride (TG) concentrations in serum were estimated using routine techniques (Cobas Integra 400 plus analyzer, Roche Diagnostics, Mannheim, Germany). The concentrations were expressed in (mg/dl). The inter- and intra-assay coefficients of variations (CV) were 2.8% and 5.4%, respectively, for T-Chol; 3.2% and 5.4%, respectively, for HDL-Chol; 2.6% and 6.5%, respectively, for LDL-Chol; and 2.5% and 7.6%, respectively, for TG. The triglyceride/HDL cholesterol (TG/HDL) ratio was calculated.

2.4.4. Determination of Atherosclerosis Plaque Instability Markers and Atherosclerosis Plaque Markers. Serum pregnancy-associated plasma protein-A (PAPP-A), soluble CD40 ligand (sCD40L), and placental growth factor (PLGF) concentrations were assayed by ELISA methods with DRG Instruments GmbH (Germany). The PAPP-A and sCD40L concentrations were expressed in ng/ml and the PLGF concentration in pg/ml. The inter- and intra-assay coefficients of variations (CV) were 6.8% and 10.2%, respectively, for PAPPA-A; 5.1% and 9.4%, respectively, for sCD40L; and 6.2% and 12.1%, respectively, for PLGF.

2.5. Assay of Activity of Ankylosing Spondylitis. The activity of ankylosing spondylitis was measured by the Bath Ankylosing Spondylitis Diseases Activity Index (BASDAI) and the Bath Ankylosing Spondylitis Functional Index (BASFI).

The BASDAI has six questions related to fatigue, back pain, peripheral pain, peripheral swelling, local tenderness, and morning stiffness (degree and length). Other than the issues relating to morning stiffness, all questions were scored from 0 (none) to 10 (very severe) using a visual analogue scale (VAS). The sum was calculated as the mean of two morning stiffness issues and the four remaining issues [29].

The BASFI is the mean score of ten questions addressing functional limitations and the level of physical activity at home and work, assessed on VAS scales (0 = easy, 10 = impossible) [30].

2.6. Assay of Intima-Media Thickness. A high-resolution Doppler ultrasonography was performed with a Logic-5 device with a high-frequency (11 MHz, 15 MHz) linear probe. The sonographer was an angiologist who was unaware of subject's clinical state. The measurement of intima-media thickness (IMT) was performed in the right and left common carotid arteries, and the average of the 2 measurements was calculated. The IMT was expressed in mm.

2.7. Statistical Analyses. Statistical analyses were undertaken using the statistical package of Statistica 10 Pl software. For each parameter, the indicators of the descriptive statistics were determined (mean value and standard deviation (SD)). The normality of the data distribution was checked using the Shapiro-Wilk test, while the homogeneity of the variance was checked by applying Levene's test. In order to compare the differences between the groups, an independent sample Student t-test was used or alternatively the Mann–Whitney U test. In the case of dependent samples, the Student t-test was used or alternatively the Wilcoxon test. Correlations between particular parameters were statistically verified by means of Spearman's nonparametric correlation test. Differences at the significance level of $P < 0.05$ were considered as statistically significant.

3. Results

3.1. Inflammatory-State Parameters, BASDAI, and BASFI. In the WBC group of AS patients, who underwent a ten-day-long cycle of WBC procedures with subsequent kinesiotherapy, it was found that after the completion of the treatment, the levels of hsCRP and CER decreased significantly. In the case of hsCRP, the difference prior to post treatment values in the WBC group was significantly higher in comparison to those in the KT group patients. Also, in the WBC group, the level of sICAM-1 showed a decreasing trend. Moreover, after the completion of the WBC cycle, the level of sICAM-1 was significantly lower in comparison to the KT group. But the level of IL-6 did not change significantly in the

Table 2: Levels of inflammatory parameters as well as the value of BASDAI and BASFI (mean value ± standard deviation (SD)) in AS patients before and after the completion of a cycle of ten whole-body cryotherapy procedures with subsequent kinesiotherapy (WBC group) or a cycle of ten kinesiotherapy procedures only (KT group), with statistical analyses. (p): plasma; (s): serum; Δ: difference prior to post treatment.

Parameters		WBC group	KT group	P
hsCRP (s) (mg/l)	Before	13.5 ± 16.3	13.9 ± 15.2	0.942
	After	9.2 ± 15.3	13.6 ± 16.2	0.438
	$^*P$	**0.002**	0.623	
	Δ	−4.24 ± 5.68	−0.27 ± 3.25	**0.023**
CER (s) (mg/dl)	Before	62.83 ± 12.61	67.57 ± 12.60	0.296
	After	51.32 ± 10.74	53.51 ± 14.26	0.628
	$^*P$	**0.006**	**0.003**	
	Δ	−11.51 ± 16.6	−14.06 ± 14.47	0.646
IL-6 (p) (pg/ml)	Before	41.6 ± 8.86	41.8 ± 10.5	0.957
	After	36.6 ± 7.89	41.0 ± 10.4	0.191
	$^*P$	0.121	0.301	0.216
	Δ	−4.94 ± 11.9	−0.74 ± 5.71	
sICAM-1 (p) (ng/ml)	Before	79.0 ± 15.5	84.3 ± 21.9	0.432
	After	69.2 ± 14.2	83.9 ± 20.0	**0.023**
	$^*P$	0.088	0.642	
	Δ	−9.84 ± 23.0	−0.41 ± 16.1	0.191
BASDAI	Before	5.43 ± 1.61	5.28 ± 1.71	0.720
	After	3.29 ± 0.91	4.53 ± 1.62	**<0.05**
	$^*P$	**<0.001**	**<0.001**	
	Δ	−2.14 ± 1.23	−0.74 ± 0.38	**0.001**
BASFI	Before	5.20 ± 2.29	5.01 ± 2.06	1.00
	After	3.81 ± 2.20	4.35 ± 2.23	0.497
	$^*P$	**<0.001**	**<0.001**	
	Δ	−1.39 ± 1.03	−0.66 ± 0.39	**<0.01**

P: statistical significance of differences between both groups of patients; $^*P$: statistical significance of differences between values before and after treatment in particular groups of patients.

WBC group with subsequent kinesiotherapy after the completion of treatment.

After the completion of treatment, only the level of CER decreased significantly from the estimated inflammatory parameters in AS patients from the KT group who underwent a cycle of kinesiotherapy only, without being preceded by WBC procedures. The levels of hsCRP and sICAM-1 did not change significantly in the KT group. Also, as in the WBC group, no statistically significant changes in the level of IL-6 were observed in the KT group.

In turn, the BASDAI and BASFI decreased significantly in both groups, but in the WBC group with subsequent kinesiotherapy after the completion of the treatment, the decrease of these parameters was significantly higher in comparison to that in the KT group. Moreover, only in the WBC group after the completion of the treatment, the value of both BASDAI and BASFI was below 4 (inactive phase of AS disease) (Table 2).

3.2. Oxidative Stress. We observed that patients in the WBC group had, after the completion of the treatment, a statistically significant decrease in erythrocyte levels of MDA, serum anti-ox-LDL ab, serum TOS, and value of OSI in comparison to initial values. What is more, the differences of these parameters prior to post treatment values in the WBC group were significantly higher in comparison to the KT group. The levels of plasma MDA and serum ox-LDL did not change significantly in the WBC group. In turn, in the KT group, no significant changes in the levels of plasma and erythrocyte MDA, serum ox-LDL, serum anti-ox-LDL ab, and serum TOS and OSI were observed after the completion of the treatment, in comparison to the initial values before the beginning of the kinesiotherapy cycle (Table 3).

In the WBC group patients, we observed a statistically significant decrease in erythrocyte activity of GPx after the completion of a cycle of cryotherapy procedures with subsequent kinesiotherapy. However, the activity of plasma and erythrocyte total SOD, plasma SOD-Mn, plasma SOD-CuZn, erythrocyte CAT, and GR did not change significantly in the WBC group after treatment. But in the WBC group, the activity of plasma SOD-Mn after treatment was significantly higher in comparison to the KT group. In turn, in the KT group, the activity of erythrocyte total SOD, GPx, and GR decreased significantly after

Table 3: Levels of lipid peroxidation parameters, total oxidative status (TOS), and oxidative stress index (OSI) (mean value ± standard deviation (SD)) in AS patients before and after the completion of a cycle of ten whole-body cryotherapy procedures with subsequent kinesiotherapy (WBC group) or a cycle of ten kinesiotherapy procedures only (KT group), with statistical analyses. (p): plasma; (s): serum; (e): erythrocyte lysates; Δ: difference prior to post treatment.

Parameters		WBC group	KT group	P
MDA (p) (μmol/l)	Before	2.54 ± 0.52	2.32 ± 0.60	0.272
	After	2.30 ± 0.75	2.41 ± 0.83	0.715
	$^*P$	0.278	0.959	
	Δ	−0.24 ± 0.81	0.09 ± 1.04	0.331
MDA (e) (nmol/gHb)	Before	0.17 ± 0.04	0.18 ± 0.02	0.418
	After	0.15 ± 0.03	0.18 ± 0.04	**0.007**
	$^*P$	**0.013**	0.642	
	Δ	−0.02 ± 0.03	0.00 ± 0.04	**0.043**
ox-LDL (s) (ng/ml)	Before	249 ± 77.6	298 ± 122	0.191
	After	223 ± 100	288 ± 133	0.132
	$^*P$	0.301	0.84	
	Δ	−25.9 ± 123	−9.6 ± 149	0.738
Anti-oxLDL ab (s) (mU/ml)	Before	465 ± 209	571 ± 426	0.382
	After	347 ± 139	490 ± 316	0.111
	$^*P$	**0.013**	0.379	
	Δ	−118 ± 178	−80.5 ± 323	0.687
TOS (s) (μmol/l)	Before	26.54 ± 4.45	23.94 ± 11.60	0.414
	After	12.09 ± 2.55	24.41 ± 6.24	**<0.001**
	$^*P$	**<0.001**	0.605	
	Δ	−14.45 ± 4.83	0.46 ± 9.11	**<0.001**
OSI (p/s) (arbitrary unit)	Before	24.10 ± 15.94	18.87 ± 11.30	0.294
	After	8.20 ± 6.76	23.65 ± 15.68	**0.002**
	$^*P$	**0.003**	0.301	
	Δ	−15.90 ± 16.82	4.78 ± 13.88	**0.001**

P: statistical significance of differences between both groups of patients; $^*P$: statistical significance of differences between values before and after treatment in particular groups of patients.

treatment in comparison to the WBC group. Additionally, the activity of plasma SOD-CuZn showed also a decreased tendency in the KT group. Similarly as in the WBC group patients, the activity of plasma total SOD and erythrocyte CAT did not change significantly in the KT group after treatment (Table 4).

What is more, in the WBC group, the parameters of nonenzymatic antioxidants, FRAP values, and UA concentration increased significantly after treatment. The levels of those parameters were significantly higher in the WBC group in comparison to the KT group after the completion of the treatment. The level of PSH did not change significantly in the WBC group after treatment. In turn, in the KT group, the FRAP values and PSH level decreased significantly, but the level of UA did not change significantly after treatment (Table 5).

3.3. Markers of Lipid Profile, Atherosclerosis Plaque, and Atherosclerosis Plaque Instability. The levels of T-Chol, LDL, TG, sCD40L, PLGF, and PAPP-A decreased significantly after treatment in both groups, but the differences prior to post treatment values in the WBC group were significantly higher in comparison to the KT group, except for T-Chol. But the TG difference prior to post treatment values in the WBC group was higher in comparison to the KT group. The level of HDL-Chol did not change significantly in both groups. The TG/HDL ratio showed a decreasing tendency in the WBC group in comparison to the KT group (Table 6).

3.4. Significant Relationships among the Estimated Parameters in AS Patients Who Underwent WBC Procedures. After treatment, we noticed significant relationships in the WBC group between changes of serum hsCRP concentration and erythrocyte MDA concentration ($r = 0.6$). Also, a positive correlation between serum hsCRP change and plasma FRAP activity change ($r = 0.6$) was observed. Additionally, a negative correlation between serum hsCRP concentration and plasma SOD-CuZn activity was found ($r = -0.62$). In the case of the analysis of serum oxLDL-ab, we observed a negative correlation with CAT and SOD activities in erythrocytes (r coefficients: −0.51 and −0.53, resp.). Furthermore, the ratio of

Table 4: Activities of antioxidant enzymes (mean value ± standard deviation (SD)) in AS patients before and after the completion of a cycle of ten whole-body cryotherapy procedures with subsequent kinesiotherapy (WBC group) or a cycle of ten kinesiotherapy procedures only (KT group), with statistical analyses. (p): plasma; (e): erythrocyte lysates; Δ: difference prior to post treatment.

Parameters		WBC group	KT group	P
Total SOD (p) (NU/ml)	Before	13.4 ± 2.13	12.3 ± 1.85	0.145
	After	12.1 ± 1.88	1.7 ± 2.49	0.632
	$^*P$	0.233	0.301	
	Δ	−1.28 ± 3.13	−0.60 ± 2.65	0.512
SOD-Mn (p) (NU/ml)	Before	5.37 ± 2.75	4.56 ± 1.86	0.336
	After	6.27 ± 0.99	5.02 ± 1.64	**0.015**
	$^*P$	0.163	0.642	
	Δ	0.90 ± 2.80	0.46 ± 2.46	0.642
SOD-CuZn (p) (NU/ml)	Before	8.09 ± 2.74	7.80 ± 2.21	0.749
	After	7.15 ± 1.32	7.05 ± 3.09	0.902
	$^*P$	0.326	0.063	
	Δ	−0.93 ± 2.77	−0.75 ± 2.72	0.854
Total SOD (e) (NU/mgHb)	Before	85.5 ± 17.3	128.0 ± 11.2	**<0.001**
	After	90.5 ± 11.9	111.0 ± 15.6	**<0.001**
	$^*P$	0.438	**0.001**	
	Δ	5.02 ± 17.3	−17.1 ± 11.8	**<0.001**
CAT (e) (IU/mgHb)	Before	385.0 ± 70.3	425.0 ± 53.6	0.084
	After	375.0 ± 58.3	412.0 ± 58.6	0.088
	$^*P$	0.535	0.352	
	Δ	−9.9 ± 57.0	−13.0 ± 54.0	0.876
GPx (e) (IU/gHb)	Before	31.2 ± 4.90	29.9 ± 2.84	0.363
	After	29.1 ± 2.97	20.4 ± 5.05	<0.001
	$^*P$	**0.039**	**0.001**	
	Δ	−2.09 ± 3.61	−9.49 ± 6.74	0.001
GR (e) (IU/gHb)	Before	1.72 ± 0.56	2.07 ± 0.52	0.043
	After	1.54 ± 0.60	1.65 ± 0.59	0.078
	$^*P$	0.469	**0.002**	
	Δ	−0.18 ± 0.80	−0.42 ± 0.41	0.622

P: statistical significance of differences between both groups of patients; $^*P$: statistical significance of differences between values before and after treatment in particular groups of subjects.

TG/HDL was positively correlated with the PLGF serum concentration after WBC procedures ($r = 0.58$). We also observed a positive correlation between plasma concentrations of sICAM-1 and MDA ($r = 0.66$) in the WBC group after treatment. In the case of erythrocyte GPx activity in AS patients who underwent WBC procedures with subsequent kinesiotherapy, a positive correlation with plasma PSH ($r = 0.54$) was visible and a negative correlation was found with plasma MDA concentration. All the correlations mentioned above were significant ($p < 0.05$).

4. Discussion

In our study, we observed that, after the completion of the treatment, the WBC group of AS patients who underwent a ten-day-long cycle of WBC procedures with subsequent kinesiotherapy had significantly decreased levels of hsCRP and CER. The level of sICAM-1 showed a decreasing trend in the WBC group. But the level of IL-6 did not change significantly.

The results of the inflammatory parameters in this study are consistent with our previous preliminary study [17], in which AS patients who underwent WBC procedures were observed to have a decrease in CRP, fibrinogen, mucoprotein, and sICAM levels.

However, in another study [31], the authors have observed a decrease in TNF-α and an increase in IL-6 in tennis players after a 5-day exposure to WBC twice a day.

Banfi et al. [32] have also confirmed that a decreased level of sICAM-1 is induced by WBC treatment and is linked to an anti-inflammatory response. In another paper, Pournot et al. [33] have found that WBC (−110°C) decreased IL-1β and CRP levels and increased the IL-1ra level after intense exercise. But the levels of TNF-α, IL-10, and IL-6 remained unchanged. Similarly, in our study, we did not observe any changes in serum IL-6 in AS patients who underwent WBC.

Table 5: Levels of nonenzymatic antioxidants (mean value ± standard deviation (SD)) in AS patients before and after the completion of a cycle of ten whole-body cryotherapy procedures with subsequent kinesiotherapy (WBC group) or a cycle of ten kinesiotherapy procedures only (KT group), with statistical analyses. (p): plasma; (s): serum; Δ: difference prior to post treatment.

Parameters		WBC group	KT group	P
FRAP (μmol/l)	Before	587.1 ± 58.3	550.0 ± 91.3	0.183
	After	636.1 ± 62.3	499.3 ± 74.6	**<0.001**
	$^*P$	**0.010**	**0.001**	
	Δ	49.0 ± 31.7	−50.8 ± 39.4	**<0.001**
PSH (s) (μmol/l)	Before	402.6 ± 91.7	393.2 ± 90.0	0.772
	After	392.6 ± 87.4	364.7 ± 28.4	0.239
	$^*P$	0.836	**0.017**	
	Δ	−9.9 ± 108.1	−28.5 ± 92.6	0.605
UA (s) (mg/dl)	Before	5.40 ± 1.39	4.34 ± 1.15	**0.025**
	After	6.62 ± 2.07	4.61 ± 1.25	**0.003**
	$^*P$	**0.011**	0.196	
	Δ	1.22 ± 1.70	0.27 ± 0.70	0.052

P: statistical significance of differences between both groups of patients; $^*P$: statistical significance of differences between values before and after treatment in particular groups of patients.

In the present study, we also saw a significant decrease in the BASDAI and BASFI after the completion of the WBC treatment in a cryochamber with cold retention. Similar results were observed in a closed cryochamber of a type called "Wrocławski", cooled by liquid nitrogen [15]. In the both studies, after the completion of a cycle consisting of ten daily 3-minute-long WBC procedures with subsequent kinesiotherapy (−120°C, with a weekend break), the BASDAI and BASFI decreased below 4. This indicates that the AS disease entered an inactive phase after the completion of treatment. Our results are also consistent with a study [16], in which the AS patients underwent 8 daily WBC procedures (−110°C, 3 minutes).

There are not many reports on the impact of WBC on the prooxidant-antioxidant balance. It has been noticed that WBC procedures may have a beneficial influence on antioxidant status. In the study performed by Dugué et al. [34], a significant increase has been seen in the TAS value in healthy men at the end of a cycle of 45 procedures of WBC (−110°C, 2 minutes, coolant liquid nitrogen) performed three times a week. In another study, Miller et al. [12] have noticed an increase in total antioxidant status, SOD activity, and uric acid level in the plasma of multiple sclerosis patients who underwent WBC treatment (−110° temperature, daily 10 procedures with weekend break, coolant medium liquid nitrogen). What is more, WBC was advocated to possibly enhance antioxidant capacities and, thus, counteract the exercise-induced reactive oxygen species production [12].

However, in a different study [13], patients with seropositive rheumatoid were observed by the authors to have only a short-term increase in TRAP during the first treatment session of WBC (−110°C, three times daily for 7 consecutive days) and the cold treatment did not cause any significant oxidative stress or adaptation.

In our study, we observed a significant decrease in oxidative stress, which may also be linked to the decrease in systemic inflammation in AS patients who underwent WBC treatment. After treatment, in the WBC group, we observed positive correlations between plasma concentrations of sICAM-1 and MDA as well as serum hsCRP and erythrocyte MDA concentrations. In addition, negative correlations between serum hsCRP concentration and plasma SOD-CuZn activity were found.

Furthermore, we observed the similar results in healthy subjects who underwent WBC procedures performed in a cryochamber with cold retention [35].

The differences in the results of various studies may be related to the type of cryochamber being used and the coolant medium, in addition to the time of exposure to cryogenic temperatures.

Only a few papers have estimated the impact of WBC on lipid profile. In rats exposed to WBC for 5 or 10 days, HDL and LDL cholesterol fraction decreased and total cholesterol levels in animals subjected to −60°C sessions for 10 days remained unchanged. The authors have also observed an increase in triglycerides in the blood serum of animals subjected to cryostimulation compared to control. A decrease in HDL cholesterol in rats after cryostimulation can be explained by the fact that HDL is the main fraction transporting cholesterol in rats, while in humans, most cholesterol is found in low-density lipoproteins [36].

In another study [9], the authors have observed reducing T-Chol, LDL-Chol, and TG and increasing HDL-Chol after 20 sessions of WBC in healthy men, but after 10 sessions of WBC, only LDL-Chol decreased, while a simultaneous HDL-Chol increase was observed in healthy men (cryogenic temperature −130°C).

In another study by these authors [14], a significant decrease in the level of LDL-Chol and TG has been observed, with a slight increase in high-density lipoprotein concentration after WBC treatment, including two cryostimulation treatments of 20 daily sessions in the second and

Table 6: Levels of lipid profile parameters, atherosclerosis plaque markers, and atherosclerosis plaque instability and values of TG/HDL ratio (mean value ± standard deviation (SD)) in AS patients before and after the completion of a cycle of ten whole-body cryotherapy procedures with subsequent kinesiotherapy (WBC group) or a cycle of ten kinesiotherapy procedures only (KT group), with statistical analyses. (p): plasma; (s): serum; (e): erythrocyte lysates; Δ: difference prior to post treatment.

Parameters		WBC group	KT group	P
T-Chol (s) (mg/dl)	Before	221.3 ± 39.17	200.33 ± 21.33	0.074
	After	202.40 ± 24.40	190.70 ± 22.57	0.51
	$^*P$	**0.0006**	**0.04**	
	Δ	−18.90 ± 20.54	−9.63 ± 18.38	0.20
LDL-Chol (s) (mg/dl)	Before	125.2 ± 32.6	145.3 ± 28.3	0.073
	After	93.3 ± 36.9	132.4 ± 24.7	**0.002**
	$^*P$	**<0.001**	**0.005**	
	Δ	−31.9 ± 28.6	−12.9 ± 15.1	**0.027**
HDL-Chol (s) (mg/dl)	Before	50.5 ± 14.1	58.0 ± 18.0	0.198
	After	47.0 ± 9.0	56.4 ± 18.2	0.078
	$^*P$	0.079	0.109	
	Δ	−3.5 ± 9.1	−1.7 ± 10.1	0.590
TG (s) (mg/dl)	Before	185.1 ± 18.9	178.6 ± 15.9	0.299
	After	156.7 ± 11.2	165.2 ± 20.4	0.158
	$^*P$	**0.001**	**0.001**	
	Δ	−28.4 ± 22.4	−13.4 ± 19.7	0.053
TG/HDL ratio	Before	3.95 ± 1.18	3.32 ± 0.96	0.150
	After	3.44 ± 0.60	3.18 ± 0.99	0.320
	$^*P$	0.055	0.250	
	Δ	−0.51 ± 0.92	−0.14 ± 0.43	0.190
sCD40L(s) (mg/ml)	Before	9.21 ± 3.88	7.25 ± 2.20	0.180
	After	5.01 ± 2.55	5.85 ± 2.06	0.171
	$^*P$	**0.0004**	**0.006**	
	Δ	−4.19 ± 2.17	−1.4 ± 1.78	**0.0001**
PLGF(s) (pg/ml)	Before	30.17 ± 10.23	21.69 ± 3.54	0.007
	After	19.32 ± 5.53	18.31 ± 2.91	0.641
	$^*P$	**0.001**	**0.004**	
	Δ	−10.84 ± 7.05	−3.38 ± 2.13	**0.0001**
PAPP-A (s) (ng/ml)	Before	17.74 ± 7.78	14.48 ± 4.52	0.162
	After	11.24 ± 3.12	11.79 ± 3.72	0.920
	$^*P$	**0.0004**	**0.003**	
	Δ	−6.51 ± 8.40	−2.69 ± 3.65	**0.008**

P: statistical significance of differences between both groups of patients; $^*P$: statistical significance of differences between values before and after treatment in particular groups of patients.

the last month of intervention, without diet modification in obese subjects.

In our study, we also observed a significant decrease in T-Chol, LDL-Chol, and TG. But the HDL-Chol level did not change after completing WBC procedures in the AS patients. What is more, in our study, we observed a significant decrease in the levels of sCD40, PAPP-A, and PLGF. Additionally, in the present study, the ratio of TG/HDL was positively correlated with the PLGF serum concentration after WBC procedures. The impact of WBC on these markers in AS patients has been estimated for the first time.

A significant decrease in lipid profile, atherosclerotic plaque and oxidative stress, and inflammatory parameters, as well as a reduction in the proportion of TG cholesterol to HDL cholesterol (TG/HDL ratio), seems beneficial enough to consider WBC treatment as a useful method for atherosclerosis prevention in AS patients.

The present study has some limitations. First, the study did not provide long-term follow-up (at least 3 months), and thus, we do not know how long the beneficial effect of WBC with subsequent kinesiotherapy would be maintained after the completion of a WBC cycle. Second, the cycle of WBC with subsequent kinesiotherapy

consisted of only ten procedures. A greater number of procedures (e.g., 20–30) could probably increase the treatment effect. Third, the study should involve a larger number of AS patients.

5. General Conclusion

Whole-body cryotherapy with subsequent kinesiotherapy facilitates a decrease in oxidative stress, lipid profile, atherosclerosis plaque, and its instability, as well as inflammatory parameters, and appears to be a useful method of atherosclerosis prevention in AS patients.

Conflicts of Interest

The authors declare that there is no conflict of interests regarding the publication of this paper.

Acknowledgments

This work was supported by grants from the Medical University of Silesia (KNW-1-045/K/7/K and KNW-640-2-1-376/17).

References

[1] A. Bremander, I. F. Petersson, S. Bergman, and M. Englund, "Population-based estimates of common comorbidities and cardiovascular disease in ankylosing spondylitis," *Arthritis Care & Research*, vol. 63, no. 4, pp. 550–556, 2011.

[2] N. Bodnar, G. Kerekes, I. Seres et al., "Assessment of subclinical vascular disease associated with ankylosing spondylitis," *The Journal of Rheumatology*, vol. 38, no. 4, pp. 723–729, 2011.

[3] A. Stanek, A. Cholewka, T. Wielkoszyński, E. Romuk, K. Sieroń, and A. Sieroń, "Increased levels of oxidative stress markers, soluble CD40 Ligand and carotid intima-media thickness reflect acceleration of atherosclerosis in male patients with ankylosing spondylitis in active phase and without the classical cardiovascular risk factors," *Oxidative Medicine and Cellular Longevity*, vol. 2017, Article ID 9712536, 8 pages, 2017.

[4] D. van der Heijde, S. Ramiro, R. Landewé et al., "2016 update of the ASAS-EULAR management recommendations for axial spondyloarthritis," *Annals of the Rheumatic Diseases*, vol. 76, no. 6, pp. 978–991, 2017.

[5] L. A. Passalent, "Physiotherapy for ankylosing spondylitis: evidence and application," *Current Opinion in Rheumatology*, vol. 23, no. 2, pp. 142–147, 2011.

[6] J. Tyrrell, W. Schmidt, D. H. Williams, and C. H. Redshaw, "Physical activity in ankylosing spondylitis: evaluation and analysis of an eHealth tool," *Journal of Innovation in Health Informatics*, vol. 23, no. 2, pp. 510–522, 2016.

[7] X. Guillot, N. Tordi, L. Mourot et al., "Cryotherapy in inflammatory rheumatic diseases: a systematic review," *Expert Review of Clinical Immunology*, vol. 10, no. 2, pp. 281–294, 2014.

[8] G. Lombardi, E. Ziemann, and G. Banfi, "Whole-body cryotherapy in athletes: from therapy to stimulation. An updated review of the literature," *Frontiers in Physiolology*, vol. 8, no. 258, pp. 1–16, 2017.

[9] A. Lubkowska, G. Banfi, B. Dolegowska, G. V. d'Eril, J. Łuczak, and A. Barrasi, "Changes in lipid profile in response to three different protocols of whole-body cryostimulation treatments," *Cryobiology*, vol. 61, no. 1, pp. 22–26, 2010.

[10] A. Lubkowska, W. Dudzińska, I. Bryczkowska, and B. Dołęgowska, "Body composition, lipid profile, adipokine concentration, and antioxidant capacity changes during interventions to treat overweight with exercise programme and whole-body cryostimulation," *Oxidative Medicine and Cellular Longevity*, vol. 2015, Article ID 803197, 13 pages, 2015.

[11] J. Rymaszewska, D. Ramsey, and S. Chładzińska-Kiejna, "Whole-body cryotherapy as adjunct treatment of depressive and anxiety disorders," *Archivum Immunologiae et Therapiae Experimentalis*, vol. 56, no. 1, pp. 63–68, 2008.

[12] E. Miller, M. Mrowiecka, K. Malinowska, K. Zołynski, and J. Kedziora, "Effects of the whole-body cryotherapy on a total antioxidative status and activities of some antioxidative enzymes in blood of patients with multiple sclerosis-preliminary study," *The Journal of Medical Investigation*, vol. 57, no. 1,2, pp. 168–173, 2010.

[13] H. Hirvonen, H. Kautiainen, E. Moilanen, M. Mikkelsson, and M. Leirisalo-Repo, "The effect of cryotherapy on total antioxidative capacity in patients with active seropositive rheumatoid arthritis," *Rheumatology International*, vol. 37, no. 9, pp. 1481–1487, 2017.

[14] L. Jagodziński, A. Stanek, J. Gmyrek, G. Cieślar, A. Sielańczyk, and A. Sieroń, "Evaluation of whole-body cryotherapy on the circulatory system in patients with ankylosing spondylitis by analysis of duration and QT interval dispersion," *Polish Journal of Physiotherapy*, vol. 7, no. 3, pp. 362–369, 2007.

[15] A. Stanek, A. Cholewka, J. Gaduła, Z. Drzazga, A. Sieroń, and K. Sieroń-Stołtny, "Can whole-body cryotherapy with subsequent kinesiotherapy procedures in closed type cryogenic chamber improve BASDAI, BASFI, some spine mobility parameters and decrease pain intensity in patients with ankylosing spondylitis?," *BioMed Research International*, vol. 2015, Article ID 404259, 11 pages, 2015.

[16] M. W. Romanowski, W. Romanowski, P. Keczmer, M. Majchrzycki, W. Samborski, and A. Straburzynska-Lupa, "Whole body cryotherapy in rehabilitation of patients with ankylosing spondylitis. A randomised controlled study," *Physiotherapy*, vol. 101, article e1294, Supplement 1, 2015.

[17] A. Stanek, G. Cieślar, K. Strzelczyk et al., "Influence of cryogenic temperatures on inflammatory markers in patients with ankylosing spondylitis," *Polish Journal of Environmental Study*, vol. 19, no. 1, pp. 167–175, 2010.

[18] S. van der Linden, H. A. Valkenburg, and A. Catts, "Evaluation of diagnostic criteria for ankylosing spondylitis," *Arthritis & Rheumatology*, vol. 27, no. 4, pp. 361–368, 1984.

[19] R. Richterich, *Clinical Chemistry: Theory and Practice*, Academic Press, New York, 1969.

[20] H. Ohkawa, N. Ohishi, and K. Yagi, "Assay for lipid peroxides in animal tissues by thiobarbituric acid reaction," *Analytical Biochemistry*, vol. 95, no. 2, pp. 351–358, 1979.

[21] O. Erel, "A new automated colorimetric method for measuring total oxidant status," *Clinical Biochemistry*, vol. 38, no. 12, pp. 1103–1111, 2005.

[22] M. Harma, M. Harma, and O. Erel, "Increased oxidative stress in patients with hydatidiform mole," *Swiss Medical Weekly*, vol. 133, no. 41-42, pp. 563–566, 2003.

[23] Y. Oyanagui, "Reevaluation of assay methods and establishment of kit for superoxide dismutase activity," *Analytical Biochemistry*, vol. 142, no. 2, pp. 290–296, 1984.

[24] H. Aebi, "[13] Catalase *in vitro*," *Methods in Enzymology*, vol. 105, pp. 121–126, 1984.

[25] D. Paglia and W. Valentine, "Studies on the quantitative and qualitative characterization of erythrocyte glutathione peroxidase," *The Journal of Laboratory and Clinical Medicine*, vol. 70, no. 1, pp. 158–169, 1967.

[26] I. F. F. Benzie and J. J. Strain, "The ferric reducing ability of plasma (FRAP) as a measure of "antioxidant power: the FRAP assay"," *Analytical Biochemistry*, vol. 239, no. 1, pp. 70–76, 1996.

[27] J. F. Koster, P. Biemond, and A. J. Swaak, "Intracellular and extracellular sulphydryl levels in rheumatoid arthritis," *Annals of the Rheumatic Diseases*, vol. 45, no. 1, pp. 44–46, 1986.

[28] Y. Zhao, X. Yang, W. Lu, H. Liao, and F. Liao, "Uricase based methods for determination of uric acid in serum," *Microchimica Acta*, vol. 164, no. 1-2, pp. 1–6, 2009.

[29] S. Garrett, T. Jenkinson, L. G. Kennedy, H. Whitelock, P. Gaisford, and A. Calin, "A new approach to defining disease status in ankylosing spondylitis: the Bath Ankylosing Spondylitis Disease Activity Index," *Journal of Rheumatology*, vol. 21, no. 12, pp. 2286–2291, 1994.

[30] A. Calin, S. Garrett, H. Whitelock et al., "A new approach to defining functional ability in ankylosing spondylitis: the development of the Bath Ankylosing Spondylitis Functional Index," *The Journal of Rheumatology*, vol. 21, no. 12, pp. 2281–2285, 1984.

[31] E. Ziemann, R. A. Olek, S. Kujach et al., "Five-day whole-body cryostimulation, blood inflammatory markers, and performance in high-ranking professional tennis players," *Journal of Athletic Training*, vol. 47, no. 6, pp. 664–672, 2012.

[32] G. Banfi, M. Melegati, A. Barassi et al., "Effects of whole-body cryotherapy on serum mediators of inflammation and serum muscle enzymes in athletes," *Journal of Thermal Biology*, vol. 34, no. 2, pp. 55–59, 2009.

[33] H. Pournot, F. Bieuzen, J. Louis et al., "Time-course of changes in inflammatory response after whole-body cryotherapy multi exposures following severe exercise," *PLoS One*, vol. 6, no. 7, article e22748, 2011.

[34] B. Dugué, J. Smolander, T. Westerlund et al., "Acute and long-term effects of winter swimming and whole-body cryotherapy on plasma antioxidative capacity in healthy women," *Scandinavian Journal of Clinical and Laboratory Investigation*, vol. 65, no. 5, pp. 395–402, 2005.

[35] A. Stanek, K. Sieroń-Stołtny, E. Romuk et al., "Whole-body cryostimulation as an effective method of reducing oxidative stress in healthy men," *Advances in Clinical and Experimental Medicine*, vol. 25, no. 6, pp. 1281–1291, 2016.

[36] B. Skrzep-Poloczek, E. Romuk, and E. Birkner, "The effect of whole-body cryotherapy on lipids parameters in experimental rat model," *Polish Journal of Balneology*, vol. 44, no. 1–4, pp. 7–13, 2002.